DESIGN OF WIND TURBINE MONOPILES FOR LATERAL LOADS

Robert B. Gilbert
The University of Texas at Austin

Shin-Tower Wang
Ensoft Inc.

Asitha Senanayake
The University of Texas at Austin

Erica Rendon
Ensoft Inc.

September 18th 2015

DISCLAIMER

This final report has been reviewed by the BSEE and approved for publication. Approval does not signify that the contents necessarily reflect the views and policies of the BSEE, nor does mention of the trade names or commercial products constitute endorsement or recommendation for use.

ACKNOWLEDGEMENT

This study was funded by the Bureau of Safety and Environmental Enforcement (BSEE), U.S. Department of the Interior, Washington, D.C., under Contract E13PC00017.

Table of Contents

LIST OF TABLES

LIST OF FIGURES

EXECUTIVE SUMMARY

The current design methods for laterally loaded offshore foundation, API RP 2A/2GEO, are unverified for the large diameter, relatively short monopiles used for offshore wind turbines. The following factors raise question as to the suitability of API RP 2A/2GEO for wind turbine monopiles: these piles have a significantly larger diameter and smaller length to diameter ratio than typical piles used for offshore structures; these piles are subjected to significant cycles of lateral loading and their design is governed by strict tolerance on rotation; and these pile may be impacted by significant scour at the sea floor.

The objective of this research was to evaluate the suitability of API RP 2A/2GEO for the design of wind turbine monopiles and to provide recommendations for improving the design method for these types of foundations. The research consisted of four tasks:

1. Lateral Load Test Database
   A database of lateral load tests, with a particular focus on large diameter and low slenderness, was compiled. Currently it includes a total of 76 tests and includes both field and laboratory tests.
2. Lateral Load Tests on Model Monopiles
   The tests in the database was supplemented with model tests conducted on monopiles that ranged from 1-in to 4-in in diameter. Tests were carried out under 1-g condition and in several different clay test beds.
3. Numerical Analyses
   Numerical analyses were performed using the Ensoft Inc. finite-difference program LPILE and using the general purpose finite-element program ABAQUS.
4. Design Guidelines
   Results from the laboratory and numerical tests were synthesized in to recommended design guidelines for wind turbine monopiles.

The project team was led by Dr. Robert Gilbert from The University of Texas at Austin and included Dr. Shin-Tower Wang (Ensoft Inc.), Erica Rendon (Ensoft Inc.), and Asitha Senanayake (The University of Texas at Austin).

The following conclusions about laterally loaded monopiles in clay are drawn based on our analysis of the laboratory, numerical modeling, and field test results:

1. Numerical modeling and model-scale testing with rigid piles of different diameters indicate that the form of the Matlock (1970) p-y curves, in which the lateral displacement is normalized by pile diameter and lateral soil resistance is normalized by the ultimate resistance, appropriately captures the effect of pile diameter. For very small L/D ratios (say less than one), the p-y curves near the tip may be affected by interaction with the soil resistance mobilized around the tip.
2. Field and model testing indicate that the Matlock (1970) p-y models consistently underestimate the lateral resistance when used to analyze laterally loaded piles in normally to moderately overconsolidated clays. This observation applies to small (2 inch) and large (54 inch) diameter piles. It even applies to the Sabine River tests (Matlock and Tucker 1961) that formed the basis of the Matlock (1970) p-y models.
3. An approximate version of the Jeanjean (2009) p-y model, in which the Matlock (1970) p-y curves are scaled by p-multipliers calculated at various depths, generally provides a

reasonable match to measured lateral displacements at the pile head when a relatively large strain at one-half the undrained shear strength is assumed, i.e., ε_{50}= 0.02. This result applies both to small scale model tests in kaolinite and large-scale field tests in high-plasticity clay provided that a gap does not form behind the pile.

4. The creation of a gap on the backside of the pile can lead to a reduction in the stiffness of the pile response and the ultimate lateral capacity. The creation of a gap is related both to the overconsolidation ratio and the magnitude of lateral displacement; as the overconsolidation ratio near the ground surface increases and the magnitude of lateral displacement increases, the potential for a gap increases. The Matlock (1970) p-y models provide a lower bound estimate for the response of a laterally loaded pile if a gap forms.
5. Field and model testing show that cyclic loading causes the secant stiffness of the lateral pile-soil response to degrade by up to 20 to 30 percent when the cyclic load amplitudes are 50 to 90 percent of the ultimate lateral capacity. The stiffness degradation occurs within the first 100 cycles, after which the stiffness is reasonably constant. Smaller or no degradation may occur if the lateral loading is a smaller percentage of the ultimate lateral capacity.
6. Model testing shows that the ultimate lateral capacity of the pile is not significantly affected by the previous cyclic loading.

For design of laterally loaded monopiles in clay, it is recommended that the following guidance be provided:

1. The form of the p-y curves for static loading in API RP 2GEO be adjusted using a bearing capacity factor of 8 versus 3 at the mudline and 12 versus 9 at depth for a normally consolidated to moderately overconsolidated clay (i.e., one in which a gap is not likely to form).
2. For cyclic loading in normally consolidated and overconsolidated clay, the currently recommended reduction in stiffness in API RP 2GEO (2011) be applied to the adjusted static p-y curves.
3. For lateral capacity checks under extreme environmental loading conditions after cyclic loading, the ultimate lateral resistance be represented by the ultimate lateral resistance for the adjusted static p-y curves.
4. The design of wind turbine structures be checked by both increasing and decreasing lateral stiffness of the soil that is predicted by the p-y curves in order to account for possible variations in the natural frequency of the structure.

1 INTRODUCTION

The current design methods for laterally loaded offshore foundation, API RP 2A/2GEO, are unverified for the large diameter, relatively short monopiles used for offshore wind turbines. This type of foundation is very common, having been used on over 75 percent of the offshore wind turbines installed in Europe (Doherty & Gavin, 2011)

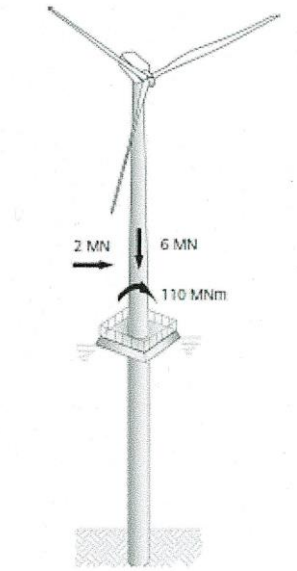

Figure 1.1: Schematic diagram of a monopile for offshore wind turbine

The following factors raise questions as to the suitability of API RP 2A/2GEO for wind turbine monopiles:

1. **Pile Diameter**
   The lateral load tests used to develop the API design method were conducted with relatively small-diameter piles. For example, the tests conducted at The University of Texas at Austin (UT Austin) for piles in clays used 12.75-in diameter steel pipe piles (Matlock, 1970). However, a monopile for a wind turbine will typically have a diameter that is ten to twenty times greater than those that were tested. Several field tests on large diameter laterally loaded piles have shown that the actual lateral displacements are much lower than those predicted based on the API design method.
2. **Pile Slenderness**
   The ratio of length to diameter (L/B) for a monopile will typically be significantly smaller than those used in the API load tests. Therefore, the response of a monopile is more like a rigid rotation, with components of axial resistance mobilized at the tip and along the sides as it rotates (Figure 1.2). This behavior is different to that of long slender piles that respond to lateral loading in bending rather than rotation.
3. **Cyclic Loading**
   Monopiles for wind turbines are subjected to cyclic loads from winds, waves, currents and tides, and they are designed with strict tolerances on rotation (typically less than 1-deg). Therefore, the primary response of interest for wind turbine monopiles is the lateral stiffness at relatively small lateral displacements and its change with time due to cyclic loading. In this project, the focus for the API design method is on the ultimate lateral capacity after cyclic loading during a

hurricane, which is not necessarily relevant when applied to wind turbine monopiles (Leblanc et al., 2010).

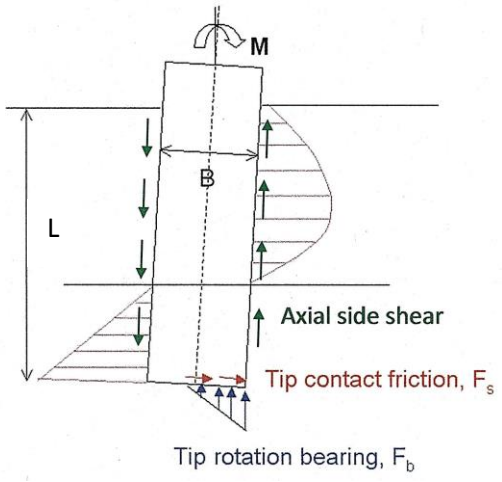

Figure 1.2: Tip and side resistance mobilized in a laterally loaded rigid pile

1.1 THE P-Y METHOD

The p-y method is the preferred method of analysis for laterally loaded piles and the API guidelines are provided in the form of p-y curves to be used with different soil conditions. This method of analysis was first proposed by McClelland & Focht (1958) and further developed by Matlock & Reese (1962).

Figure 1.3a shows a schematic of a laterally loaded pile. If the axial load on the pile is negligible then, its structural response can be found by solving the differential equation shown below. 1 where 'y' is the lateral displacement, 'z' is the depth, and 'p' is the lateral soil resistance with units of force per unit length.

$$EI\frac{d^4y}{dz^4} = p$$

The caveat is that 'p' is nonlinear function of both 'y' and 'z' i.e. $p = p(y, z)$. Under these conditions, a simple analytical solution to is not available for the above equation so a numerically solution has to be sought instead. According to the p-y method, the soil continuum around the pile is discretized in to a series of springs and the behavior of each spring is modeled by a corresponding p-y curve (see Figure 1.3b). The above equation is then solved numerically.

Published p-y curves are available in the literature for different soils and the API guidelines for the design of laterally loaded piles are presented in the form of design p-y curves.

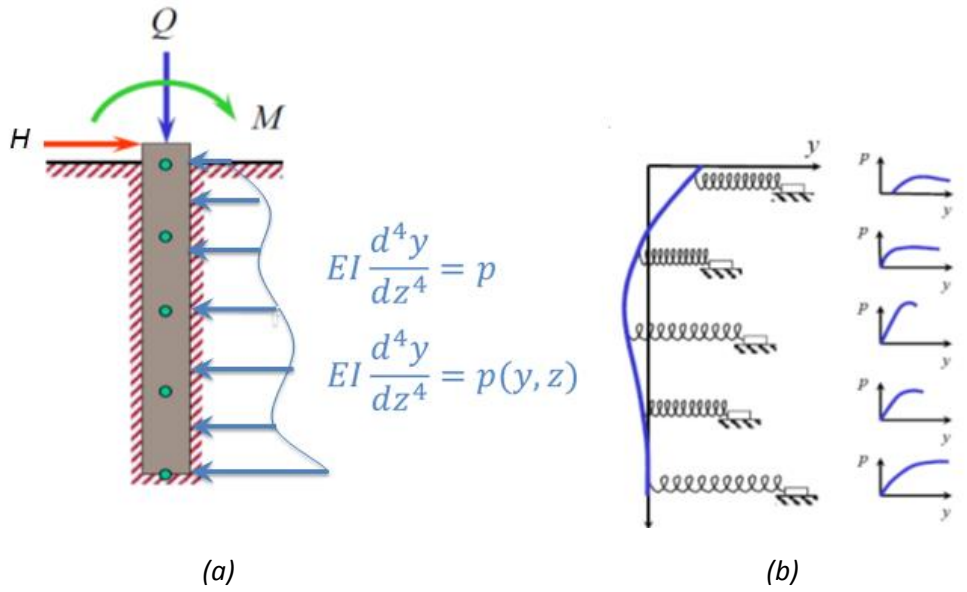

Figure 1.3: Schematic showing p-y model used for analysis of laterally loaded piles (Ref: LPILE Technical Manual)

1.2 MATLOCK (1970) P-Y CURVES

Matlock (1970) proposed a family of p-y cures to be used with "soft" clay, based on field tests carried out at Sabine River and Lake Austin in Texas. "Soft" clays are those with an undrained shear strength less than 2000-psf (Stevens & Audibert, 1979). P-y curves for use with static, cyclic, and post-cyclic reloading were proposed and the complete set of these curves is shown in Figure 1.4.

The normalized static form of these p-y curves follow the power law function shown below.

$$\frac{p}{p_{ult}} = 0.5\left(\frac{y}{y_{50}}\right)^{1/3} \quad for\ \frac{y}{y_{50}} \leq 8$$

$$\frac{p}{p_{ult}} = 1.0 \qquad for\ \frac{y}{y_{50}} > 8$$

Where p – lateral soil resistance (force/unit length), p_{ult} – ultimate lateral soil resistance (force/unit length), y – lateral displacement, y_{50} or y_c– normalizing parameter

The above normalized curves can be scaled up based on soil and pile properties by calculating p_{ult} and y_{50} as follows:

$$p_{ult} = N_p S_u D$$

$$y_{50} = 2.5\varepsilon_{50} D$$

Where N_p – lateral bearing capacity factor, S_u – undrained shear strength of the soil at depth of interest, D – pile diameter, ε_{50} – strain at which half the shear strength of the soil sample is mobilized in laboratory compression test

$$N_p = 3 + \frac{\sigma_v{}'}{S_u} + J\frac{z}{D} \quad but\ N_p \leq 9$$

σ_v' - effective vertical stress at depth of interest, z – depth of interest, J – scaling factor typically assumed to be 0.5 for marine clay (based on fit to data from the Sabine River tests by Matlock).

Under cyclic loading, the static curves should be modified as follows:

$$p_{ult,cyclic} = p_{ult} \quad for \ \frac{y}{y_{50}} \leq 3$$

$$p_{ult,cyclic} = 0.72\left(\frac{z}{z_{cr}}\right)p_{ult} \quad for \ \frac{y}{y_{50}} > 15$$

z_{cr} – critical depth i.e. depth at which $N_p = 9$ or full plastic flow (plane strain conditions) are mobilized

The above values should be linearly interpolated to obtain $p_{ult,cyclic}$ in the range $3 < \frac{y}{y_{50}} < 15$.

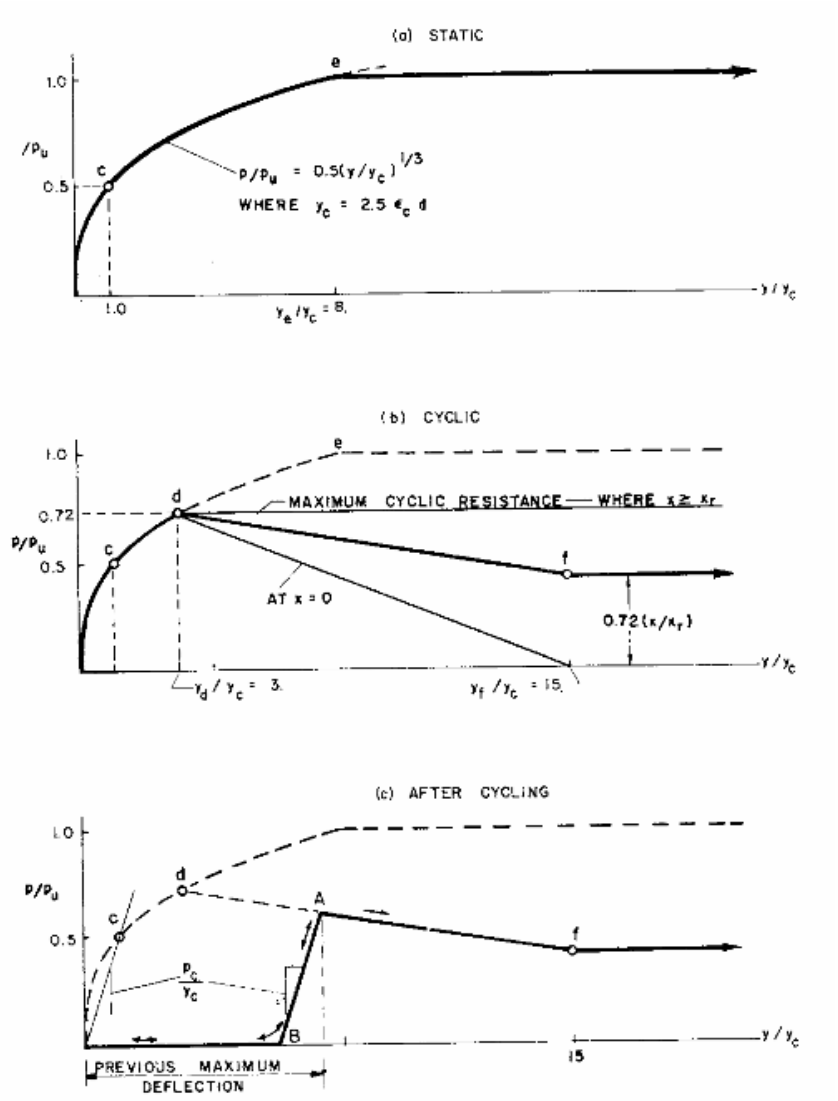

Figure 1.4: The complete set of normalized p-y curves proposed by Matlock (1970)

1.3 API RP 2GEO (2011) P-Y CURVES

API RP 2GEO presents its design guidelines in the form of design p-y curves. Table 1.1 and Table 1.2 were taken directly from API RP 2GEO (2011) and they define the design p-y curves for static and cyclic loads respectively. These API RP 2GEO (2011) p-y curves are discretized versions of the Matlock (1970) p-y curves, as is illustrated by Figure 1.5. Therefore, in this report API "soft clay" p-y curves will be referred as the Matlock (1970) p-y curves.

Table 1.1: API "soft clay" normalized p-y curve for static loading (API RP 2GEO, 2011)

p / p_u	y / y_c
0.00	0.0
0.23	0.1
0.33	0.3
0.50	1.0
0.72	3.0
1.00	8.0
1.00	∞

Key

p_u is the ultimate lateral capacity, unit of pressure;

p is the mobilized lateral resistance, unit of pressure;

y is the local pile lateral displacement;

y_C equals $2.5 \times \varepsilon_c \times D$;

D is the pile diameter;

ε_c is the strain at one-half the maximum deviator stress in laboratory undrained compression tests of undisturbed soil samples.

Table 1.2: API "soft clay" normalized p-y curves for cyclic loading (API RP 2GEO, 2011)

$z > z_R$		$z < z_R$	
p / p_u	y / y_c	p / p_u	y / y_c
0	0	0.00	0.0
0.23	0.1	0.23	0.1
0.33	0.3	0.33	0.3
0.50	1.0	0.50	1.0
0.72	3.0	0.72	3.0
0.72	∞	0.72 z / z_R	15.0
		0.72 z / z_R	∞

Key

Z	is the depth below seafloor;
z_R	is the depth below seafloor to bottom of reduced capacity zone for uniform soils (see Equation 25);
p_u	is the ultimate lateral capacity, unit of pressure;
p	is the mobilized lateral resistance, unit of pressure;
y	is the local pile lateral displacement;
y_c	equals 2.5 × εc ×D;
D	is the pile diameter;
ε_c	is the strain at one-half the maximum deviator stress in laboratory undrained compression tests of undisturbed soil samples.

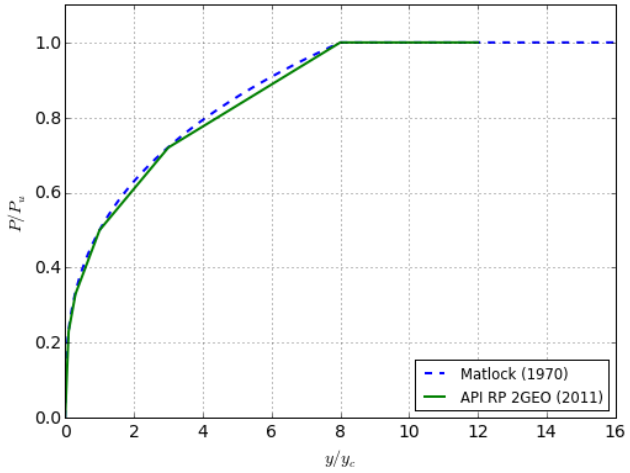

Figure 1.5: Comparison of API recommended normalized p-y curve for "soft clay" with the Matlock (1970) p-y model for static loading

1.4 JEANJEAN (2009) P-Y CURVES

Jeanjean (2009) carried out lateral load tests on model piles in a centrifuge to re-assess the p-y curves for "soft" clays as he believed that those recommended by API RP 2GEO and Matlock (1970) underestimated the lateral soil resistance on offshore oil well conductors. The conductors he modeled were vertical steel pipes so, the results are equally valid for laterally loaded piles.

Two changes to the Matlock (1970) curves were proposed in this paper. First, the shape of the p-y curves was changed to a hyperbolic form. Second, the range of the lateral bearing capacity factor (N_p) and its variation versus depth were modified.

The equation for a generic p-y curve according Jeanjean (2009) is similar to that proposed by O'Neill (1990), and is shown below.

$$\frac{p}{p_u} = \tanh\left[\frac{G_{max}}{100 S_u}\left(\frac{y}{D}\right)^{0.5}\right]$$

Figure 1.6 shows how this curve compares against the p-y curves by Matlock (1970) and API RP 2GEO (2011).

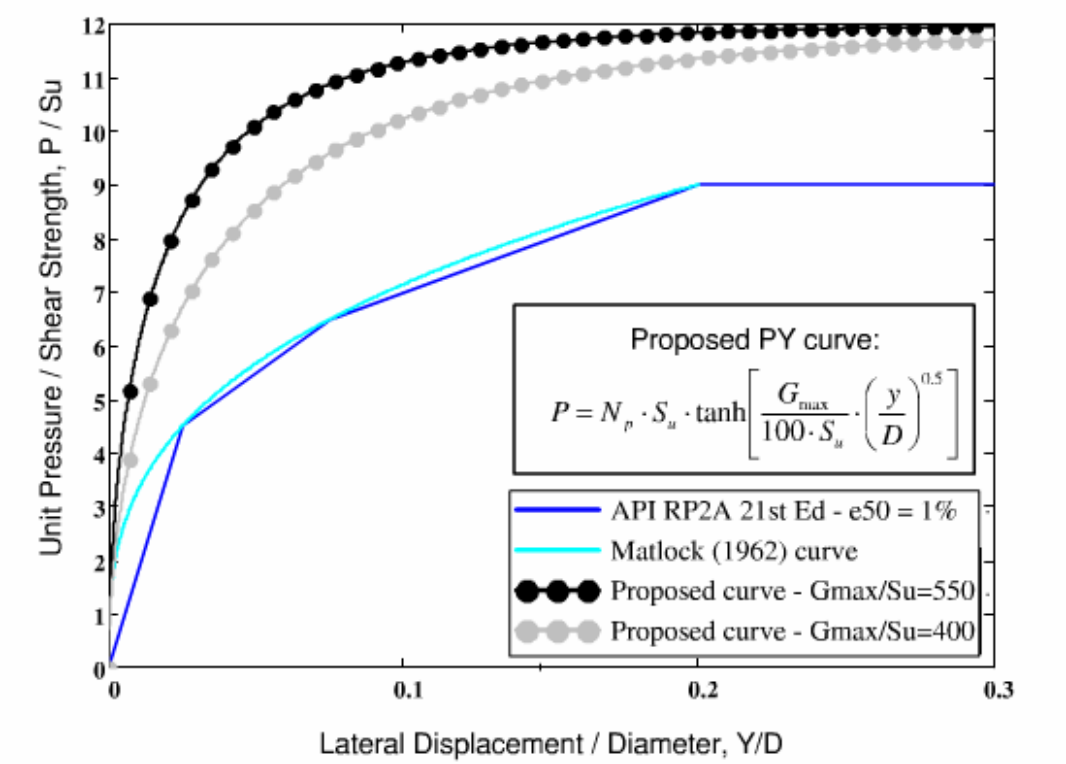

Figure 1.6: Comparison of p-y curves (Jeanjean, 2009)

The p-y curves derived from these tests were stiffer than the API RP 2GEO (2011) curves and the ultimate pressure also exceeded the value of $9S_u$ given by API/Matlock. The average value of N_p was 13.4 from the centrifuge tests but he proposed that it be limited to 12 for use in actual designs. The proposed value of N_p at the mudline is 8 and its variation versus depth (as shown in Figure 1.7) is based on the framework proposed by Murff & Hamilton (1993) for a linearly increasing shear strength profile. The mathematical formulation for N_p versus depth is as follows:

$$N_p = 12 - 4e^{-\varepsilon z/D}$$

$$\varepsilon = 0.25 + 0.05\lambda \quad for\ \lambda < 6$$
$$\varepsilon = 0.55 \quad for\ \lambda \geq 6$$

$$\lambda = \frac{S_{u0}}{S_{u1}D}$$

Where S_{u0}- undrained shear strength at the mudline, S_{u1}- rate of increase of undrained shear strength with depth, D- pile diameter, z – depth of interest

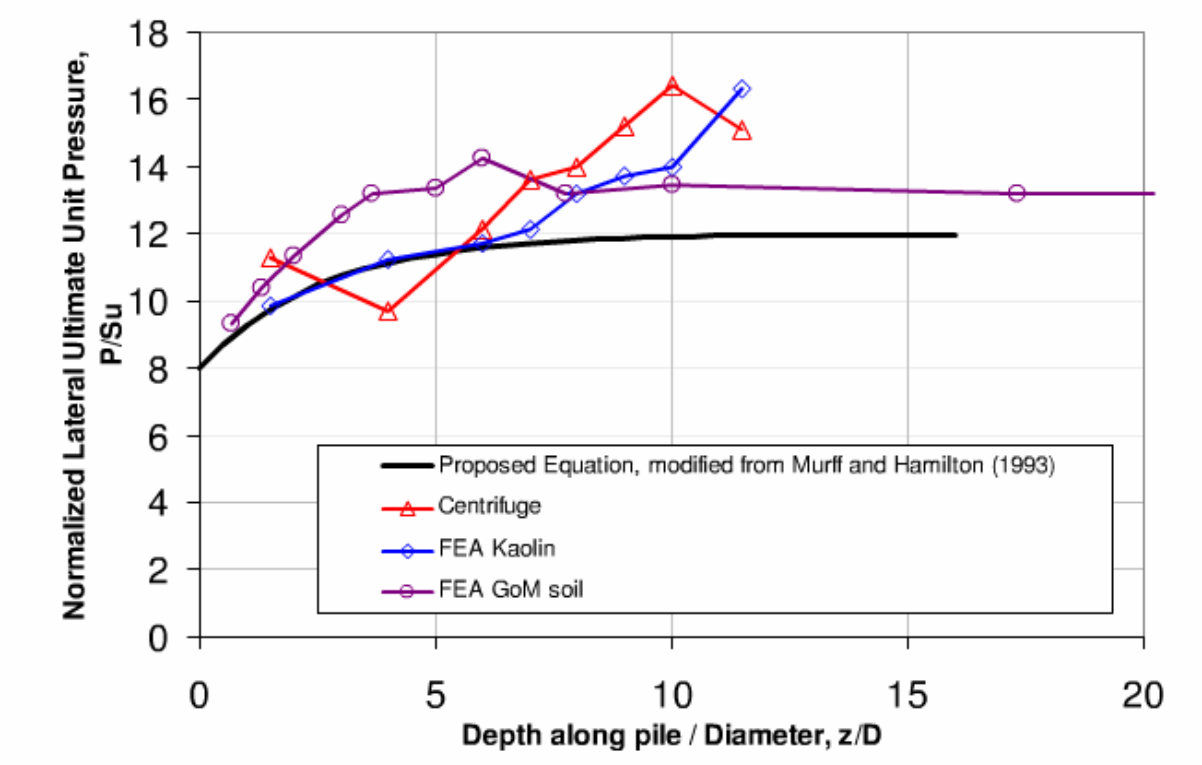

Figure 1.7: Variation of N_p versus normalized depth proposed by Jeanjean (2009)

2 DATABASE OF LATERALLY LOADED PILE TESTS

A database was created is to store, organize and analyze publicly-available results from lateral load tests, with a particular focus on the effects of pile diameter and slenderness. This database is attached as Appendix – Database of Lateral Load Tests.

Sources from which test data was obtained included text books, journal papers, conference papers, technical reports submitted to government agencies (including state DOTs, US Army Corp of Engineers and Naval Facilities Engineering Command), previously published databases on deep foundation testing, and unpublished data from tests carried out at The University of Texas at Austin and by Ensoft, Inc.. The majority of the load test results in this database were obtained from papers and/or reports published by the original researchers who conducted the tests. These data were supplemented by load test results extracted from the Deep Foundation Load Test Database (DFLTD) by the Federal Highway Administration (FHWA) and by the Laterally Loaded Pile Database by the University of Florida.

Data from over 150 lateral load tests were obtained, out of which 76 tests were chosen to be included in this database. Key criteria used in the selection process were soil stratigraphy, shape of foundation, and diameter of foundation. Since the objective of this research project was to evaluate design methods for large diameter monopile foundations, the selected test results were limited to piles/shafts with circular cross-sections. Tests performed at sites with soil profiles consisting of materials other than clays or siliceous sands (e.g., calcareous sand or rock) were also excluded since primarily clays and siliceous sands will be encountered in U.S. waters. Furthermore, an emphasis was put on obtaining load tests for piles/shafts with large diameters. Hence, the majority of the tests herein will be on foundations with diameters greater than 24 inches.

2.1 FORMAT OF DATABASE

This database is compiled in the form of an MS Excel® spreadsheet (Appendix – Database of Lateral Load Tests). Each test result was saved in a numbered worksheet and in some cases a single worksheet holds multiple test results. The worksheet named "Contents" provides a table of all the test results together with some key attributes of the load tests and the numbered worksheet in which each test result can be found. This table can sorted as required by the user via the "Sort & Filter" option in Excel, however, the order of worksheet tabs will not change.

Each test record contains two pages of data. The first page contains qualitative information about the load test such as source, type of lateral load test (monotonic and/or cyclic loading), pile head constraints (rotational fixity at pile head), date of installation & testing. Information regarding method of installation, soil stratigraphy, loading sequence, test results, and references are provided in greater detail. A schematic diagram of the pile setup including a simplified soil stratigraphy was also provided.

The second page contains quantitative data such as foundation dimensions, structural properties, soil properties, and load-deflection data. A graph of Load vs Deflection is shown at the bottom of the page.

A worksheet named "Template" is included for the purpose of adding new data in the future.

2.2 SUMMARY OF DATABASE

The database has the following attributes:

- Total of 76 tests on laterally loaded deep foundations
- Tests conducted in Soft & Stiff Clays (39 tests), Siliceous Sands (25), and Layered Clay-Sand Stratigraphy (12)
- Steel Piles, Reinforced Concrete Drilled Shafts, and Prestressed Concrete Piles/Shafts
- Field tests and laboratory tests (including one-g and centrifuge) on models
- Pile/Shaft diameters ranging from 6 inches to 97 inches
- Pile/Shaft aspect ratios (Length/Diameter) ranging from 1 to 80

2.3 PRINT INSTRUCTIONS

The worksheets that contain the test results are formatted to fit in two pages and are in shown in the "Page Break Preview" mode by default. This format allows the user to conveniently print the whole spreadsheet to a PDF document or a hardcopy. Follow the instructions below to obtain a printed copy:

1. Go to "File" → "Print"
2. Select "Print Entire Workbook" under "Settings"
3. Check Print Preview to make sure the data tables and charts fit in to the pages properly
4. Click "Print"

Note that the "Enable Editing" button should be selected when the spreadsheet is first opened in order for the page formats to be correct.

3 LABORATORY TESTS IN CLAY

A series of laboratory tests was conducted on model-scale monopiles installed in clay. Pile diameters ranged from 1 to 4 inches, all with a length of 8 times the diameter. A variety of soil profiles were used, including normally consolidated, moderately overconsolidated, heavily overconsolidated, moderately overconsolidated with a heavily overconsolidated crust, and kaolinite and marine clay from the Gulf of Mexico. Loading conditions included static, cyclic and static after cyclic. The models, soil profiles and loading conditions are described in this section. Characteristics for all tests conducted are summarized in Appendix B.

3.1 MODEL MONOPILES

The model piles were made with circular aluminum pipes, as they were well suited for underwater testing over long periods of time due to their corrosion resistance. Aluminum was also easy to machine, which made it easy to build models and integrate them to the existing loading system in our laboratory. Model piles of diameter 1-in, 2-in, 3-in, and 4-in were prepared and the wall thickness of each of these piles was 0.125-in (Figure 3.1).

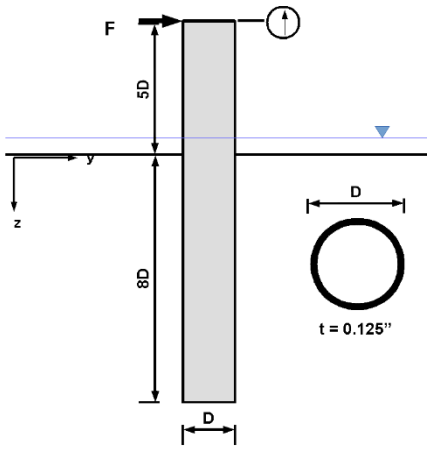

Figure 3.1: Schematic diagram of model piles, D = 1-in, 2-in, 3-in, 4-in (Senanayake et al., 2015)

Typical monopile foundations used to support offshore wind turbines have L/D ratios in the range of 5 – 10. According to Murff & Hamilton (1993), the peak lateral resistance in a soil with uniform strength will only be mobilized at a depth of greater than approximately 5D. This depth increases to approximately 12D in the case of a soil with linearly increasing strength. Hence, the pile models for this test program were chosen to have an embedded length to diameter ratio of eight (L/D = 8). This L/D ratio was both within the range for typical monopile foundations and long enough to mobilize peak lateral soil resistance near the pile tip. It also allowed us to test models with different diameters but with lengths small enough to be tested in the soil tanks in our laboratory, where the soil depths are limited to 24-in to 40-in.

Draft design calculations for a proposed offshore wind turbine in 20 m of water in the Gulf of Mexico indicated that the moment at the mud line imposed by the lateral loading has an eccentricity that is about five times the diameter. Hence, an eccentricity of 5D has been used in the testing. The same load eccentricity was used by Leblanc et al. (2010). To account for an embedded depth of 8D and a lateral

load eccentricity of 5D, the total length of the model piles was 13D. The model piles were installed by pushing them to the required depth and then the lateral loads were applied at height of 5D above the mudline, as shown in Figure 3.1.

For the purpose of comparison, Table 3.1 provides a summary of the characteristics of previous laboratory testing programs carried out on laterally loaded model piles in clay.

Table 3.1: Summary of previous laboratory testing programs on model piles in clay under lateral loading

Author	D (in)	t (in)	L/D	Model Details	Gravitational Field	Lateral Loading	Soil
Hamilton and Murff (1995)	0.5	0.04	9, 29	Circular Steel Suction Can, Pile Head Free	49 g and 93 g (Centrifuge)	Monotonic and Cyclic	Normally Consolidated Clay (Kaolinite), Overconsolidated Clay (Kaolinite)
Zhang et al. (2011)	0.5	0.04	5	Circular Aluminum Tube, Pile Head Fixed	50 g (Centrifuge)	Monotonic and Cyclic	Overconsolidated Clay (Kaolinite)
Jeanjean (2012)	0.75	0.05	22	Circular Steel Tube, Pile Head Free	48 g (Centrifuge)	Monotonic and Cyclic	Normally Consolidated Clay (Kaolinite)
Chen (2013)	6, 12	0.125	1	Circular Steel Suction Can, Pile Head Free	1 g	Monotonic and Cyclic	Normally Consolidated Clay (Kaolinite), Overconsolidated Clay (Kaolinite)

3.2 T-BAR PENETROMETER

A T-bar penetrometer was used to measure the undrained shear strength of the clay test beds. T-bar penetration tests have a history of being used to characterize the shear strength of clays and are particularly suited for applications involving laterally loaded piles and subsea pipelines (Stewart & Randolph, 1994). The main advantage of T-bar penetrometer is its ability to relate the penetration force directly to the shear strength of the soil directly to the shear strength of the soil using the plasticity based solutions by Randolph & Houlsby (1984) rather than relying on empirical correlations. Moreover, it can produce continuous shear strength profiles throughout the depth of the soil bed.

The T-bar that was used during this project was 1-in in diameter and 4-in in length as shown in Figure 3.2. It was attached to a 0.375-in diameter stainless steel rod that was 6-ft long. The whole setup of the T-bar with the rod is shown in Figure 3.3. Weights were attached to the rod at an intermediate height and this load was used to push the T-bar into the soil. The whole T-bar setup was attached to a motor

via a system of pulleys and the penetration rate was maintained at a rate of 0.8-in/s. More information about the performance and calibration of this T-bar is provided in Vanka (2004).

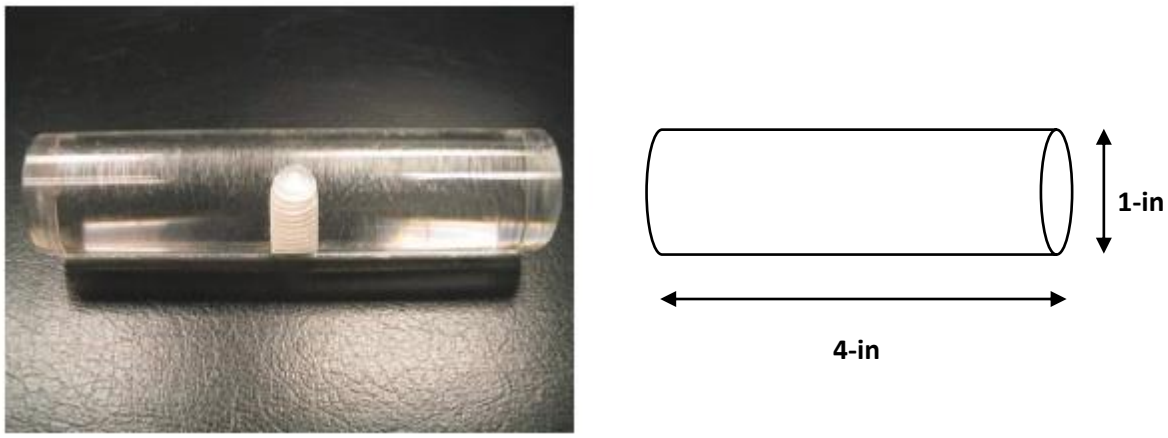

Figure 3.2: T-bar penetrometer

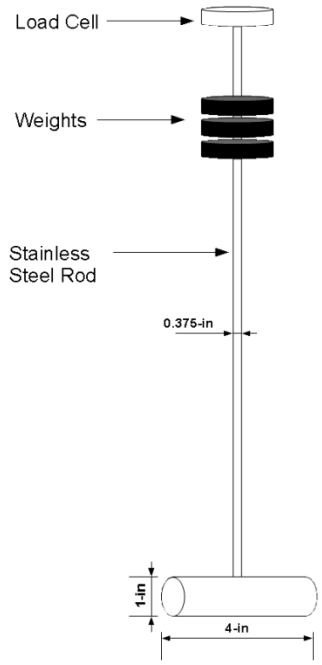

Figure 3.3: T-bar setup with rod, weights, and load cell attached

The forces acting on the T-bar and the rod are shown in Figure 3.4. Based on these forces, the soil resistance acting on the T-bar is given by:

$$F_{Soil\ Resistance\ on\ T-bar} = Load\ Cell\ Reading - W_{weights} - W_{Rod\ and\ T-bar} - F_{Rod\ Friction}$$

The soil resistance on the T-bar is related to the undrained shear strength of the soil as follows:

$$F_{Soil\ Resistance\ on\ T-bar} = N_c S_u A$$

$$\therefore S_u = \frac{F_{Soil\ Resistance\ on\ T-bar}}{N_c A}$$

Where N_c – bearing capacity factor, S_u – undrained shear strength of the soil, A – projected area of the T-bar.

According to Randolph & Houlsby (1984), N_c ranges from approximately 9 to 12, based on roughness of the T-bar surface, under fully plastic flow conditions. The standard practice for T-bar test interpretation is to assume an average bearing capacity factor therefore, $N_c = \frac{9+12}{2} = 10.5$.

$$S_u = \frac{F_{Soil\ Resistance\ on\ T-bar}}{10.5A}$$

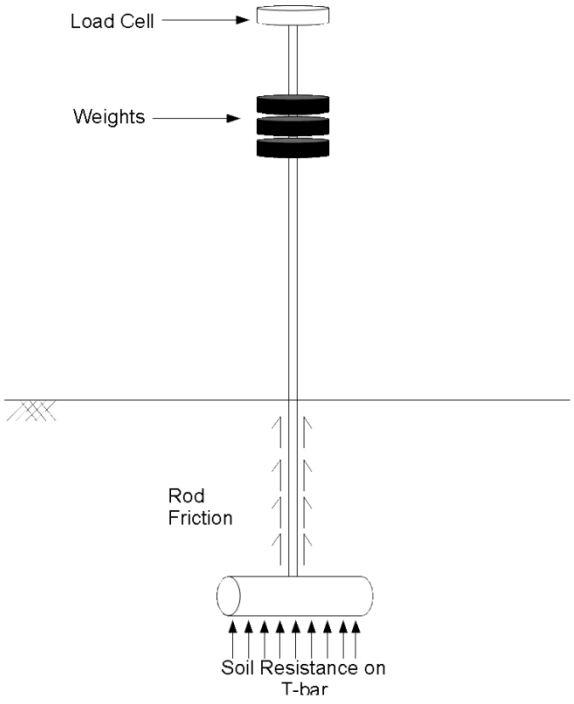

Figure 3.4: Loads acting on T-bar and the rod

3.3 TEST BEDS

Model piles were installed in test beds consisting of different soil types:

1. Normally to moderately overconsolidated kaolinite clay
2. Heavily overconsolidated kaolinite clay
3. Heavily overconsolidated kaolinite clay with a stiff crust
4. Heavily overconsolidated Gulf of Mexico clay
5. Normally consolidated Gulf of Mexico clay

Details of each soil type and how the test beds were prepared are given in the following sections.

3.3.1 Normally to Moderately Overconsolidated Kaolinite Clay Bed

The normally to moderately overconsolidated kaolinite clay bed had overconsolidation ratios ranging from approximately two to five, and an increasing undrained shear strength (S_u) versus depth. The undrained shear strength of the soil bed was measured by conducting T-bar tests at each location where model piles were to be placed. These tests were typically performed before the lateral load tests were done and the results are shown in Figure 3.5 and Figure 3.6.

Each figure shows a displacement versus time plot indicating the rate and depth of the T-bar penetration, a shear strength versus depth plot, and an overconsolidation ratio versus depth plot. Several tests were done at each location in order to determine the undisturbed and the remolded shear strength profiles. The undisturbed shear strength profile was obtained from the very first test at that location. Subsequent tests at the same location provide lower strength profiles as the soil is being remolded.

A typical S_u versus depth profile for a normally consolidated kaolinite clay is plotted with the T-bar results as a benchmark against which the actual undrained shear strength can be compared. This benchmark S_u versus depth was based on a value of $S_u/\sigma_v' = 0.19$, which in turn was based on correlations with the plasticity index for the kaolinite clay used in this soil bed. The same S_u/σ_v' ratio was reported by Jeanjean (2009) whose tests laterally loaded risers were also conducted in kaolinite clay.

The overconsolidation ratio was calculated based on the empirical equations shown in and $m = 0.67$ as reported by Jeanjean (2009):

$$\frac{(S_u/\sigma_v')_{OC}}{(S_u/\sigma_v')_{NC}} = OCR^m$$

$$OCR = \left[\frac{(S_u/\sigma_v')_{OC}}{(S_u/\sigma_v')_{NC}}\right]^{1/m}$$

$$m = 0.67 \rightarrow OCR = \left[\frac{(S_u/\sigma_v')_{OC}}{(S_u/\sigma_v')_{NC}}\right]^{1/0.67}$$

Results indicated that the soil bed had an overconsolidation ratio of about two. This soil bed was constructed in the early 2000s by sedimentation of soil slurry and since then it has undergone secondary consolidation resulting in an overconsolidation ratio of about two. We compared the original T-bar tests results from El-Sherbiny (2005) and the found that the undrained shear strength profile matched well with the theoretical value of $S_u/\sigma_v' = 0.19$. The T-bar test results from El-Sherbiny (2005) are shown in Figure 3.7.

A water content and unit weight versus depth profile of the soil bed was taken to check the shear strength values against correlations versus water content presented by El-Sherbiny (2005). The water contents and the unit weights (which were calculated assuming 100% saturation) are shown in Figure 3.8.

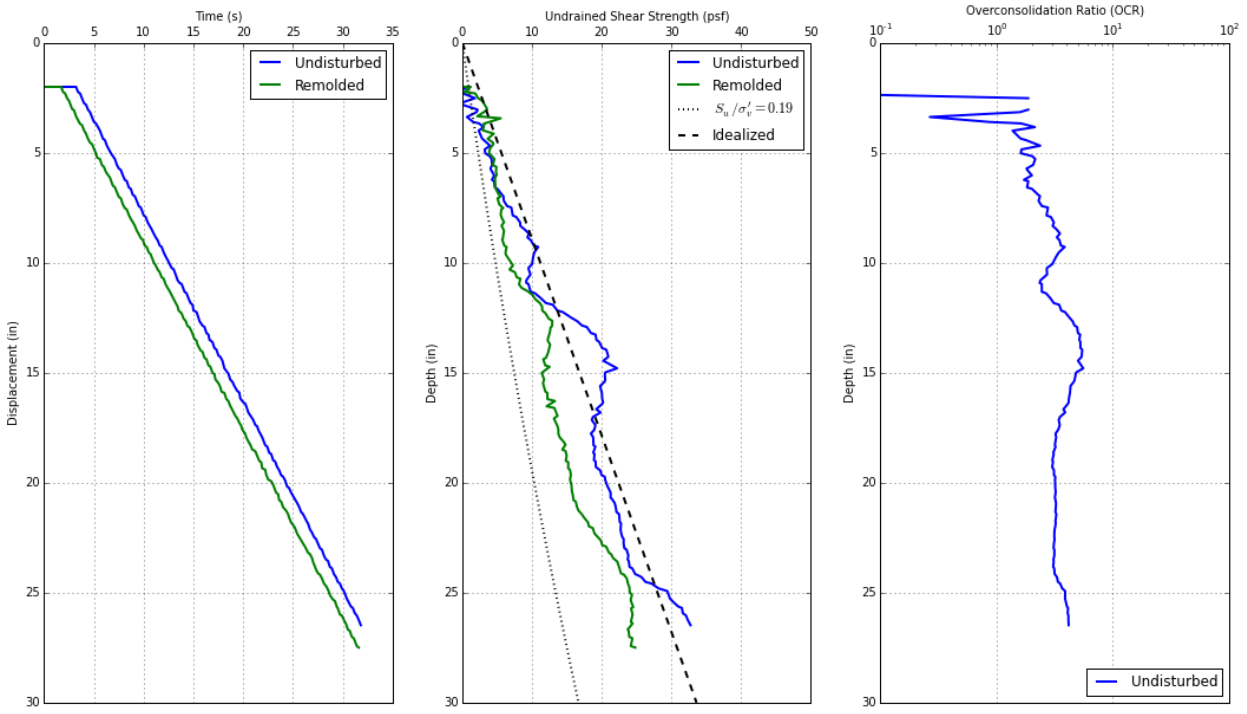

Figure 3.5: T-bar test results, normally to moderately overconsolidated kaolin clay bed, D=2-in pile location

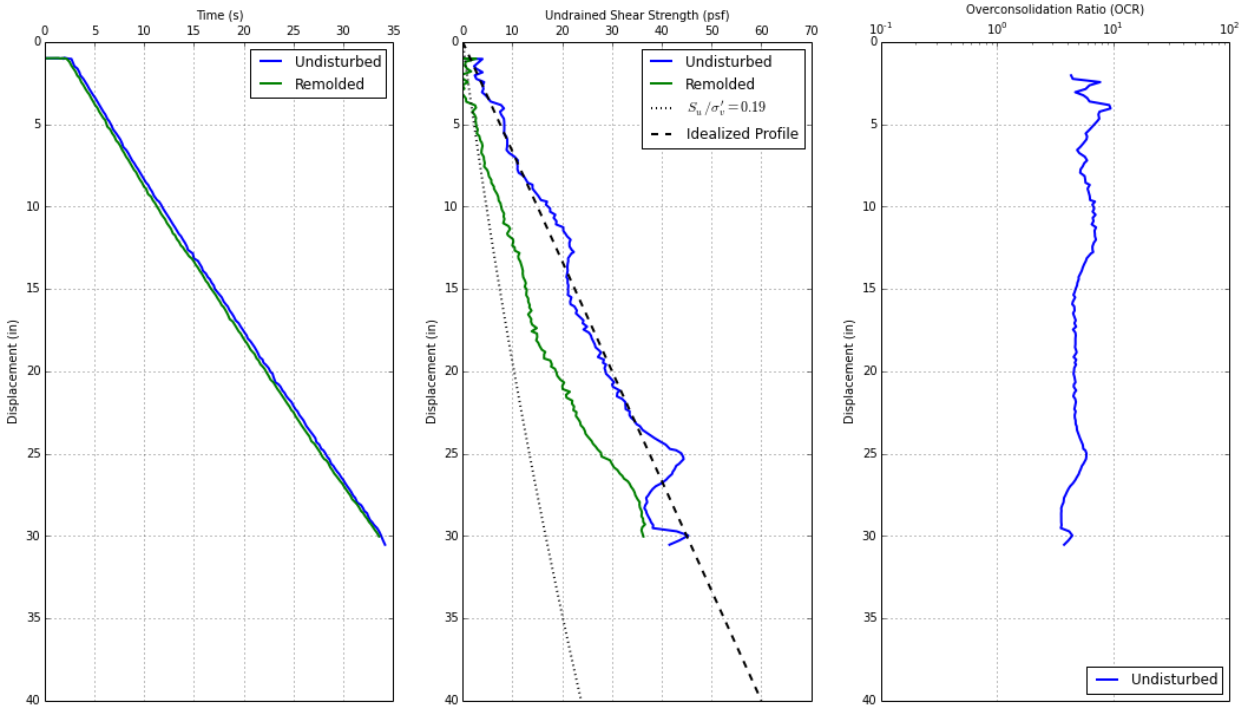

Figure 3.6: T-bar test results, normally to moderately overconsolidated kaolin clay bed, D=3-in and D=4-in pile locations

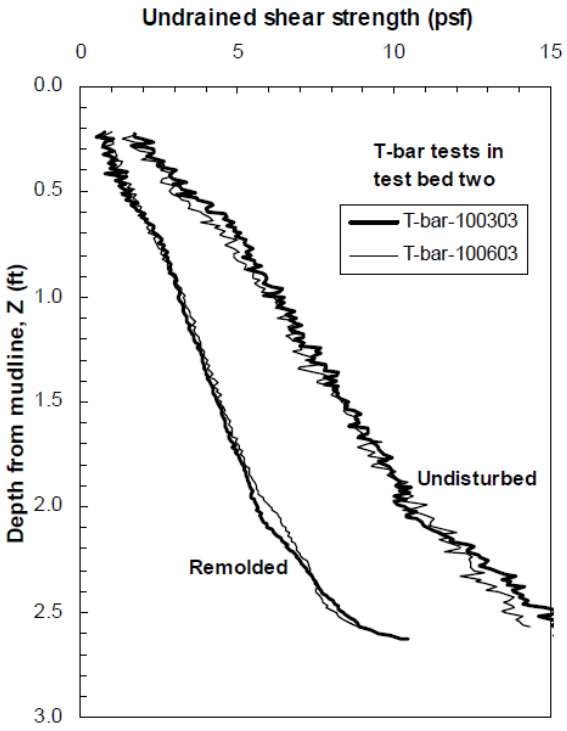

Figure 3.7: T-bar test results in normally consolidated soil bed from El-Sherbiny (2005)

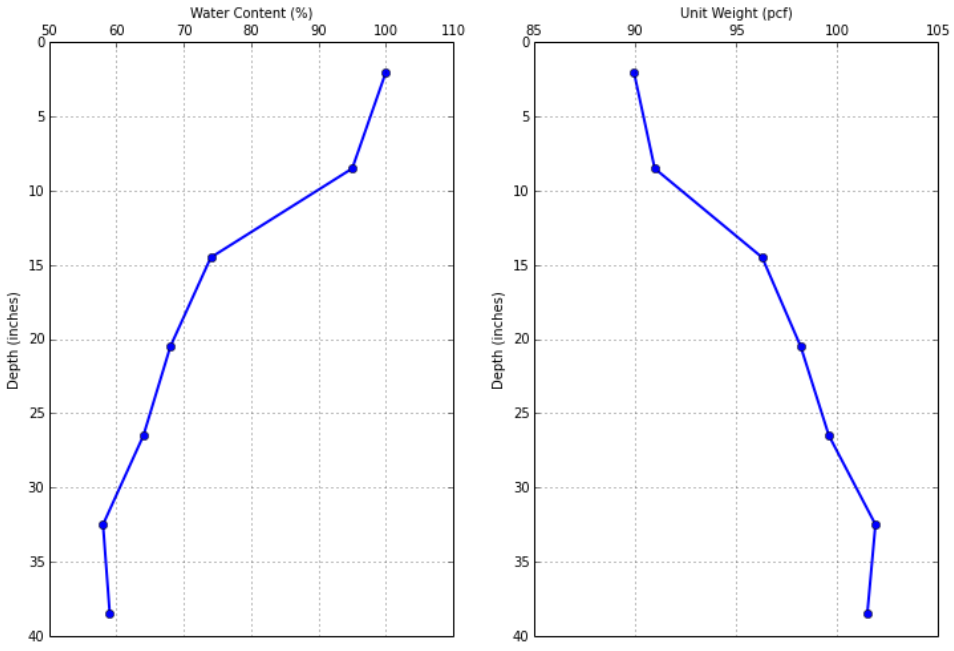

Figure 3.8: Variation of water content and unit weight with depth in the normally to moderately overconsolidated soil bed

3.3.2 Heavily Overconsolidated Kaolinite Clay Test Bed

The heavily overconsolidated kaolinite clay test bed had approximate overconsolidation ratios of ten at the surface and two at mid-depth. The undrained shear strength was constant versus depth. It was

prepared by mixing kaolinite clay with water so that the water content was constant with depth. This uniformity was achieved by thoroughly mixing the soil using an industrial paint mixer. The soil bed had a starting water content of approximately 100% and it was reduced by adding dry clay in order to increase the shear strength to accommodate pile testing.

The model piles were installed after 15-20 minutes of continuous mixing so that soil bed was uniform and the shear strength of the soil was close as possible to the remolded value. They were placed in the middle of the tank to minimize end effects as much as possible. A picture of the soil tank is shown in Figure 3.9 and the plan dimensions together with the area in which the piles were installed (rectangle with dashed line) is shown in Figure 3.10.

The water content and unit weight versus depth profiles in the soil bed is shown in Figure 3.11. T-bar tests in this soil test bed were carried out before the model piles were installed and the results are shown in Figure 3.12.

It was ensured that the water content in the soil did not change appreciably during the testing period in order to make sure the soil did not gain strength. The soil was mixed and T-bar tests were run on each day of testing in order to make sure the undrained shear strength profile was consistent for all tests.

All tests except one were done in the soil with an undrained shear strength of 10-psf as shown in Figure 3.12. (A repeat monotonic test on the 1-inch pile was done and S_u was 8-psf. This result is presented separately from the other tests on the 1-inch pile.)

Figure 3.9: 100-gallon Rubbermaid stock tank which contained the soil bed with the heavily overconsolidated kaolinite clay (1-inch diameter pile installed is also shown)

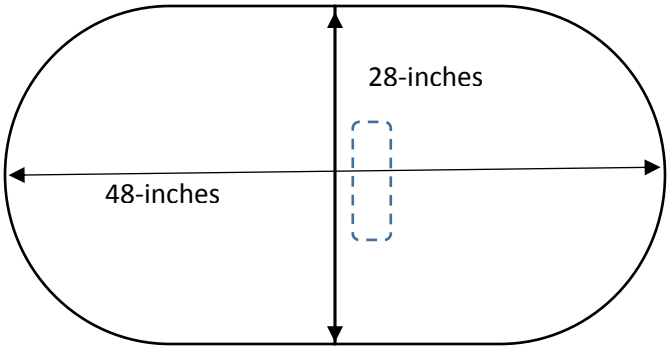

Figure 3.10: Plan dimensions of the tank containing the heavily overconsolidated kaolinite clay bed

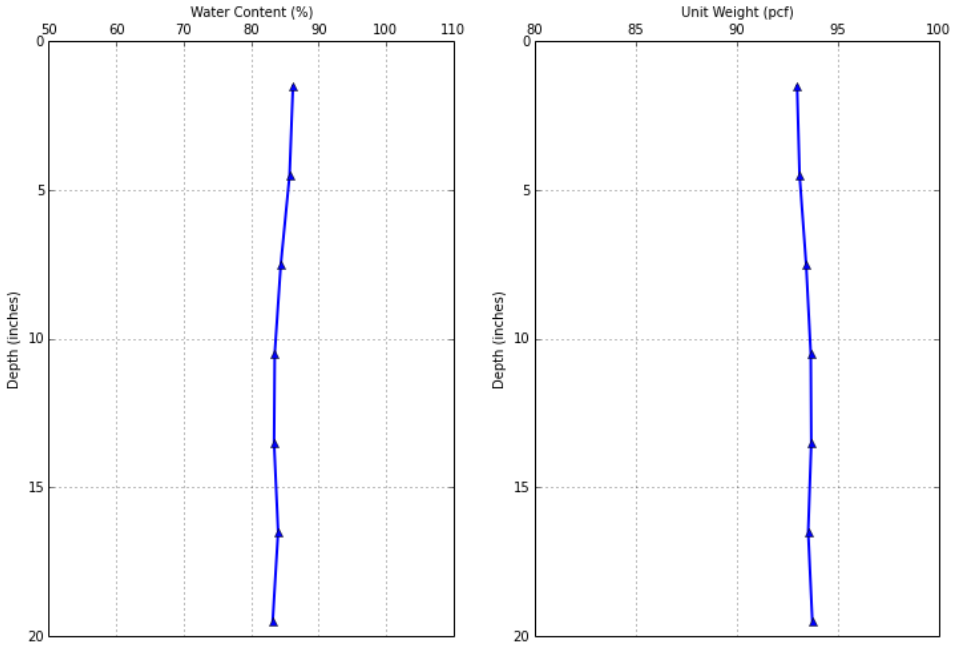

Figure 3.11: Variation of water content and unit weight with depth in the heavily overconsolidated kaolinite clay bed (S_u = 10-psf)

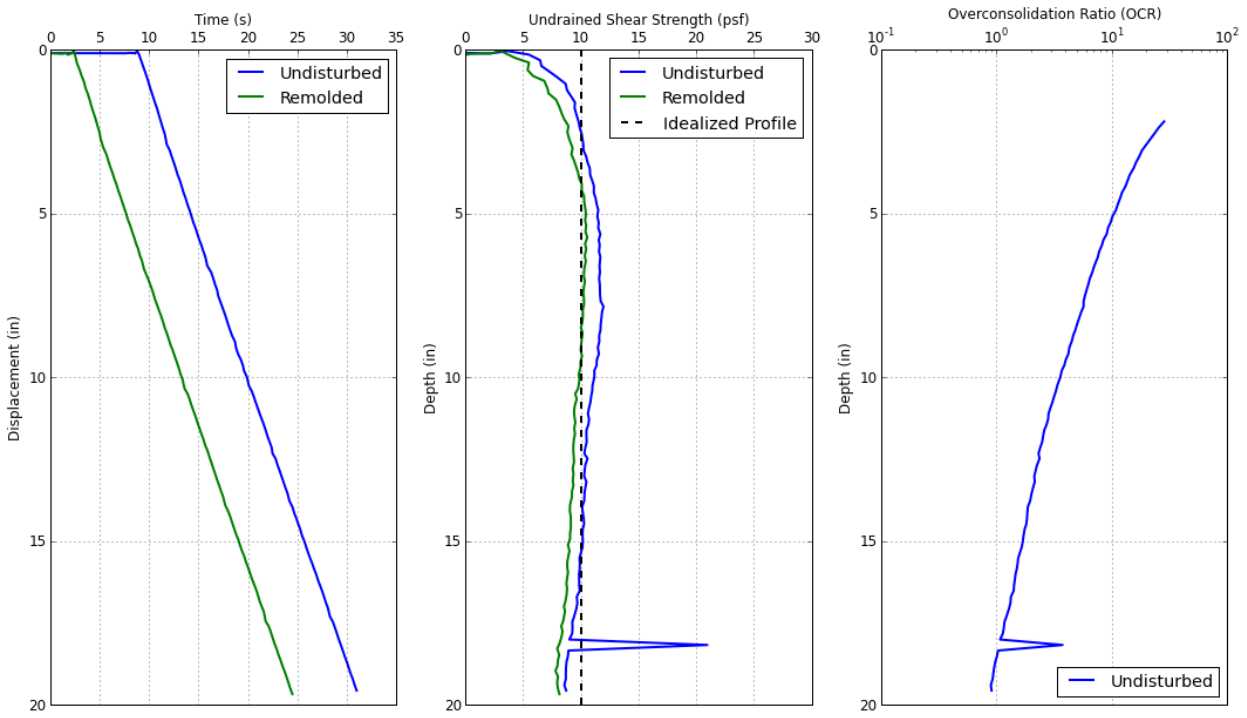

Figure 3.12: T-bar test results, heavily overconsolidated kaolinite bed (tested on August 4th 2014)

3.3.3 Heavily Overconsolidated Kaolinite Clay Bed with a Stiff Crust

The heavily overconsolidated kaolinite clay bed with a stiff crust was prepared by mixing kaolin clay with water so that the water content was constant with depth. After a uniform mix was obtained, a 2-inch thick layer of clay with a lower water content was added on top to create a stiff crust. This soil bed had approximate overconsolidation ratios of 100 at the surface and ten at mid-depth. The undrained shear strength in the clay underlying the stiff crust was approximately constant versus depth. The stiff top crust had an undisturbed undrained shear strength of about 1.25 times that of the underlying layer. A picture of this test bed, with a 2-in diameter pile installed, is shown in Figure 3.13.

Figure 3.13: Heavily overconsolidated kaolinite clay bed with a stiff crust with 2-inch diameter pile installed and ready to be tested

Figure 3.14 and Figure 3.15 show the S_u versus depth profiles as measured using T-bar tests. The undisturbed S_u profile was obtained from the first T-bar push and the remolded profile was obtained from the third push at the same location. The overconsolidation ratio was back-calculated based on a $\frac{S_u}{\sigma_v'}$ value of 0.19 and it is only applicable to the undisturbed S_u profile. The idealized S_u is shown here since it was the input for the LPILE analyses on piles tested in this clay bed.

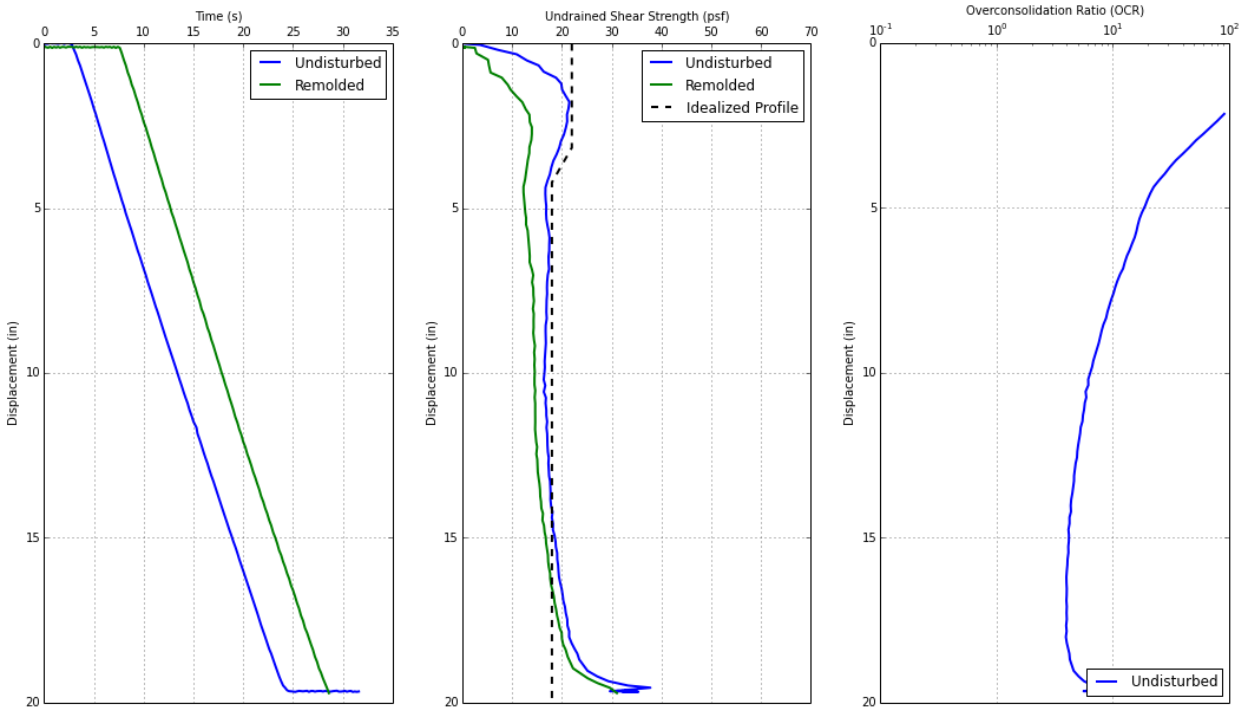

Figure 3.14: T-bar test results, heavily overconsolidated kaolinite clayl bed with stiff crust, approximately 30-minutes of setup time (tested on December 08th 2014)

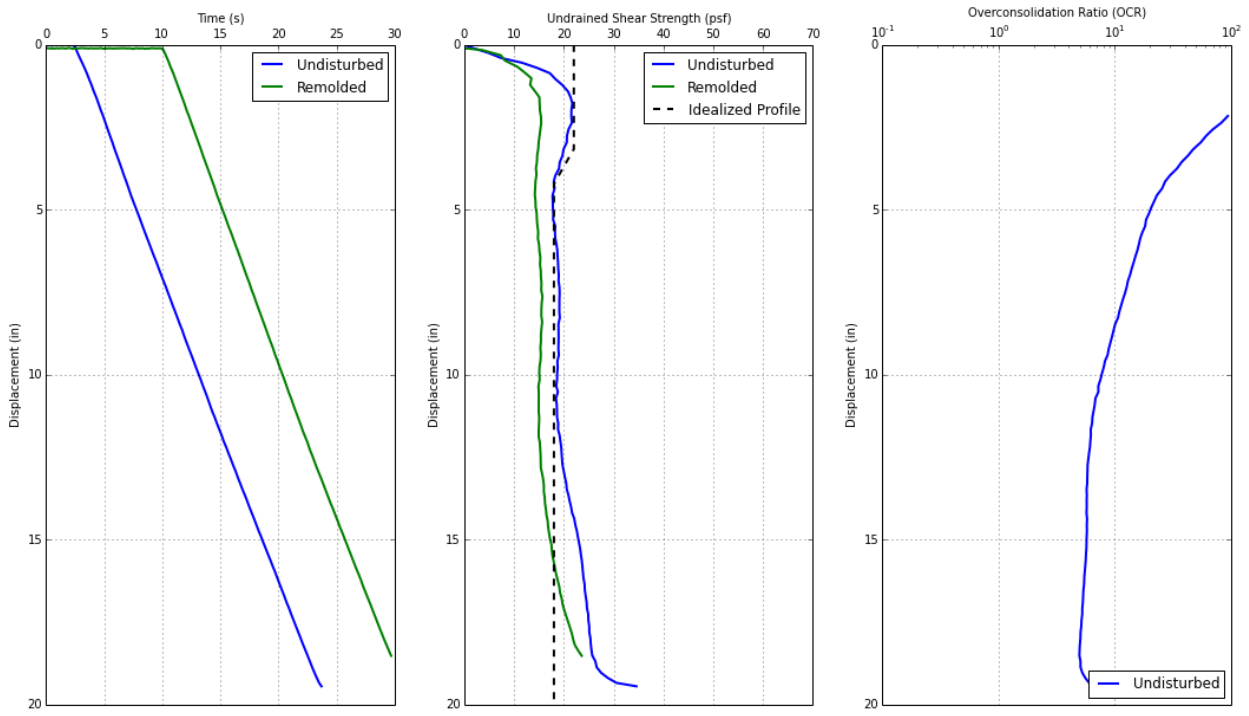

Figure 3.15: T-bar test results, heavily overconsolidated kaolinite clay bed with stiff crust, approximately 4-days of setup time (tested on December 12th 2014)

The model piles were installed almost immediately after the soil bed was prepared. The piles were placed in the middle of the tank to minimize end effects as much as possible. The area in which the piles were installed (rectangle with dashed line) in the soil tank is shown in Figure 3.16.

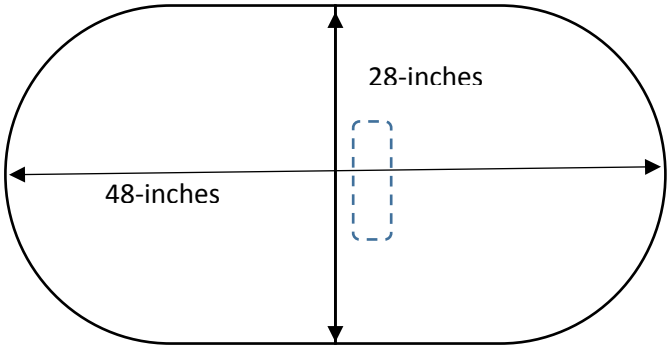

Figure 3.16: Plan dimensions of the tank containing heavily overconsolidated kaolinite clay bed with stiff crust

3.3.4 Heavily Overconsolidated Gulf of Mexico Clay Bed

The soil for heavily overconsolidated Gulf of Mexico clay test bed was a composite of deep water marine clay samples from a variety of locations, providing a generic profile that is representative of marine clays in the Gulf of Mexico.

The clay was in the form of Shelby tube samples before it was remolded and formed into a uniform test bed. These samples were first immersed in water with a salinity of 35 g/l for a few days and then

transferred to the soil tank. The soil was then thoroughly mixed using an industrial paint mixer until a uniform test bed was created. A picture of this test bed, with a 2-in diameter pile installed in it, is shown in Figure 3.17.

Figure 3.17: Heavily overconsolidated Gulf of Mexico clay bed with a 2-inch diameter pile installed and ready to be tested

Figure 3.18, Figure 3.19, and Figure 3.20 show the S_u versus depth profiles corresponding to 30-minutes, 48-hours, and 4-weeks respectively. These results are shown separately because each S_u profile is applicable to a different pile load test in this test bed. The overconsolidation ratios were back-calculated based on a $\frac{S_u}{\sigma_v'}$ value of 0.25 and is only applicable to the undisturbed S_u profiles. The idealized S_u profile is also shown here since it was the input for the LPILE models on piles tested in this clay bed.

The S_u profile was approximately constant versus depth with a value of about 30-psf and a soil sensitivity of about 1.2 after 30-minutes of setup time. After 48-hours, the average S_u had increased to about 33-psf and the sensitivity had increased to about 1.3. After 4-weeks of setup time, the S_u profile had a gradient of about 14psf/ft instead of being constant with depth. The sensitivity near the mudline had not changed (eg: 1.3 at a depth of 5-inches) but it had increased with depth and was about 1.4 at a depth of 17 inches.

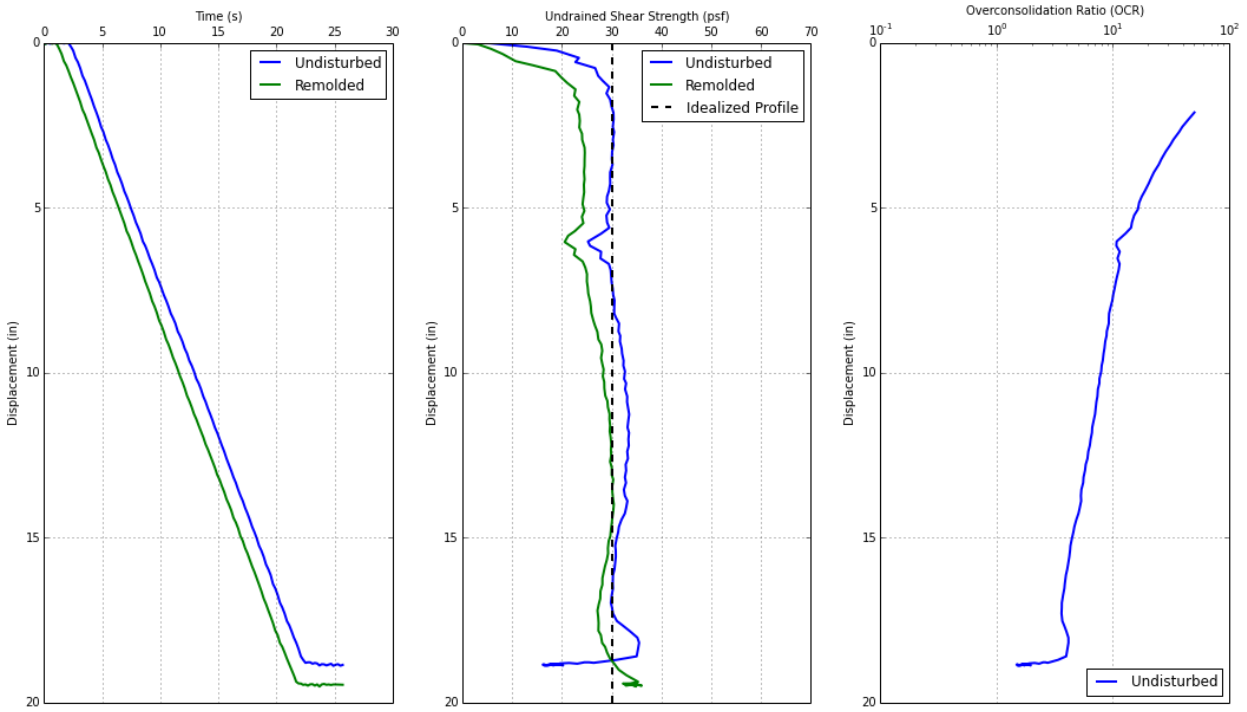

Figure 3.18: T-bar test results, overconsolidated Gulf of Mexico clay bed, approximately 30-minutes of setup time (tested on December 16th 2014)

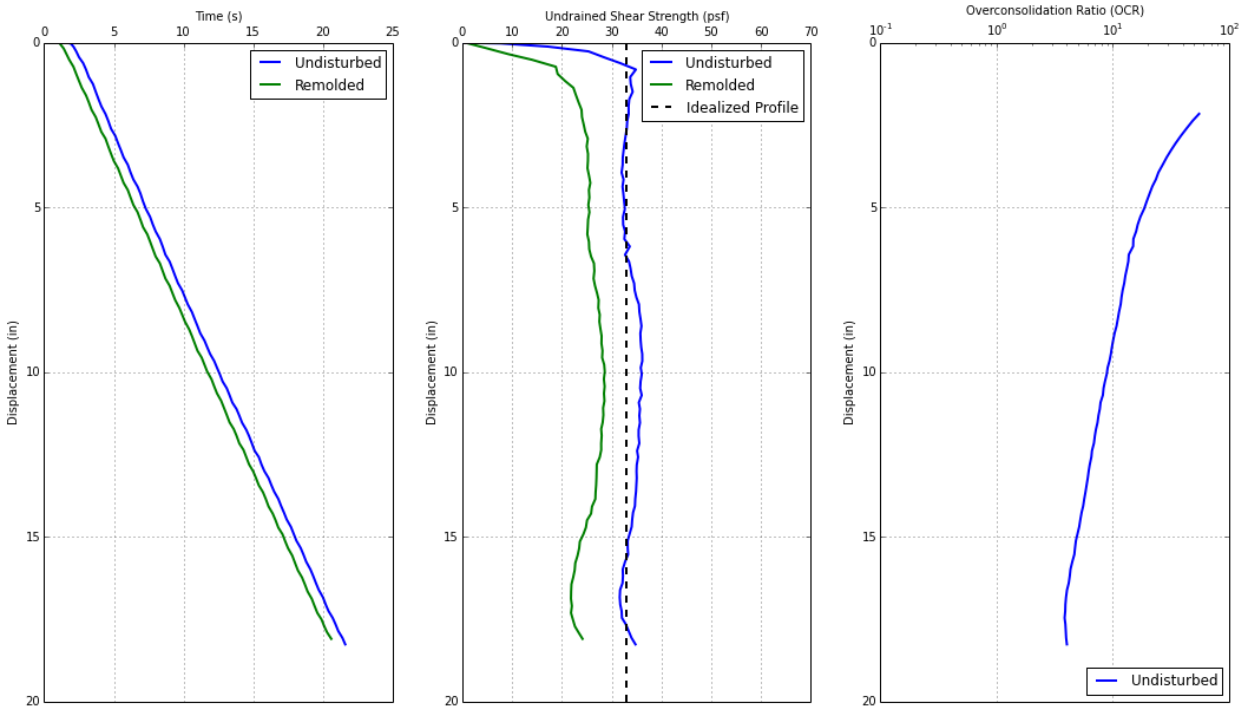

Figure 3.19: T-bar test results, overconsolidated Gulf of Mexico clay bed, approximately 48-hours of setup time (tested on December 18th 2014)

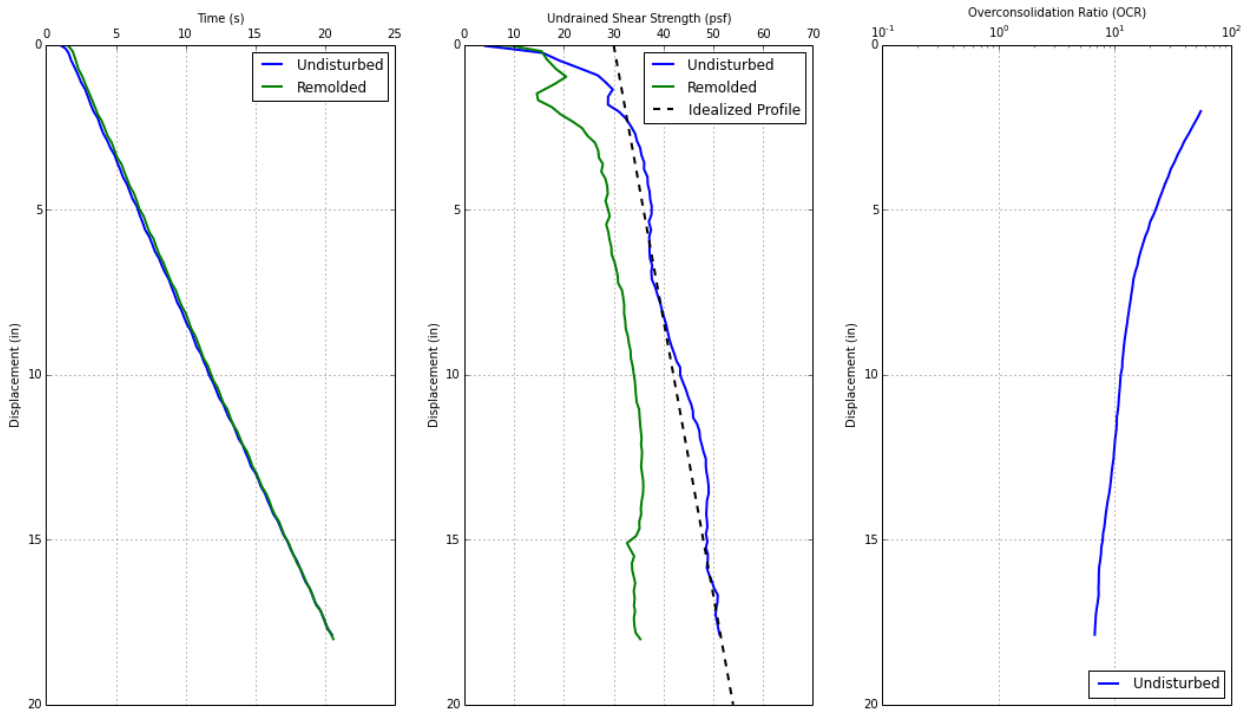

Figure 3.20: T-bar test results, overconsolidated Gulf of Mexico clay bed, approximately 4-weeks of setup time (test results from January 13th 2014)

3.3.5 Normally consolidated Gulf of Mexico Clay Bed

The normally consolidated Gulf of Mexico clay test bed consisted of a composite of deep water marine clay samples from a variety of locations, which provided a generic profile that is representative of marine clays in the Gulf of Mexico. It was prepared in several stages over a period of two months.

The clay was originally in the form of Shelby tube samples before it was remolded and formed into a uniform test bed. These samples were first immersed in water with a salinity of 35 g/l for up to a week to soften them and then transferred to a mixing barrel. The soil was then thoroughly mixed in batches of 20 – 30 gallons using an industrial paint mixer until a uniform mixture was created. The preparation of each batch took approximately a week.

A normally consolidated clay bed is ideally prepared through the process of sedimentation of a soil slurry. However, this process can take many months or even years before the test bed has completely consolidated; therefore we chose an expedited method in which soil samples of different shear strengths were prepared by controlling the water content and then constructing the test bed in lifts that were four to six inches thick. Since we used undrained shear strength (S_u) as the primary variable in this procedure, we defined "normally consolidated GoM clay" as one having an undisturbed undrained shear strength versus depth profile of 7.5-psf/ft (Figure 3.21). More details about this method and undrained shear strength profiles in the Gulf of Mexico are provided in Lee (2008) and Cheon (2010) respectively.

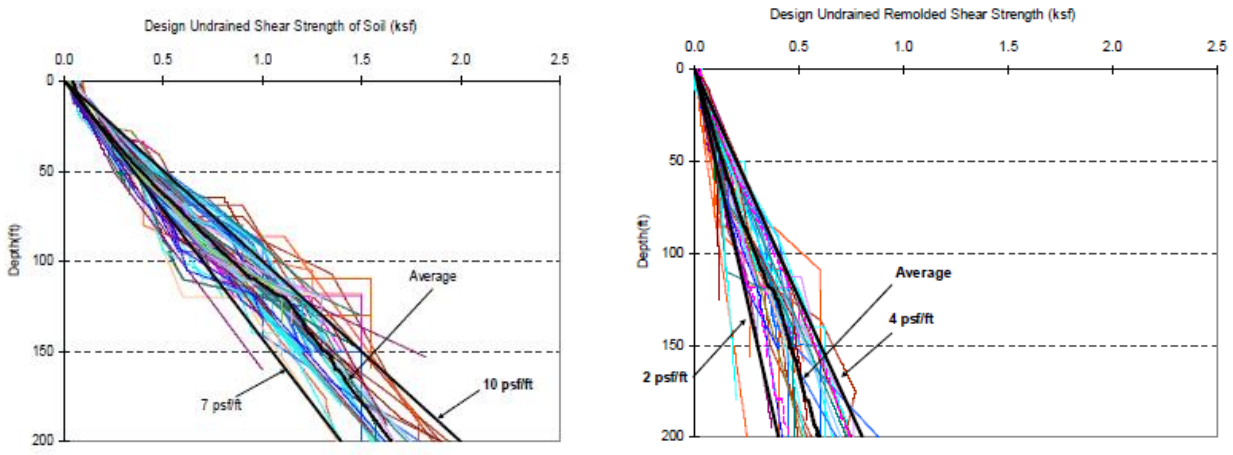

Figure 3.21: Design undrained shear strength versus depth in the Gulf of Mexico (Cheon, 2010)

The first step in this procedure was to obtain a relationship between undrained shear strength and water content for the GoM clay that was being used. T-bar penetration tests on remolded soil mixes with varying water contents provided an empirical relationship of $S_u = 376e^{-3.25w}$ for the undrained shear strength and the water content as shown in Figure 3.22. This empirical relationship was then used to construct a test bed with a remolded S_u versus depth profile of approximately 2.5-psf/ft and allowed to consolidate and setup for two weeks. The finished test bed is shown in Figure 3.9.

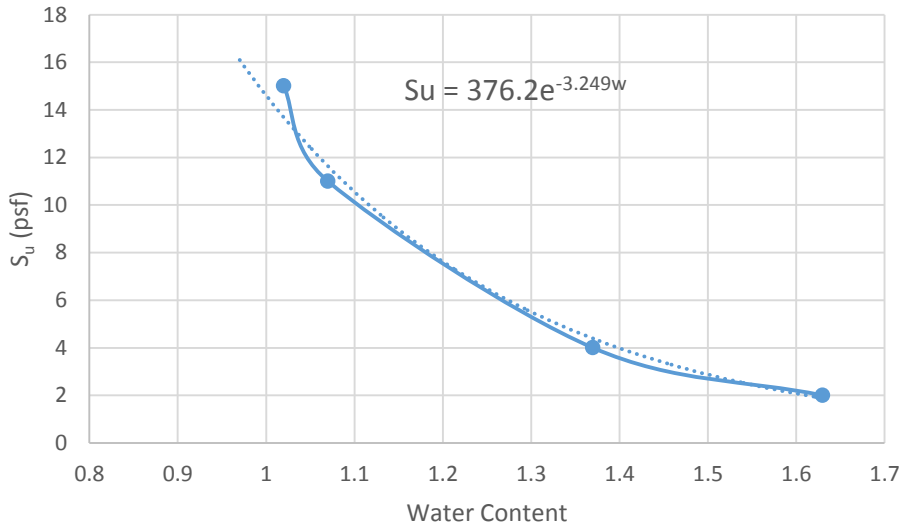

Figure 3.22: Variation of the undrained shear strength

Figure 3.23: Normally consolidated GoM clay bed with 1-inch diameter pile installed and ready to be tested

Figure 3.24 shows the result from a T-bar penetration test done 10-days after the test bed was prepared. The measured S_u versus depth profile is close to the target of 7.5-psf/ft.

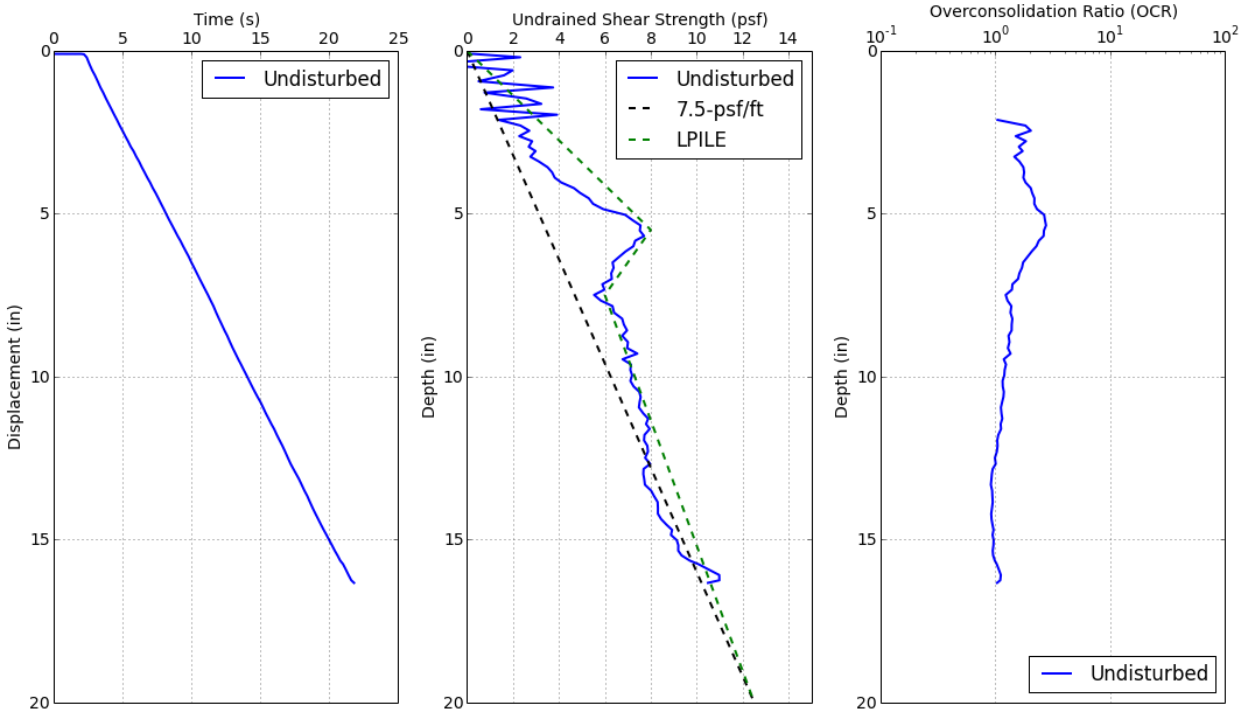

Figure 3.24: T-bar test results, normally consolidated GoM clay test bed, 10-days after preparation (tested on April 10th 2015)

The piles were placed in the middle of the tank to minimize end effects. The piles were installed in the soil tank is shown in Figure 3.10 (rectangle with dashed line), one week after the soil bed was prepared.

One and three days of setup time was allowed for the 1-inch and 2-inch piles respectively based on the solution to the problem of radial consolidation by Soderberg (1962) as cited in Stevens et al. (2015).

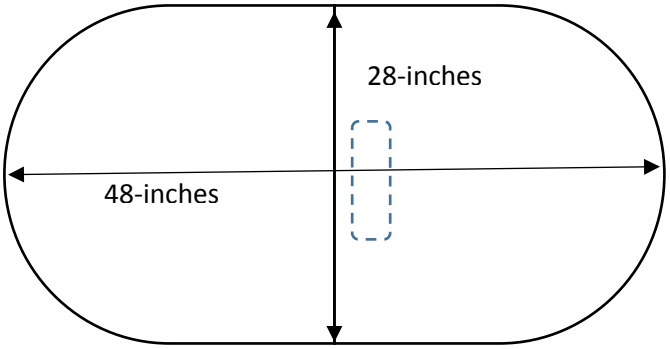

Figure 3.25: Plan dimensions of the tank containing normally consolidated GoM clay bed

3.4 TESTS IN NORMALLY CONSOLIDATED TO MODERATELY OVERCONSOLIDATED KAOLINITE CLAY

3.4.1 Monotonic/Static Lateral Load Tests

Selected results from tests on 2-inch, 3-inch and 4-inch piles are shown in Figure 3.26, Figure 3.27 and Figure 3.28 respectively. Three tests on the 3-inch pile at different loading rates are shown in Figure 3.27. All three load-displacement curves are very similar, indicating that the effect of the rate of displacement on the load-displacement behavior of the pile was not significant over this range of loading rates.

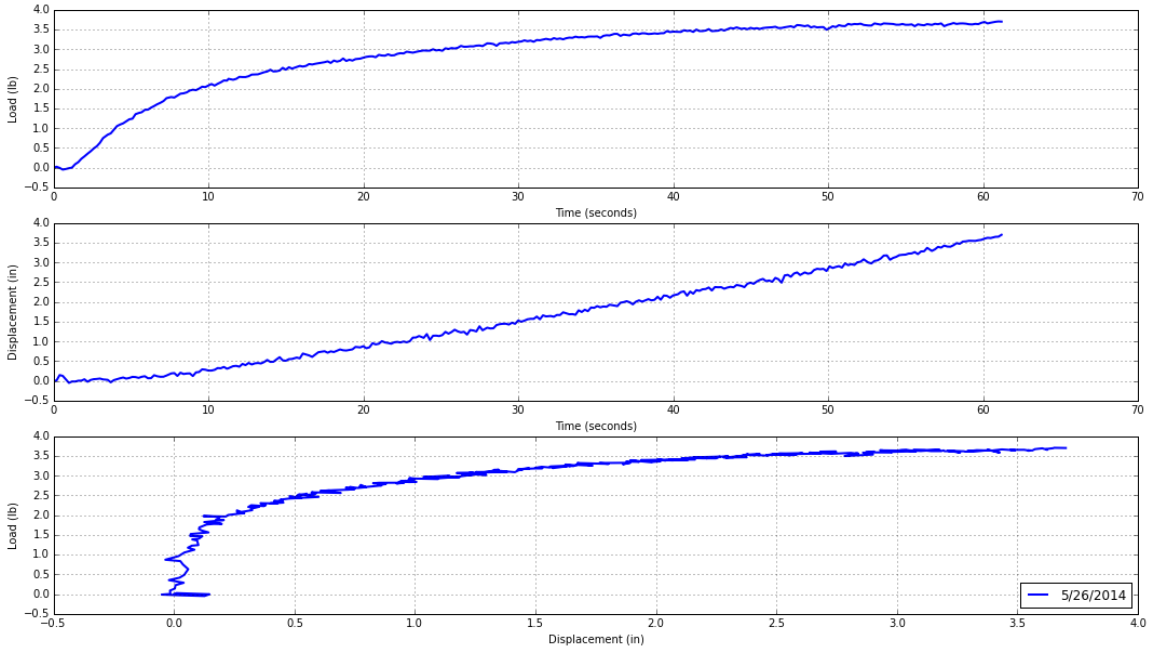

Figure 3.26: Monotonic load test: diameter=2-inches, embedment = 8D, load eccentricity = 5D, target lateral displacement = D

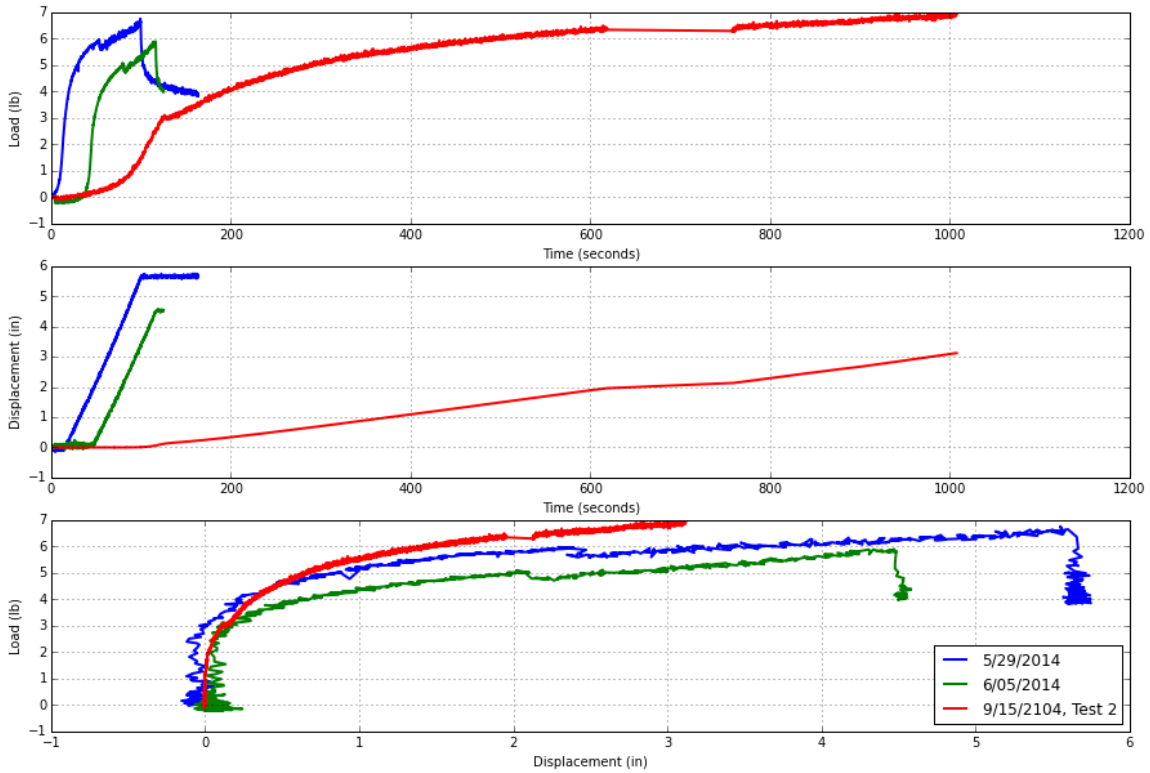

Figure 3.27: Monotonic load test: diameter=3-inches, embedment = 8D, load eccentricity = 5D, target lateral displacement = D

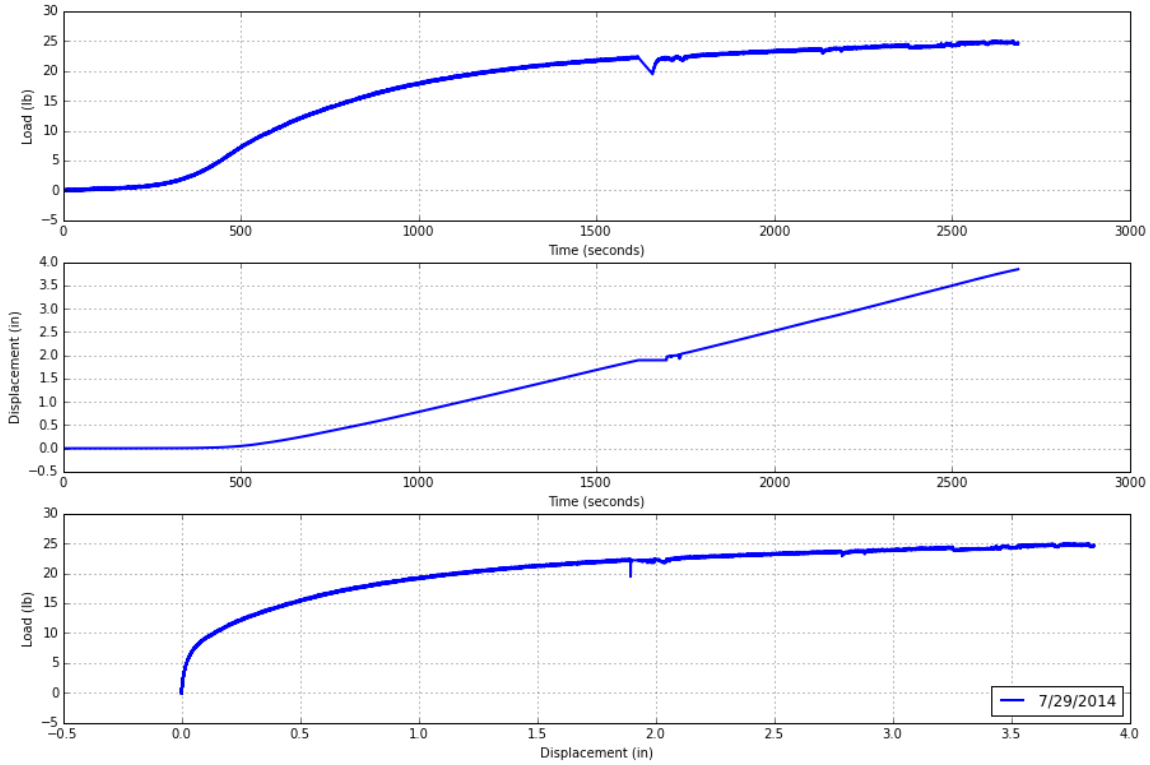

Figure 3.28: Monotonic load test: diameter=4-inches, embedment = 8D, load eccentricity = 5D, target lateral displacement = D

Several static tests were conducted with a tactile pressure sensor wrapped around the 4-in diameter model pile were carried out in the normally consolidated to moderately overconsolidated kaolinite clay bed. The objective of these tests was to measure the lateral soil resistance directly. The sensor was 12.6-in by 32-in in area and approximately 1/8-in thick. Figure 3.29 (a) and (b) show pictures of the 4-in pile with the pressure sensor installed. Two monotonic (displacement controlled) tests and five static (load controlled) tests were performed on the 4-inch diameter pile while it was instrumented with a tactile pressure sensor. The sensor readings were not usable in the first six tests (conducted in the fall of 2014) due to problems with calibrating the sensor when it was wrapped around the pile and over the range of pressures applied by the soil. We subsequently calibrated the sensor wrapped around the pile in a deep swimming pool and were able to obtain usable pressure readings in the final test conducted in the summer of 2015.

For the tests in which the pressure sensor readings are not usable, the measurements of load and displacement at the pile head were usable and are included here (Figure 3.30 and Figure 3.31). The pile tested on 10/28/2014 (Figure 3.30) was installed on 10/23/2014. It was preceded by a cyclic test that was aborted after 15-cycles due to a malfunction in the test system. This sequence is highlighted because it gives some insight in to how cyclic loading preceding a monotonic or static load test affects the pile response (see section 5.3.2). The pile tested on 11/18/2014 (Figure 3.30) was installed on the same day and had an hour of setup time before loading. The first three static tests (Figure 3.31) were performed immediately after the pile was installed, while the fourth test performed on 12/12/2014 (Figure 3.31) was conducted after 20-cycles of one-way displacement was applied to the pile in order to investigate the effect of cyclic loading on the subsequent ultimate capacity of the pile (see section 5.3.2).

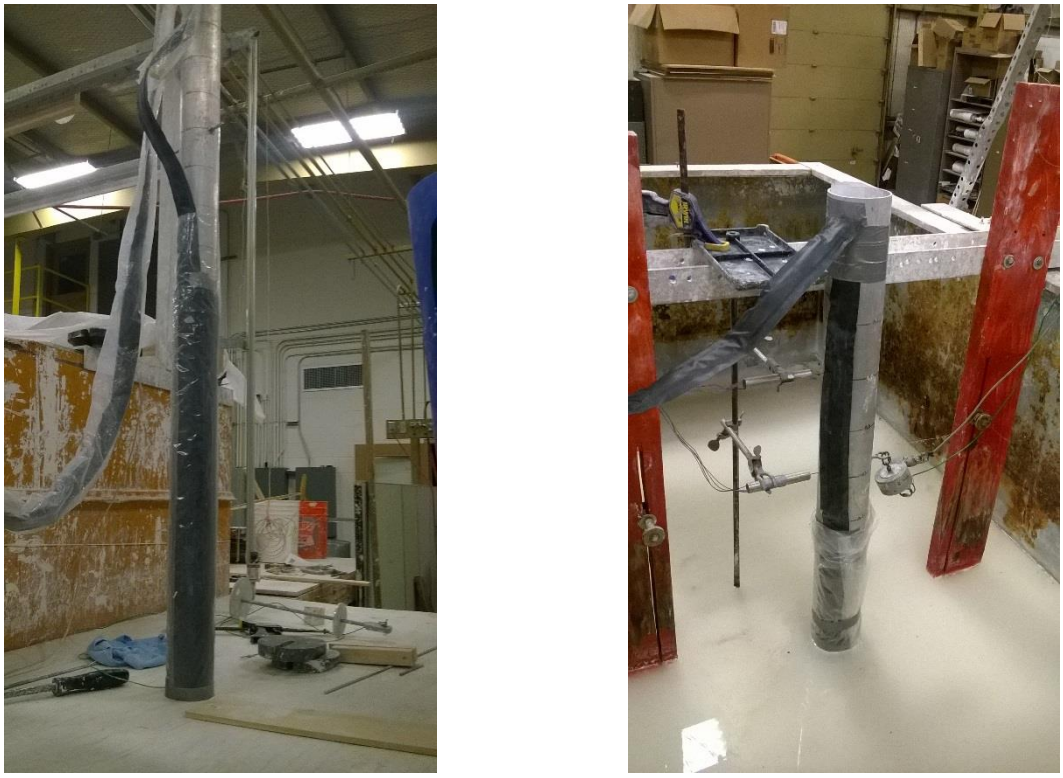

(a) (b)

Figure 3.29: 4-in diameter model pile with tactile pressure sensor installed

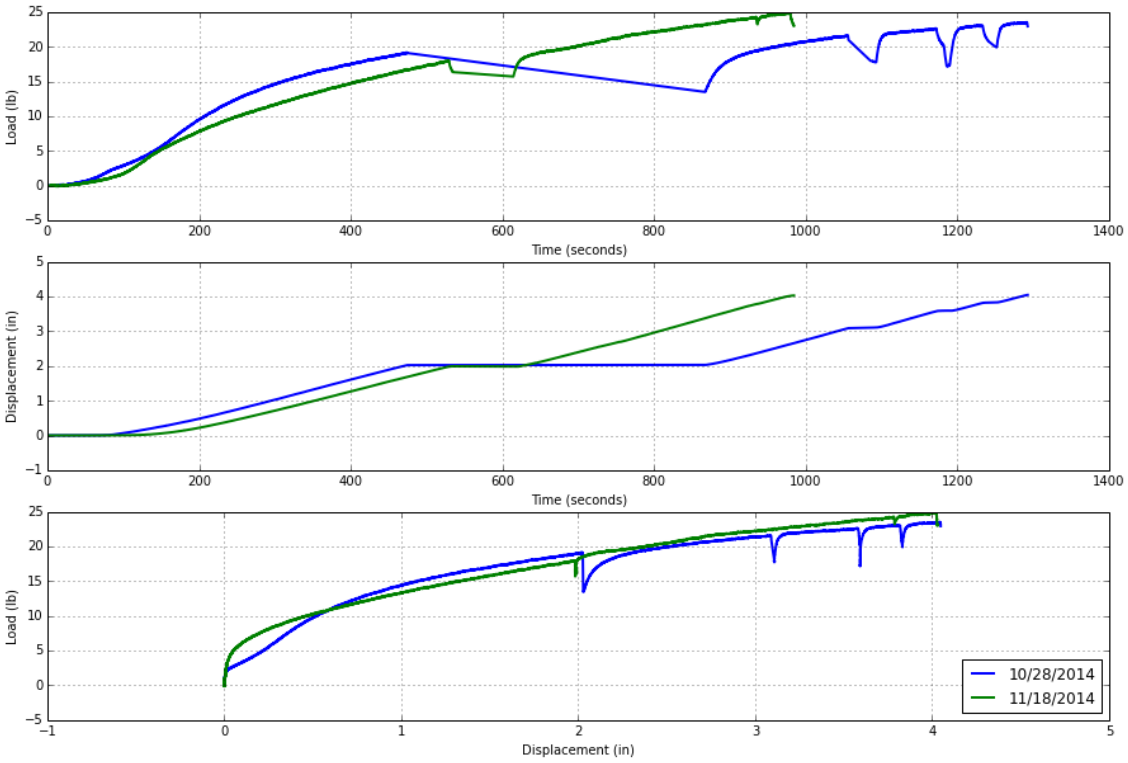

Figure 3.30: Monotonic load tests, D=4-inches, embedment = 8D, load eccentricity = 5D, target lateral displacement = D, normally to moderately overconsolidated kaolin clay

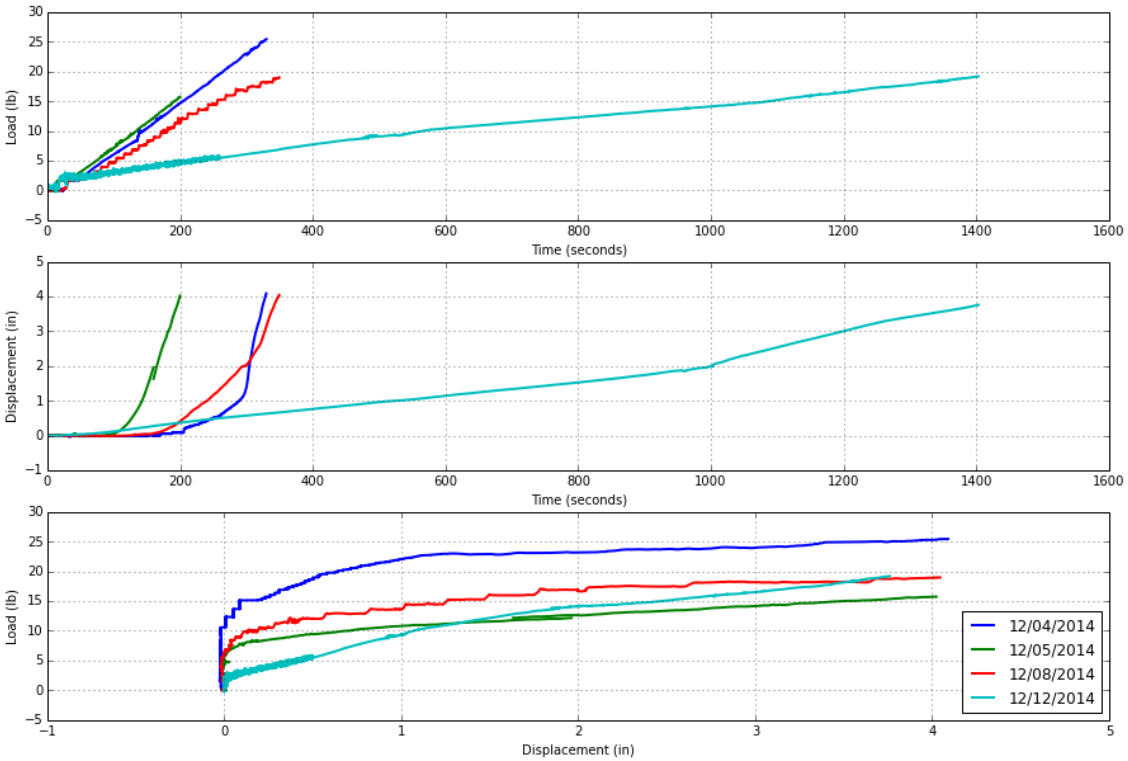

Figure 3.31: Static load tests, D=4-inches, embedment = 8D, load eccentricity = 5D, target lateral displacement = D, normally to moderately overconsolidated kaolin clay

The load versus displacement results for the static load test with the usable (properly calibrated) pressure sensor measurements are shown in (Figure 3.32). The pressure sensor readings are provided and discussed in section **Error! Reference source not found.**.

Figure 3.32: Static load test with pressure sensor, D=4-inches, embedment = 8D, load eccentricity = 5D, target lateral displacement = 1-in, normally to moderately overconsolidated kaolin clay

3.4.2 Cyclic Lateral Load Tests

Cyclic tests were conducted by imposing constant a target tilt of 'α' degrees for 1,000 cycles of one-way loading (α degrees to the imposed tilt and back to 0 degrees constitutes one cycle). The period of loading is similar to wave loading, 10 seconds. The tilt angle 'α' had values of 0.5°, 1.0°, and 2.0°.

Cyclic load test results are shown in Figure 3.33 to Figure 3.41 for each pile diameter. These data are plotted in several ways: load versus time, displacement versus time and load versus displacement. Also, photos of the soil around the pile at the mudline are provided in Figure 3.42 to Figure 3.44.

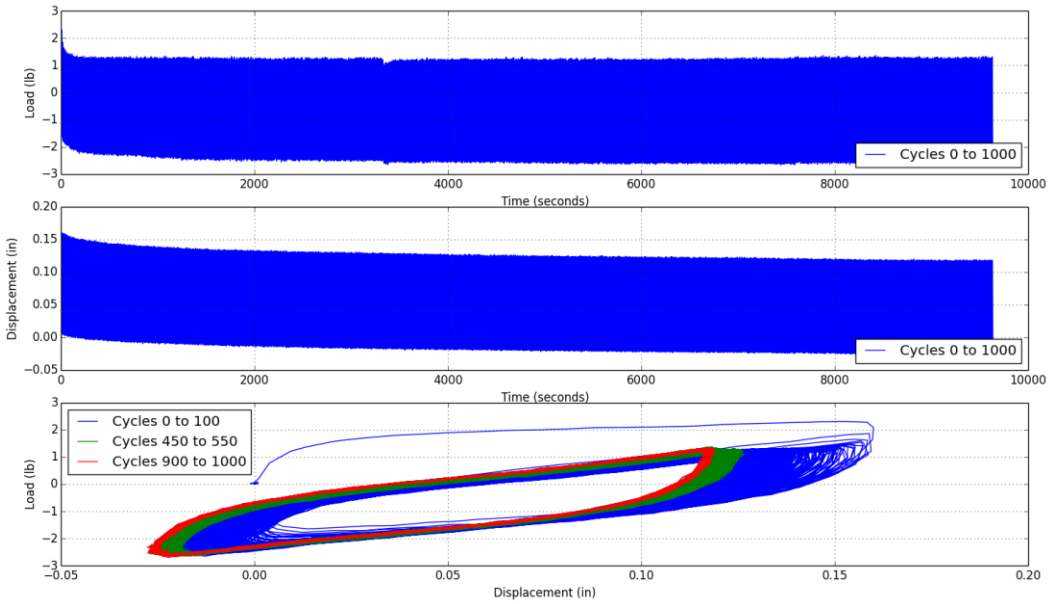

Figure 3.33: Cyclic Load Test Results: Diameter=2", Embedment = 8D, Load Eccentricity = 5D, Target Tilt Angle = 0.5°

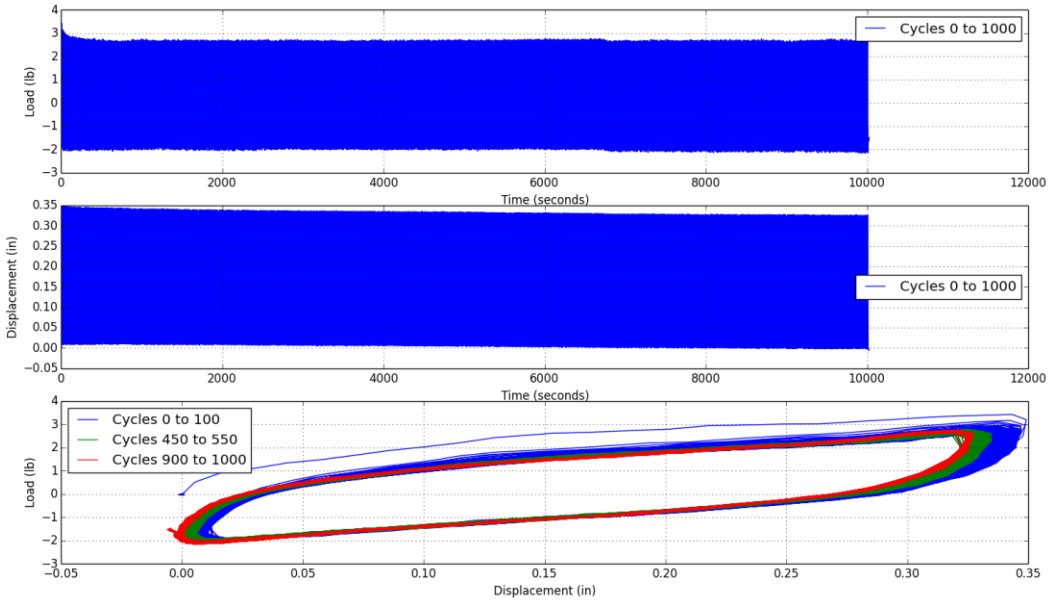

Figure 3.34: Cyclic Load Test Results: Diameter=2", Embedment = 8D, Load Eccentricity = 5D, Target Tilt Angle = 1.0°

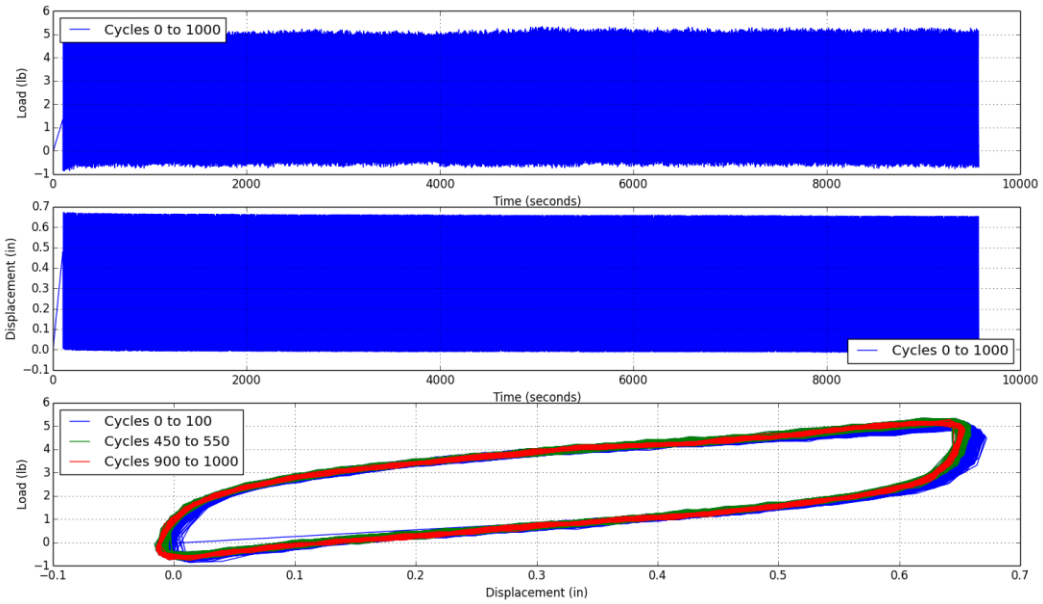

Figure 3.35: Cyclic Load Test Results: Diameter=2", Embedment = 8D, Load Eccentricity = 5D, Target Tilt Angle = 2.0°

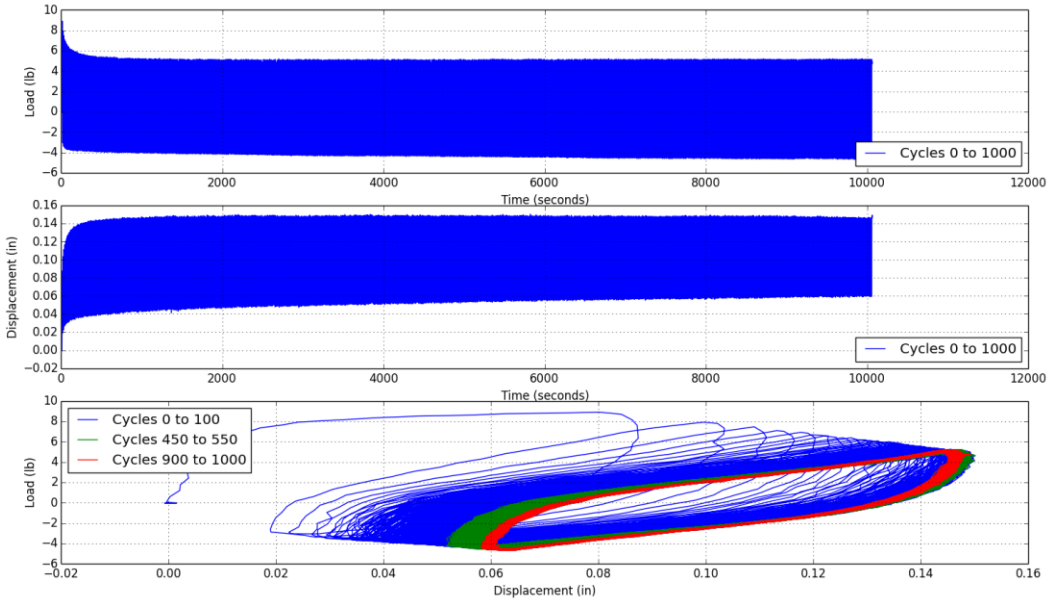

Figure 3.36: Cyclic Load Test Results: Diameter=3", Embedment = 8D, Load Eccentricity = 5D, Target Tilt Angle = 0.5°

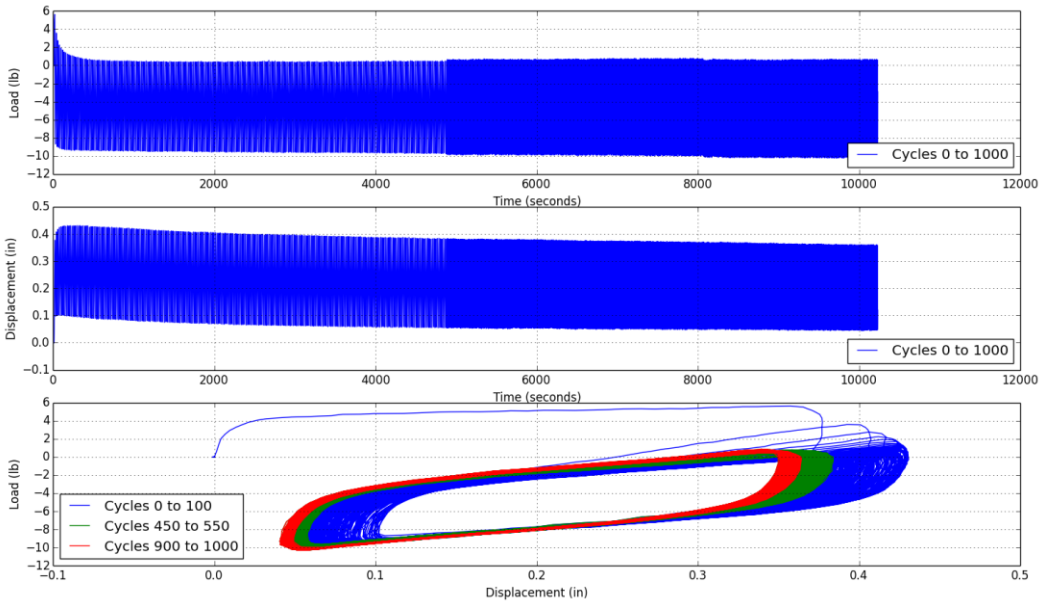

Figure 3.37: Cyclic Load Test Results: Diameter=3", Embedment = 8D, Load Eccentricity = 5D, Target Tilt Angle = 1.0°

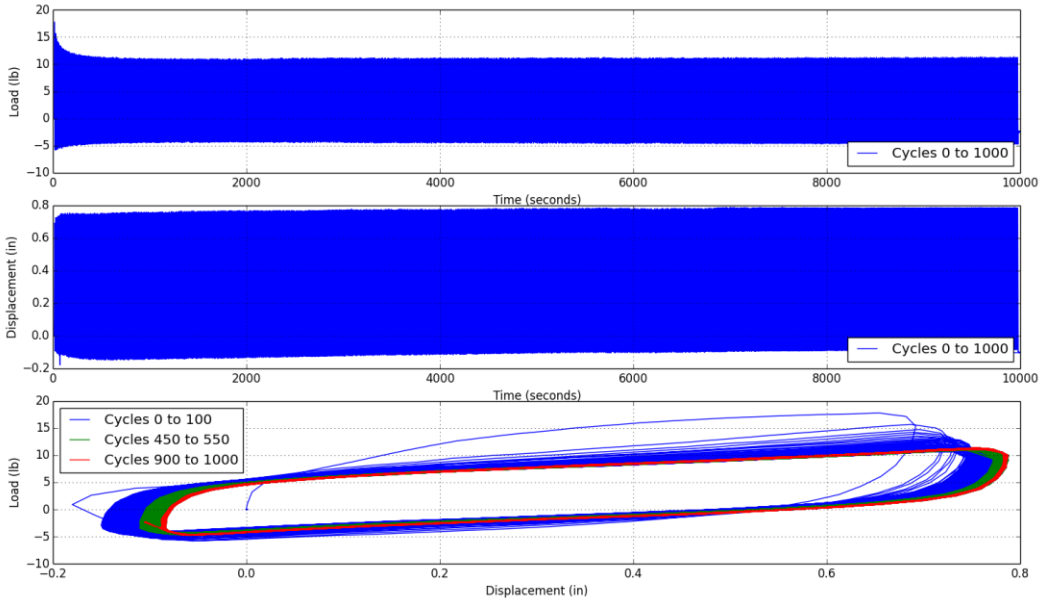

Figure 3.38: Cyclic Load Test Results: Diameter=3", Embedment = 8D, Load Eccentricity = 5D, Target Tilt Angle = 2.0°

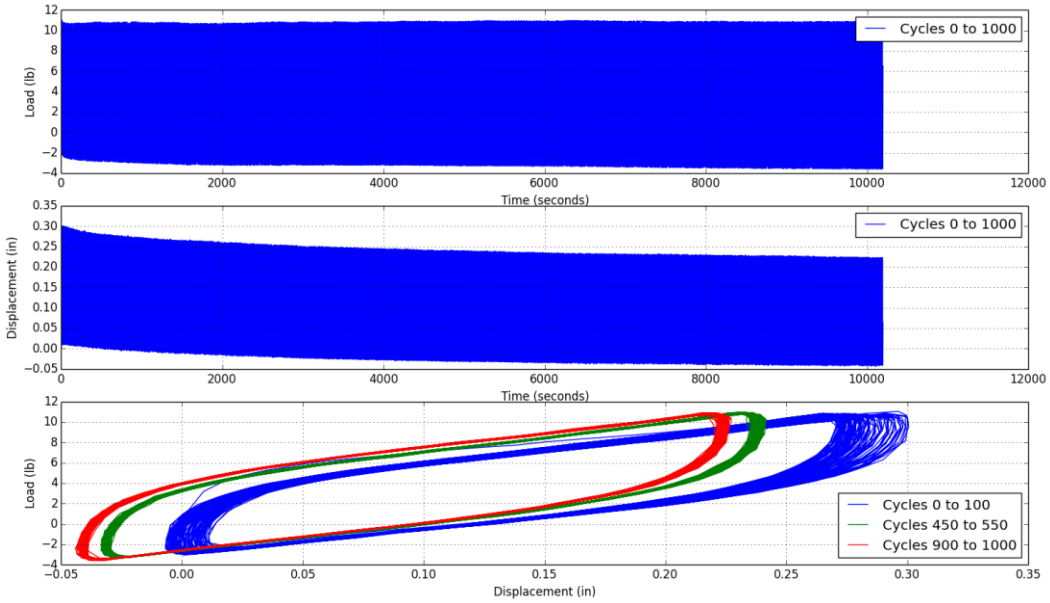

Figure 3.39: Cyclic Load Test Results: Diameter=4", Embedment = 8D, Load Eccentricity = 5D, Target Tilt Angle = 0.5°

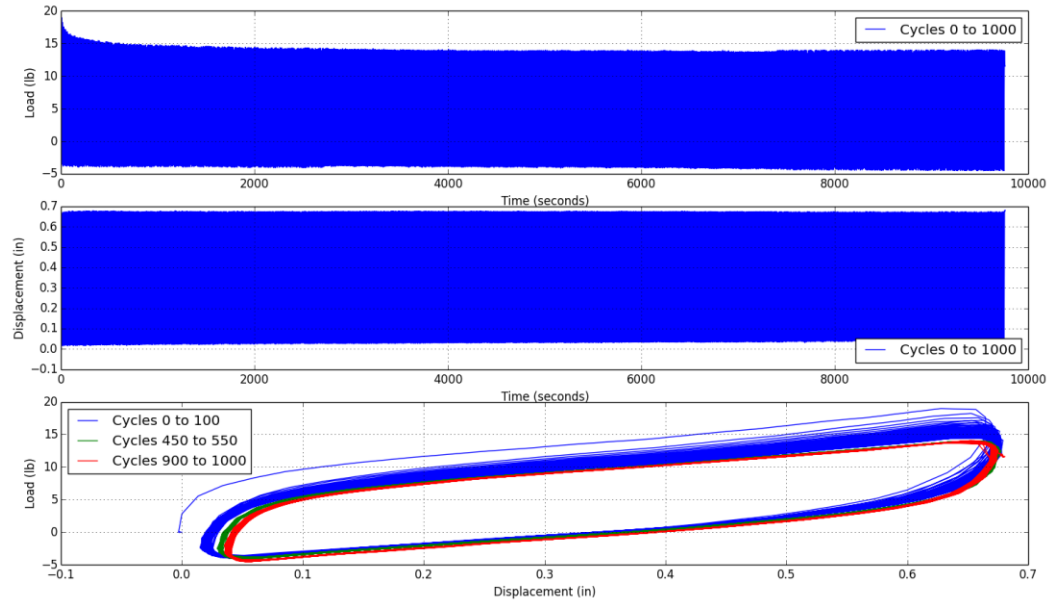

Figure 3.40: Cyclic Load Test Results: Diameter=4", Embedment = 8D, Load Eccentricity = 5D, Target Tilt Angle = 1.0°

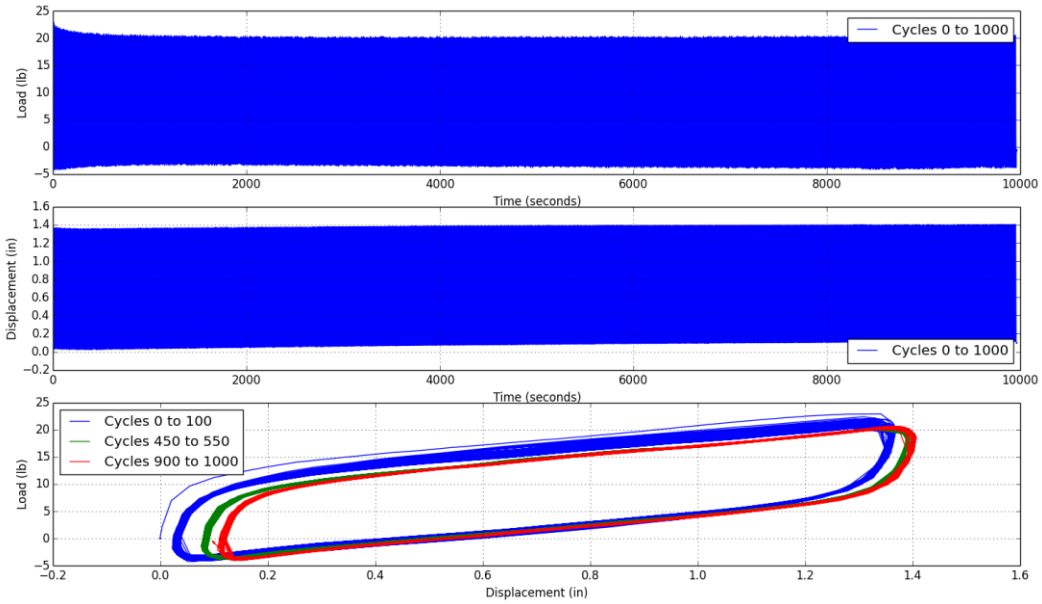

Figure 3.41: Cyclic Load Test Results: Diameter=4", Embedment = 8D, Load Eccentricity = 5D, Target Tilt Angle = 2.0°

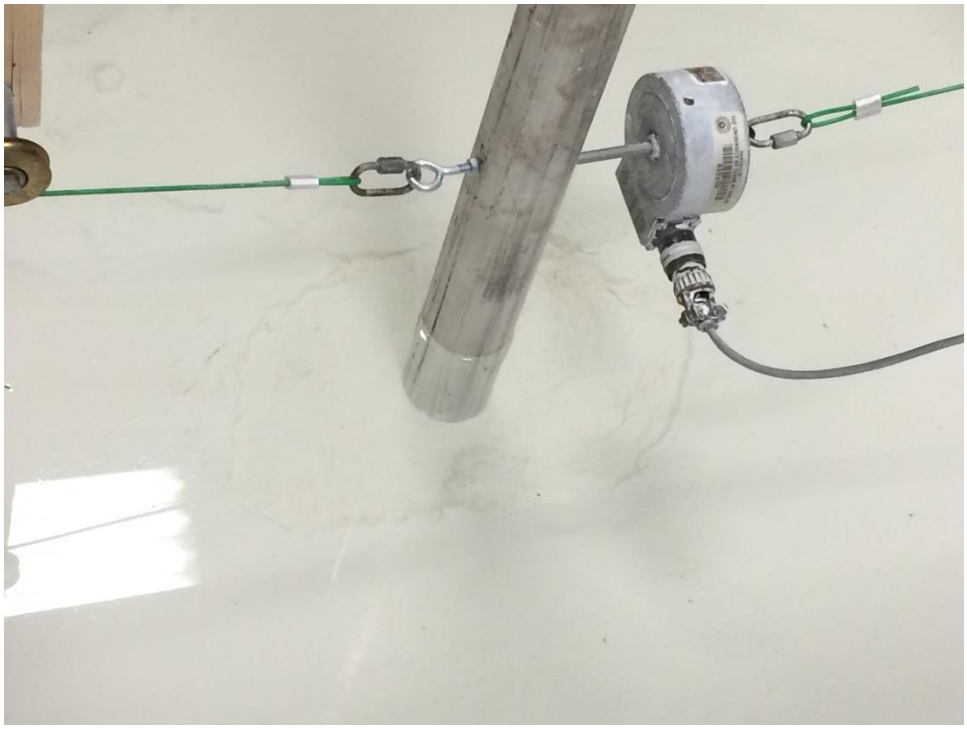

Figure 3.42: Disturbed Soil around 2" Diameter Monopile after Cyclic Tests

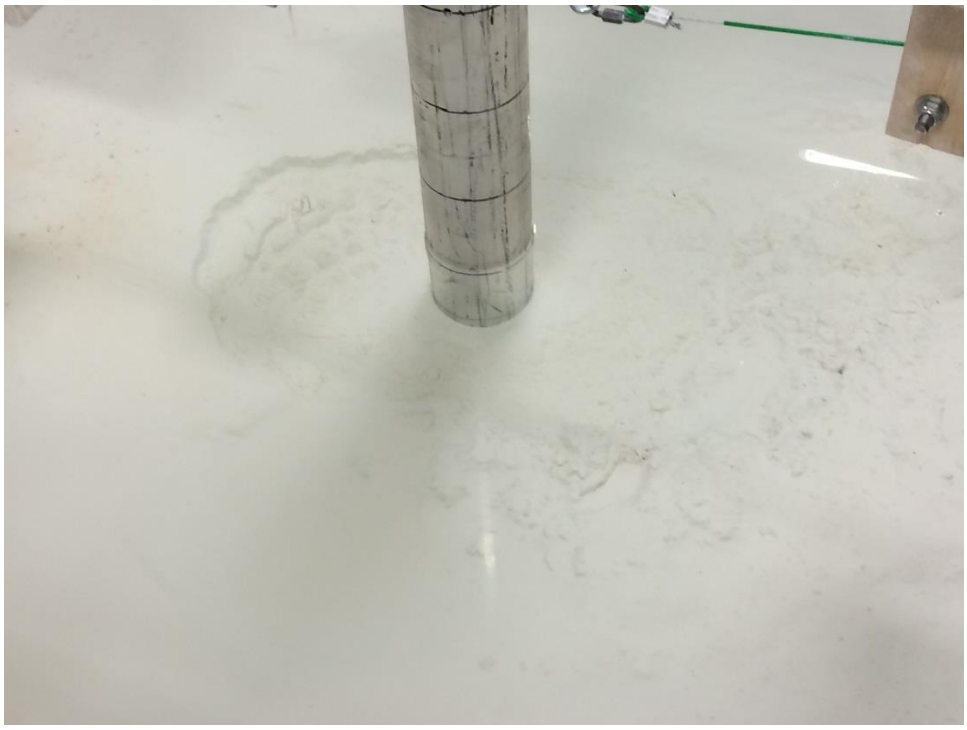

Figure 3.43: Disturbed Soil around 3" Diameter Monopile after Cyclic Tests

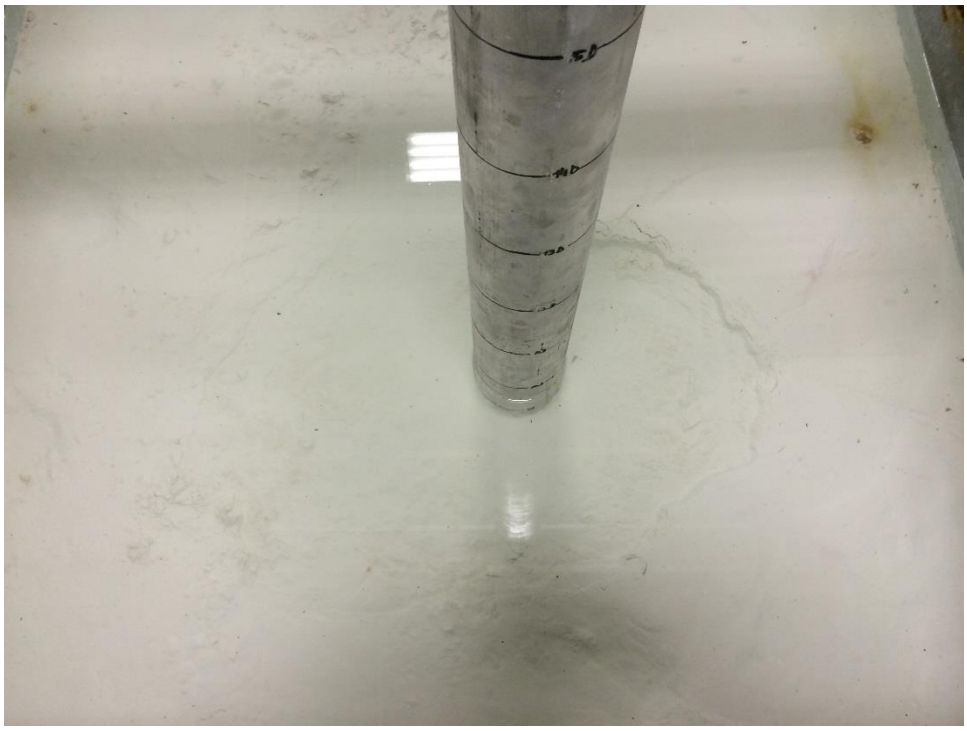

Figure 3.44: Disturbed Soil around 4" Diameter Pile after Cyclic Load Tests Lateral Load Tests to Failure

Results shown in Figure 3.33 to Figure 3.41 were from the first set of cyclic load tests that were carried out in this project. The variation in stiffness of the pile response during the cycling was analyzed (see Section **Error! Reference source not found.**) and seven out of the nine test results showed a decrease in he stiffness during the initial 50 cycles which was consistent with what was expected. However, two of the tests showed an increase in the stiffness. In order to verify that the stiffness does indeed decrease we retested the piles under 50 load cycles. The results from these tests are shown in Figure 3.45 - Figure 3.53.

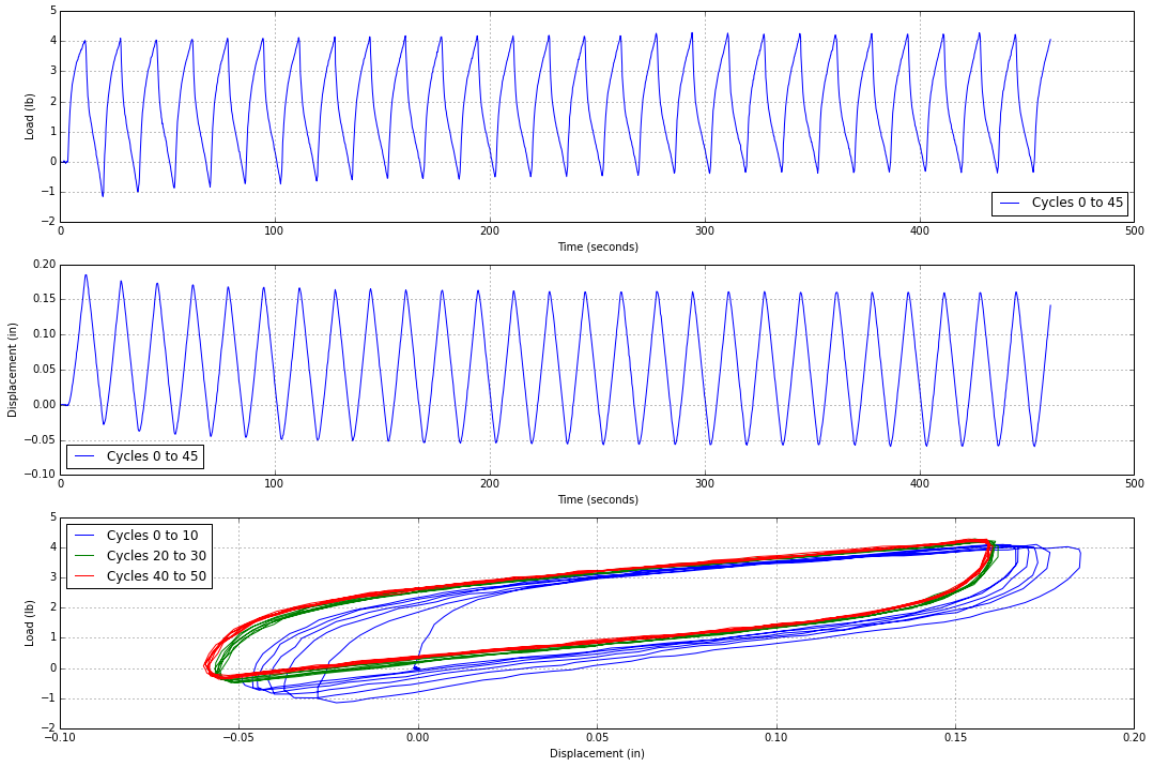

Figure 3.45: Cyclic load test results, 2-inch diameter, embedment = 8D, load eccentricity = 5D, target tilt angle = 0.5°, normally to lightly overconsolidated soil bed

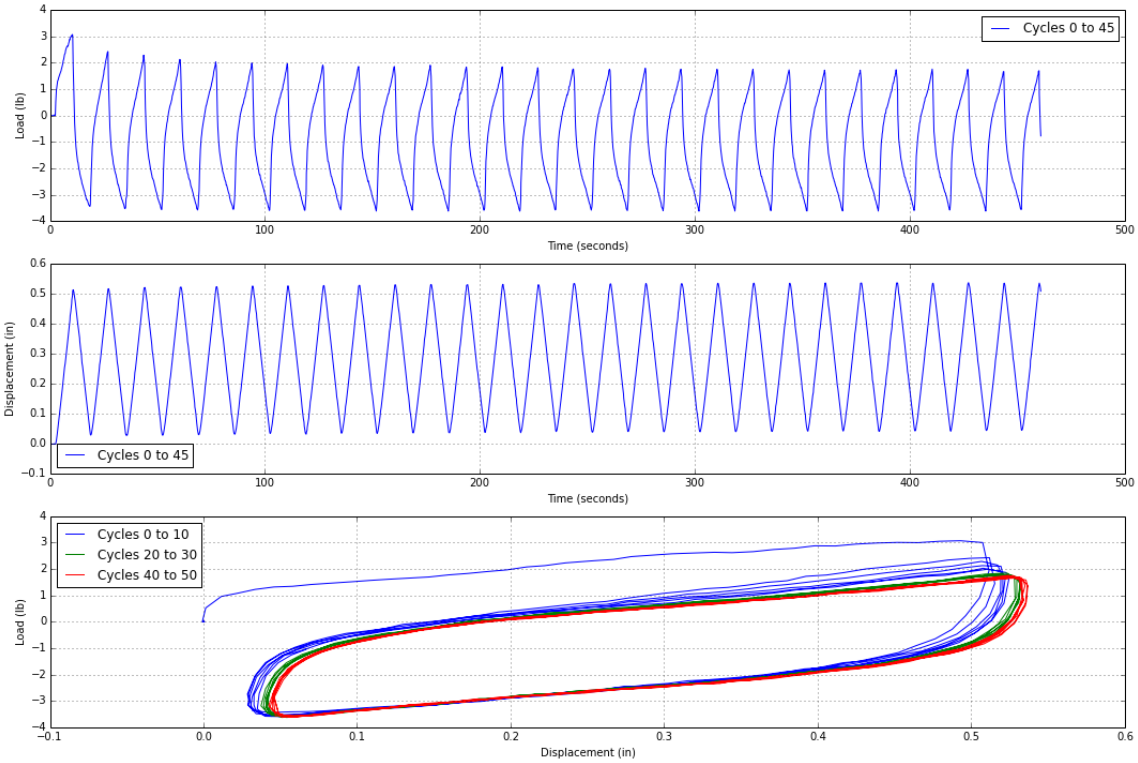

Figure 3.46: Cyclic load test results, 2-inch diameter, embedment = 8D, load eccentricity = 5D, target tilt angle = 1.0°, normally to lightly overconsolidated soil bed

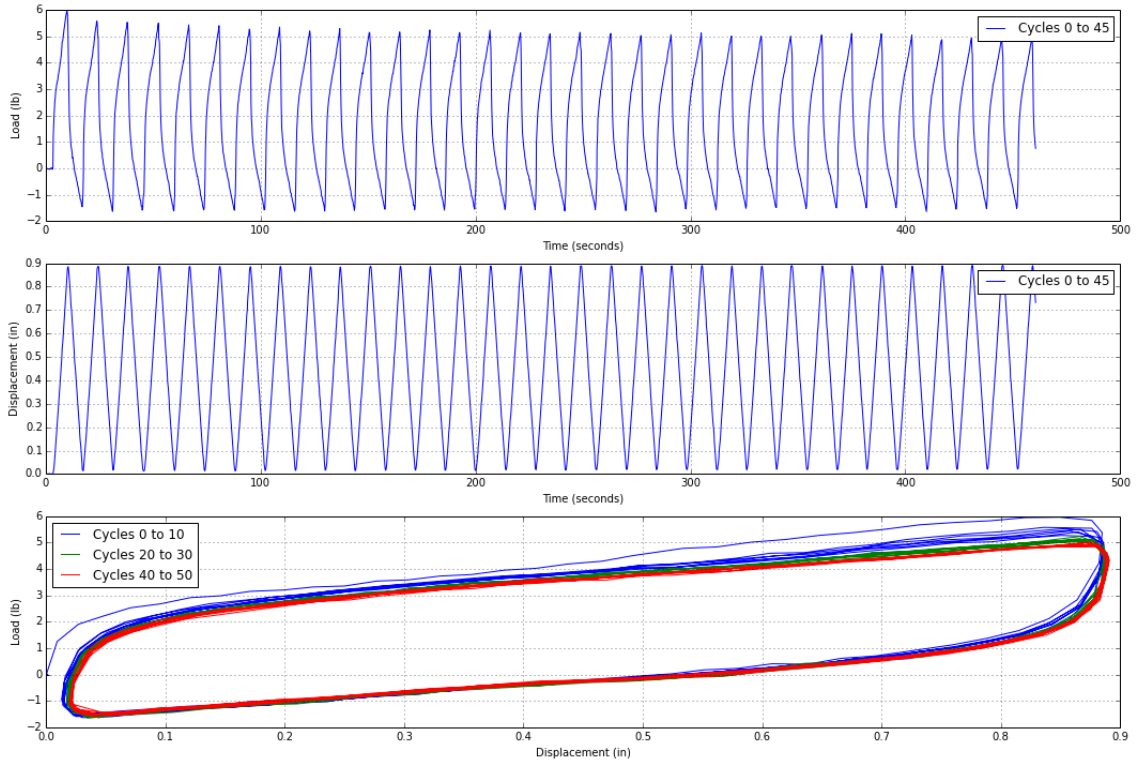

Figure 3.47: Cyclic load test results, 2-inch diameter, embedment = 8D, load eccentricity = 5D, target tilt angle = 2.0°, normally to lightly overconsolidated soil bed

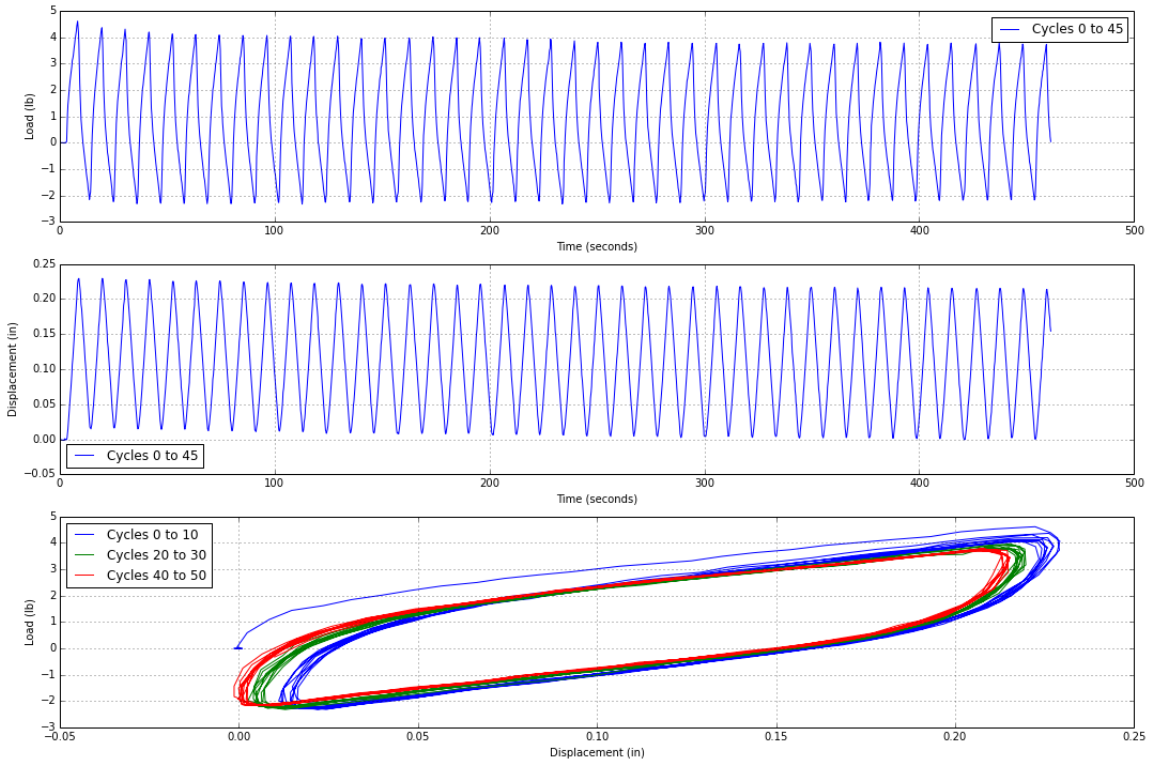

Figure 3.48: Cyclic load test results, 3-inch diameter, embedment = 8D, load eccentricity = 5D, target tilt angle = 0.5°, normally to lightly overconsolidated soil bed

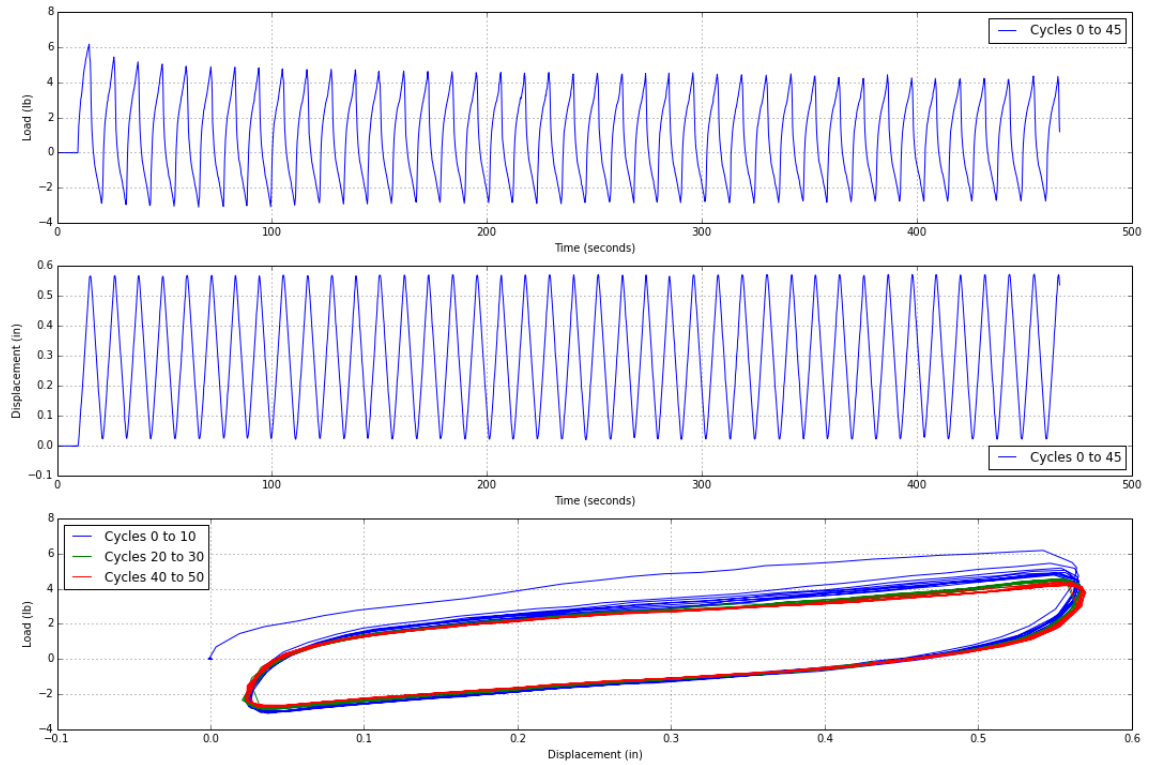

Figure 3.49: Cyclic load test results, 3-inch diameter, embedment = 8D, load eccentricity = 5D, target tilt angle = 1.0°, normally to lightly overconsolidated soil bed

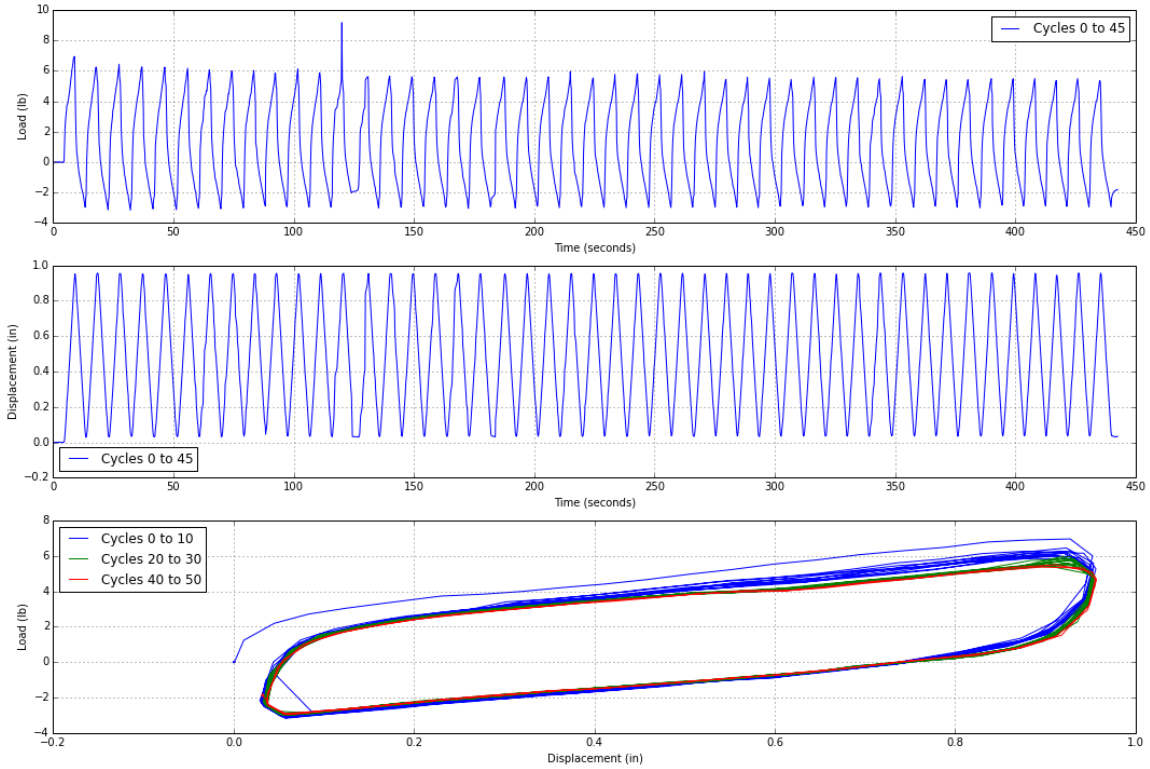

Figure 3.50: Cyclic load test results, 3-inch diameter, embedment = 8D, load eccentricity = 5D, target tilt angle = 1.0°, normally to lightly overconsolidated soil bed

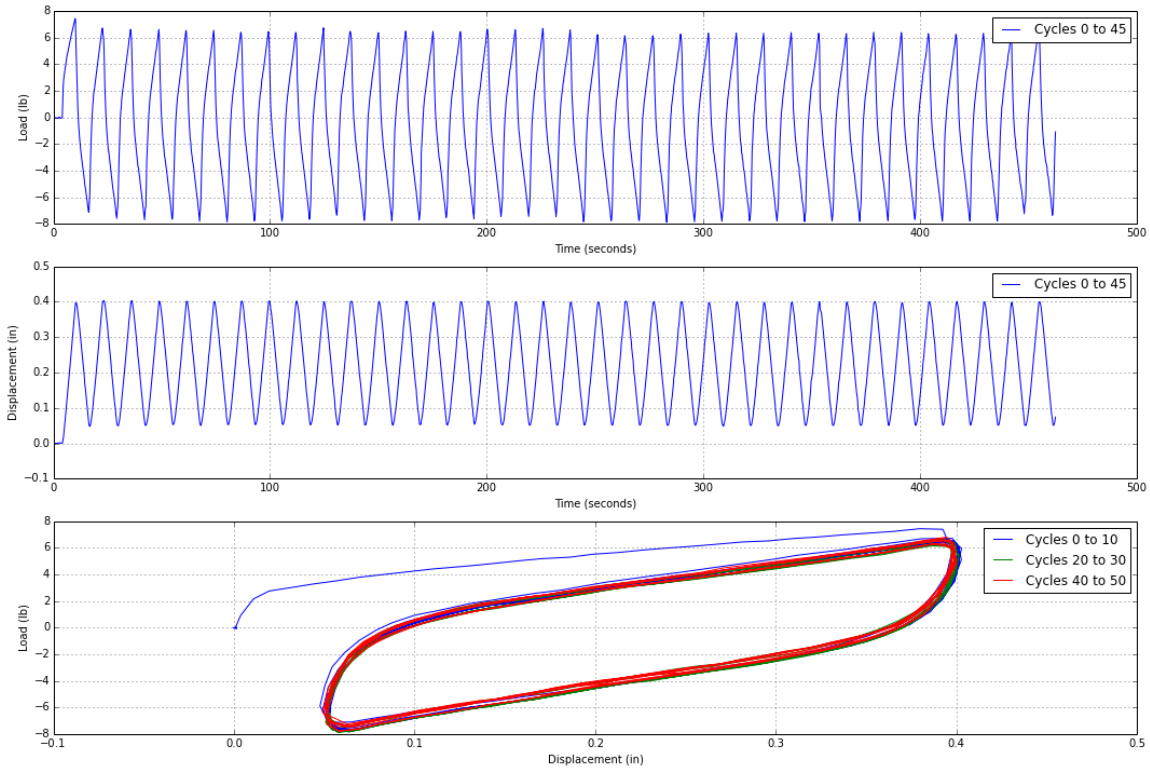

Figure 3.51: Cyclic load test results, 4-inch diameter, embedment = 8D, load eccentricity = 5D, target tilt angle = 0.5°, normally to lightly overconsolidated soil bed

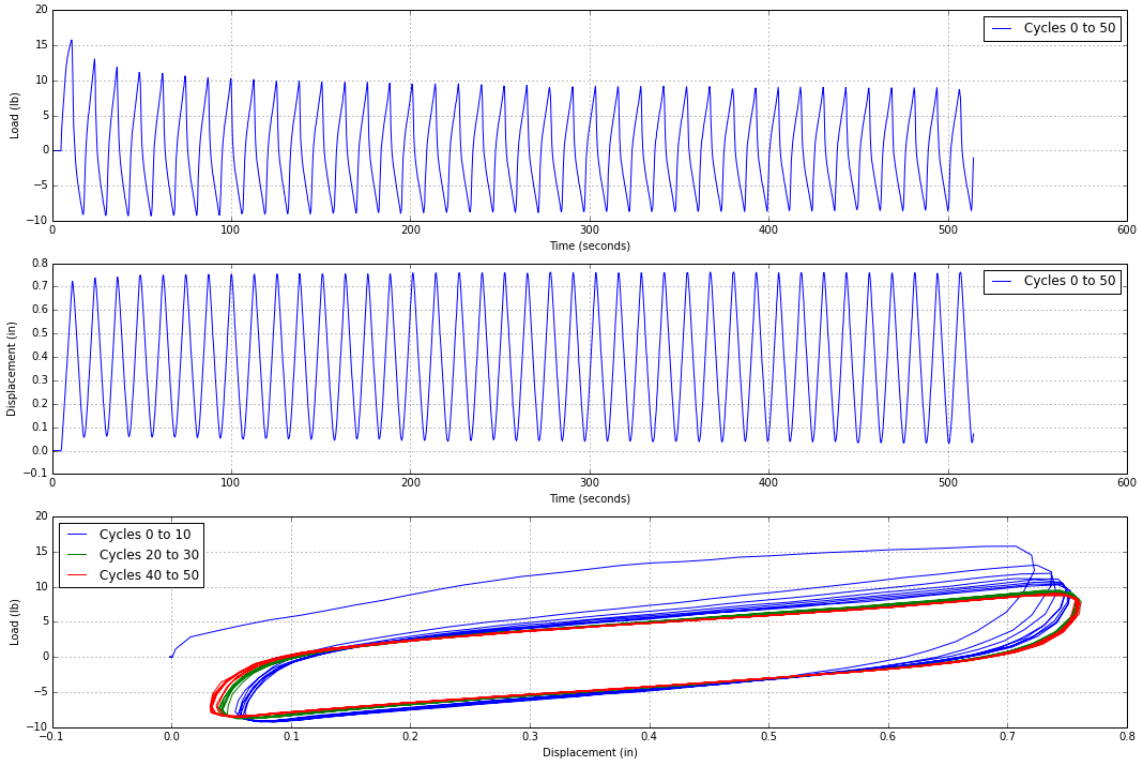

Figure 3.52: Cyclic load test results, 4-inch diameter, embedment = 8D, load eccentricity = 5D, target tilt angle = 1.0°, normally to lightly overconsolidated soil bed

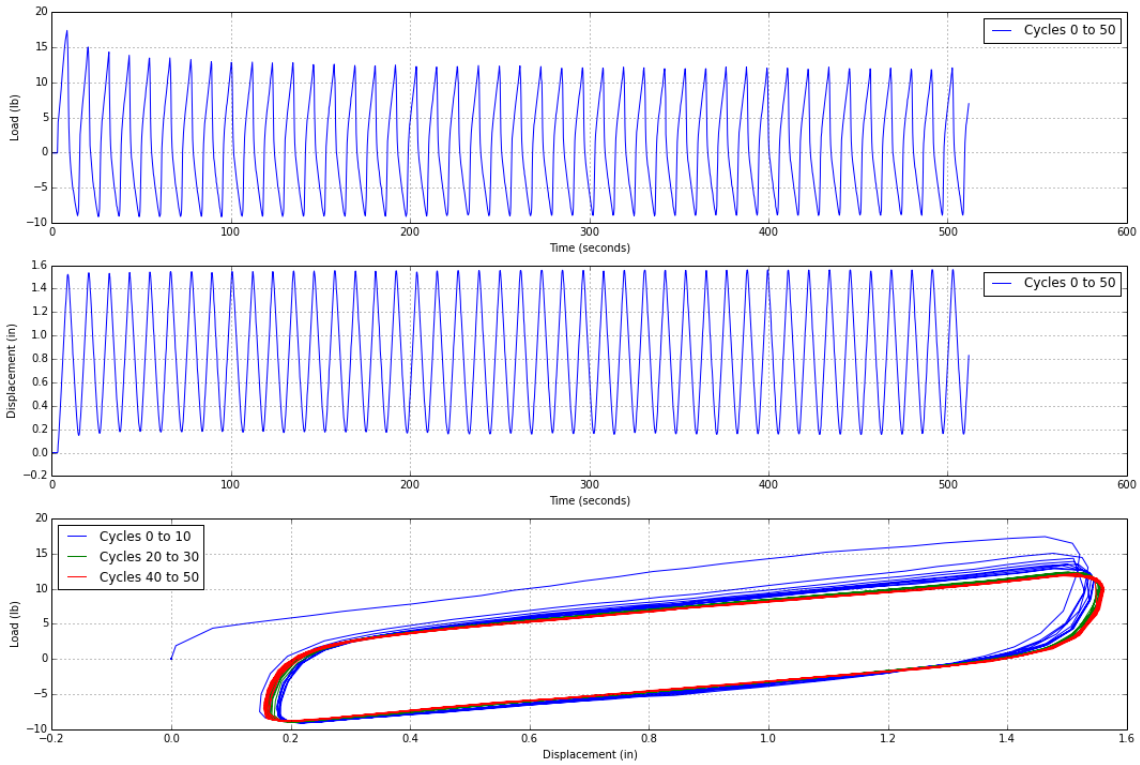

Figure 3.53: Cyclic load test results, 4-inch diameter, embedment = 8D, load eccentricity = 5D, target tilt angle = 2.0°, normally to lightly overconsolidated soil bed

3.5 TESTS IN HEAVILY OVERCONSOLIDATED KAOLINITE CLAY

3.5.1 Monotonic/Static Lateral Load Tests

All test models had an embedment depth of 8D and lateral loads were applied at a height of 5D above the mudline. The depth of the soil bed was 20-inches, as a result, the pile diameters were limited to 1-inch and 2-inches.

These tests were monotonic (displacement controlled) tests and were carried out at a displacement rate of 0.002in/s which was slower than the earlier reported tests. Trial tests did not show any appreciable influence of the displacement rate on the results but this lower displacement rate was adopted to ensure the avoidance of viscous effects in the soft soil beds. The load test results are shown in Figure 3.54 and Figure 3.55 for the two pile diameters. These data are plotted in several ways: load versus time, displacement versus time and load versus displacement.

Note: In Figure 3.54, the test on 8/28/2014 shows a softer load-deformation response because the soil bed had a lower shear strength at only 8-psf compared with 10-psf in the case of the tests carried out on 8/06/2014.

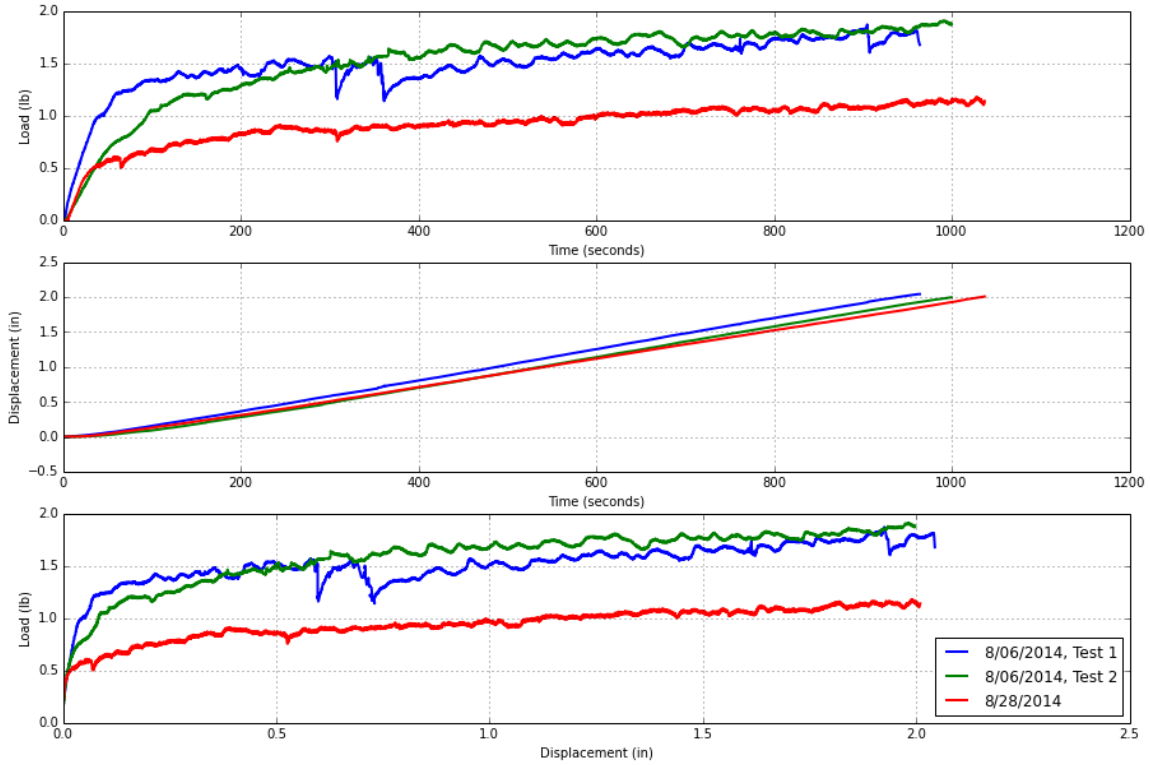

Figure 3.54: Monotonic load test: diameter=1-inch, embedment = 8D, load eccentricity = 5D, target lateral displacement = 2D

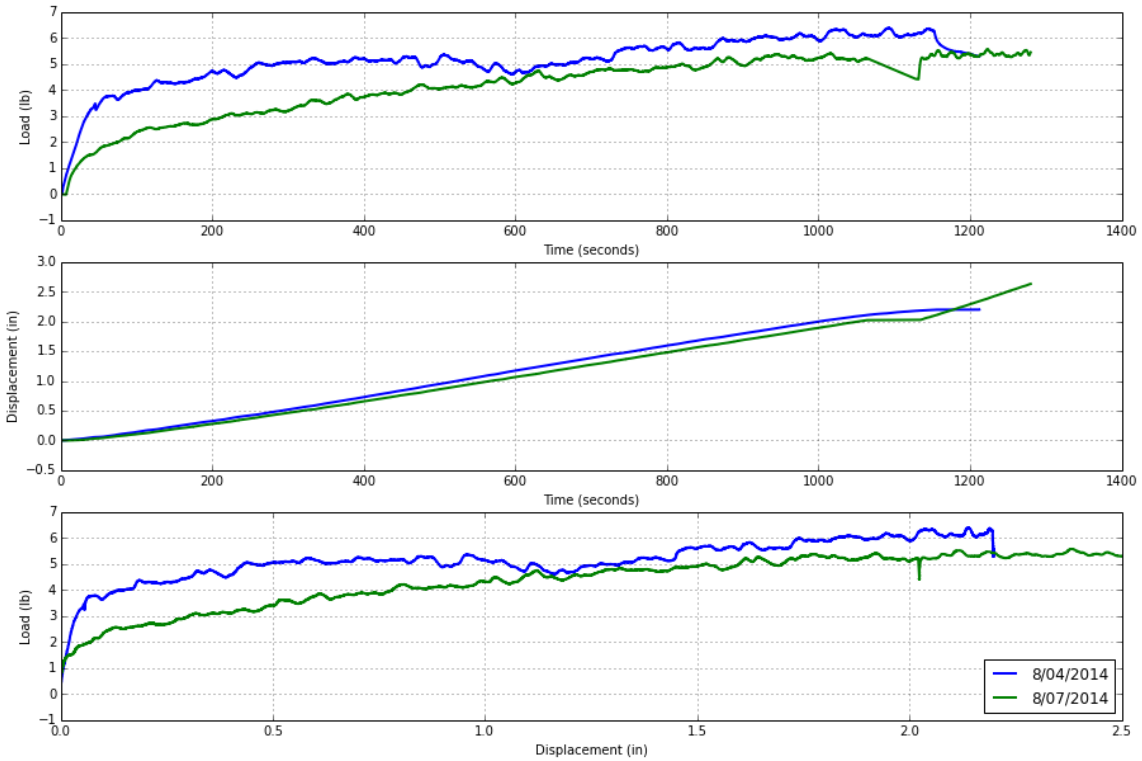

Figure 3.55: Monotonic load test: diameter=2-inches, embedment = 8D, load eccentricity = 5D, target lateral displacement = 2D

3.5.2 Cyclic Lateral Load Tests

Cyclic tests were conducted by imposing constant a target tilt of 0.5 degrees for 1,000 cycles of one-way loading (0.5 degrees to the imposed tilt and back to 0 degrees constitutes one cycle). The period of loading is similar to wave loading, 10 seconds. The previous report included cyclic tests with tilts of 1.0 and 2.0 degrees as well but, these resulted in mobilized capacities which were very close to the ultimate capacity. Therefore, it was deemed that a 1000 cycles of 1.0 and 2.0 degrees would be much too high and unrealistic.

Cyclic load test results for two pile diameters are shown in Figure 3.56 and Figure 3.57. These data are plotted in several ways: load versus time, displacement versus time and load versus displacement. Also, photos of the soil around the pile at the mudline are provided in Figure 3.58 and Figure 3.59.

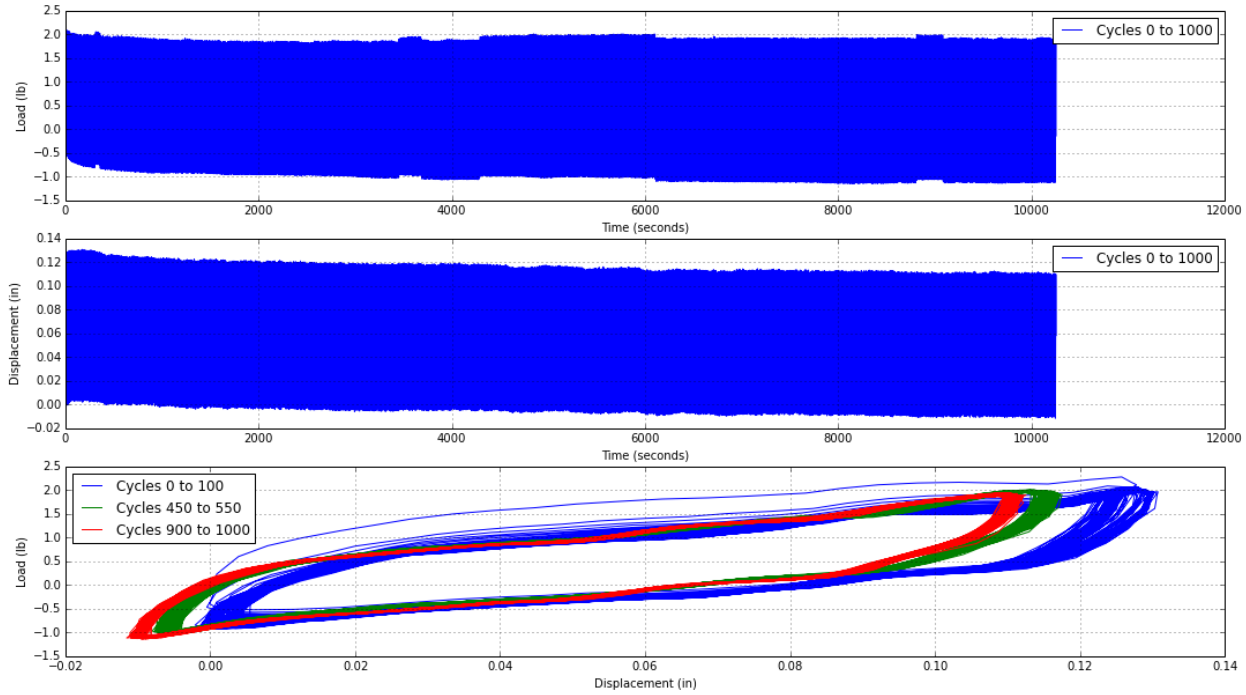

Figure 3.56: Cyclic load test results, diameter=1-inch, embedment = 8D, load eccentricity = 5D, target tilt angle = 0.5°, overconsolidated soil bed

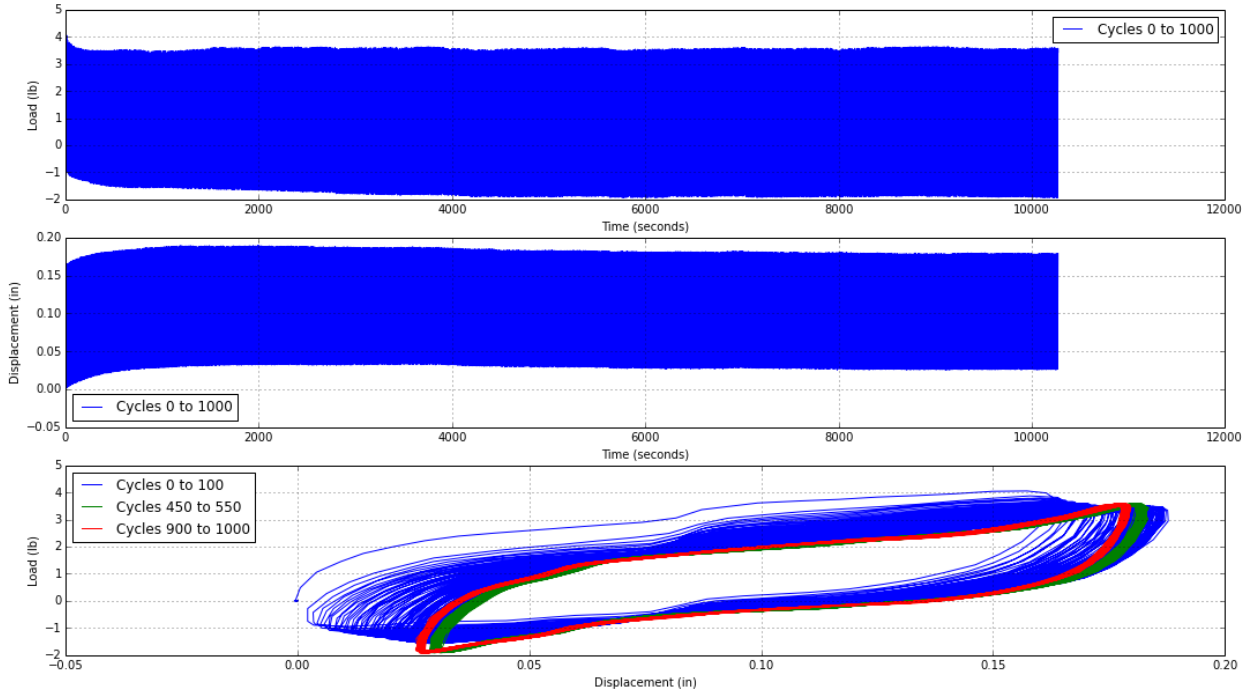

Figure 3.57: Cyclic Load test results, diameter=2-inches, embedment = 8D, load eccentricity = 5D, target tilt angle = 0.5°, overconsolidated soil bed

Figure 3.58: 1-inch diameter monopile during cyclic test, overconsolidated soil bed

Figure 3.59: 2-inch diameter monopile during cyclic test, overconsolidated soil bed

3.6 TESTS IN HEAVILY OVERCONSOLIDATED KAOLINITE CLAY BED WITH A STIFF CRUST

3.6.1 Monotonic/Static Lateraly Load Tests

Two static lateral load tests were done in the overconsolidated kaolin clay bed with a stiff crust. Details of these tests are provided in Figure 3.60 and the information is plotted in several ways: load versus time, displacement versus time, and load versus displacement.

The pile was installed on 12/08/2014 and the first test was done about an hour after installation. After that the pile was reset to its original position and tested again after four days on 12/12/2014. This second test was done in order to see the effect of setup time on the lateral response of the pile.

The S_u profiles for these tests were slightly different as the soil beyond depth of about 10-inches had gained strength by the time the second test was done. However, this difference was neglected in the idealized S_u profile used in the LPILE analyses since the maximum gain in soil strength was not more than 2-psf and it only affected the bottom two pile diameters.

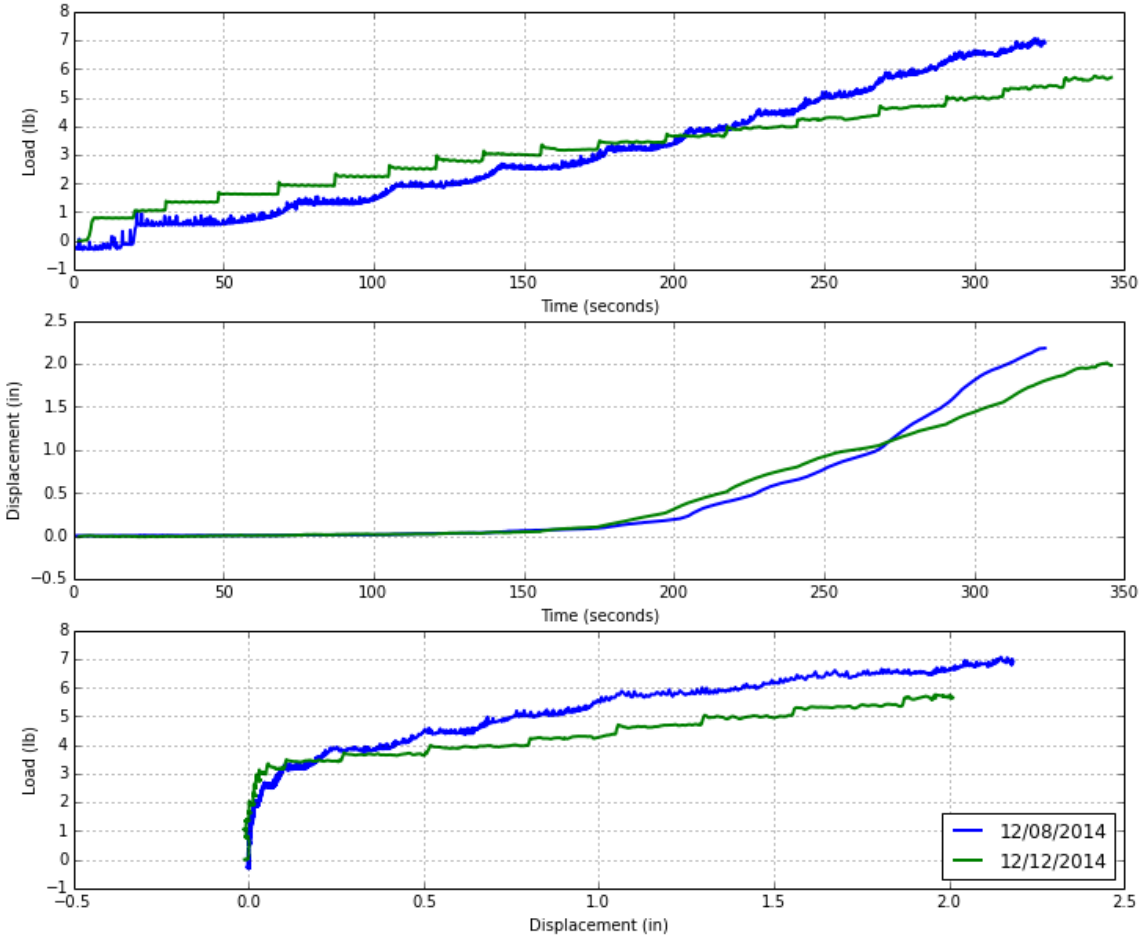

Figure 3.60: Static load tests, overconsolidated kaolin clay with stiff top crust, D = 2-inches, embedment = 8D, load eccentricity = 5D, target lateral displacement = D

3.6.2 Cyclic Load Tests

No cyclic tests were done in this clay bed.

3.7 TESTS IN NORMALLY CONSOLIDATED GULF OF MEXICO CLAY

3.7.1 Monotonic/Static Lateral Load Tests

Two static lateral load tests were done on the 1-inch diameter pile and the results are shown in Figure 3.61. The second test was carried out since the pile was disturbed while installing the instrumentation during the first test. It should be pointed out that the pile response was very weak owing to its small size and load cell used to the measure the lateral loads was heavier than the model pile itself. So these results are not as reliable as those from the 2-inch diameter pile.

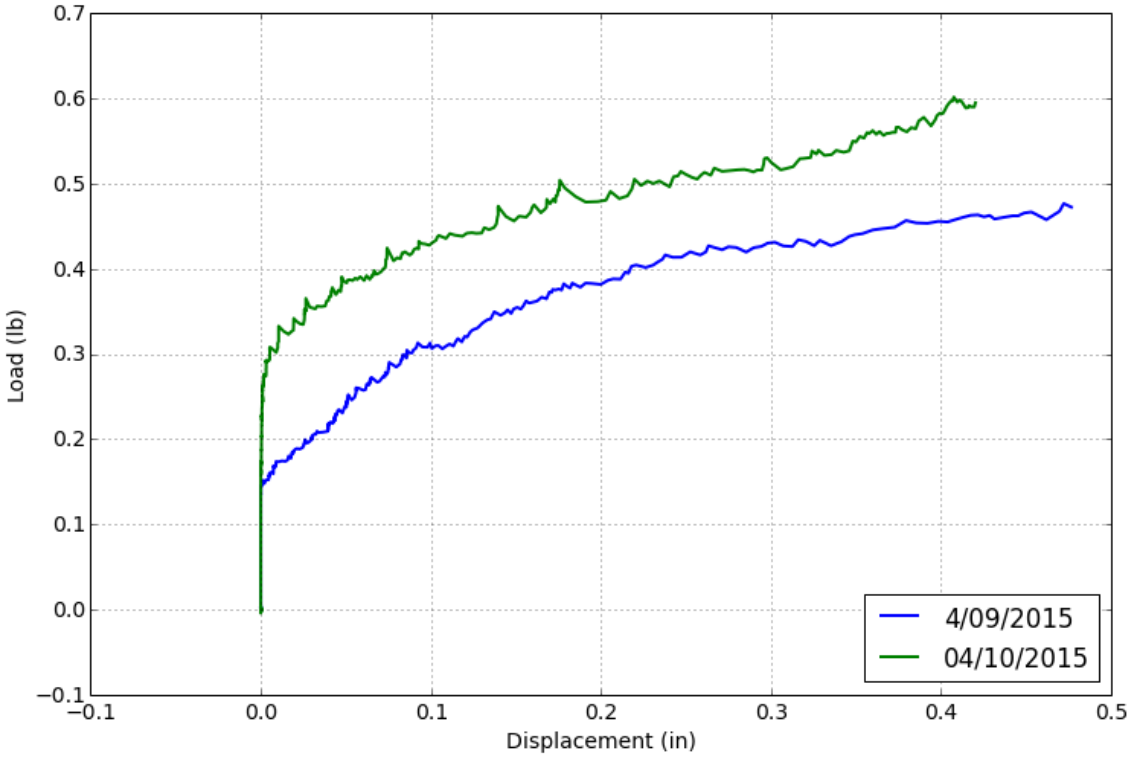

Figure 3.61: Static load tests, normally consolidated GoM clay, D = 1-inch, embedment = 8D, load eccentricity = 5D

One monotonic (displacement controlled) load test was done on the 2-inch diameter pile (see Figure 3.62) and the results are shown in Figure 3.63.

Figure 3.62: Normally consolidated GoM clay bed with 2-inch diameter pile installed and ready to be tested

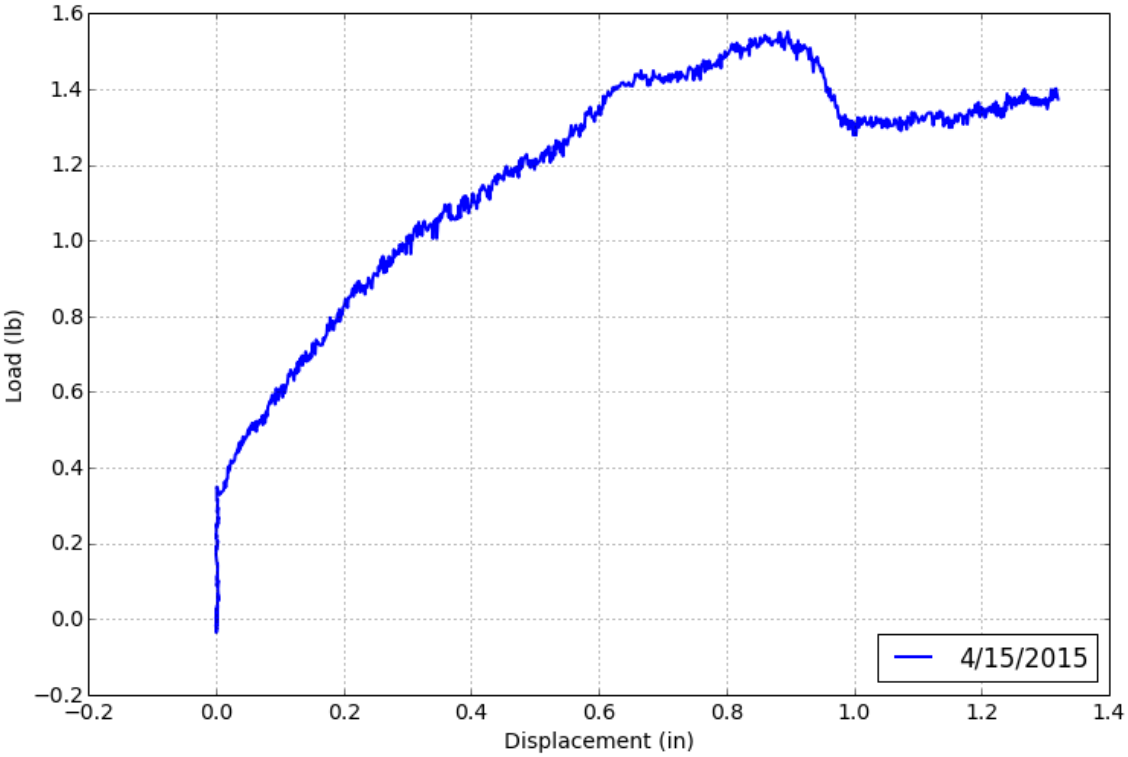

Figure 3.63: Static load test, normally consolidated GoM clay, D = 2-inches, embedment = 8D, load eccentricity = 5D

3.7.2 Cyclic Lateral Load Tests

A displacement controlled cyclic test was done on the 2-inch pile with a target tilt of 0.5-degree as shown in Figure 3.64. The objective of this test was to check the validity of the conclusions that were drawn from previous tests in kaolinite test beds regarding the cyclic degradation of the lateral soil resistance.

A second cyclic test was also done but the results are not shown here due to a lack of clarity.

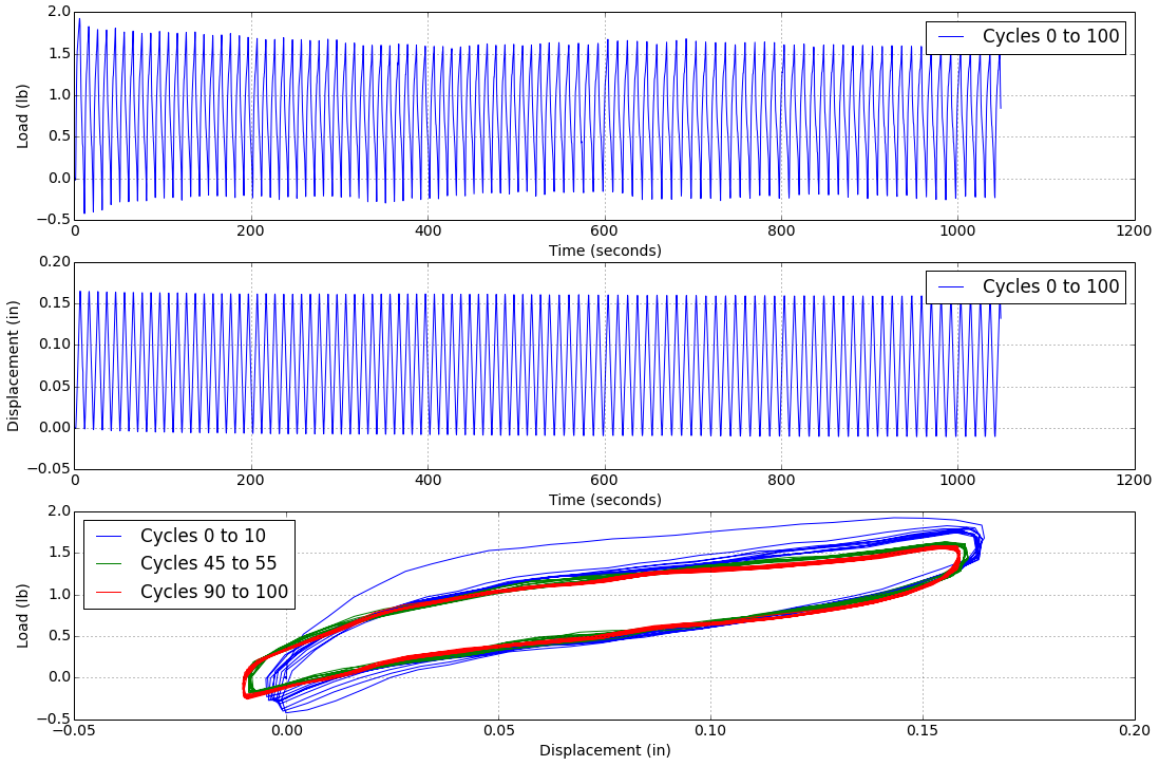

Figure 3.64: Cyclic load test, normally consolidated GoM clay, D = 2-inches, embedment = 8D, load eccentricity = 5D, 0.5-deg tilt

3.8 TESTS IN HEAVILY OVERCONSOLIDATED GULF OF MEXICO CLAY

3.8.1 Monotonic/Static Lateral Load Tests

Two static lateral load tests were done in this soil bed as well and the details are provided Figure 3.65.

The pile was installed on 12/16/2014 and the first test was done within about an hour after installation. After the completion of this test, the pile was reset to its original position and tested again after two days on 12/18/2014. This second test was done in order to see the effect setup time on the lateral response of the pile.

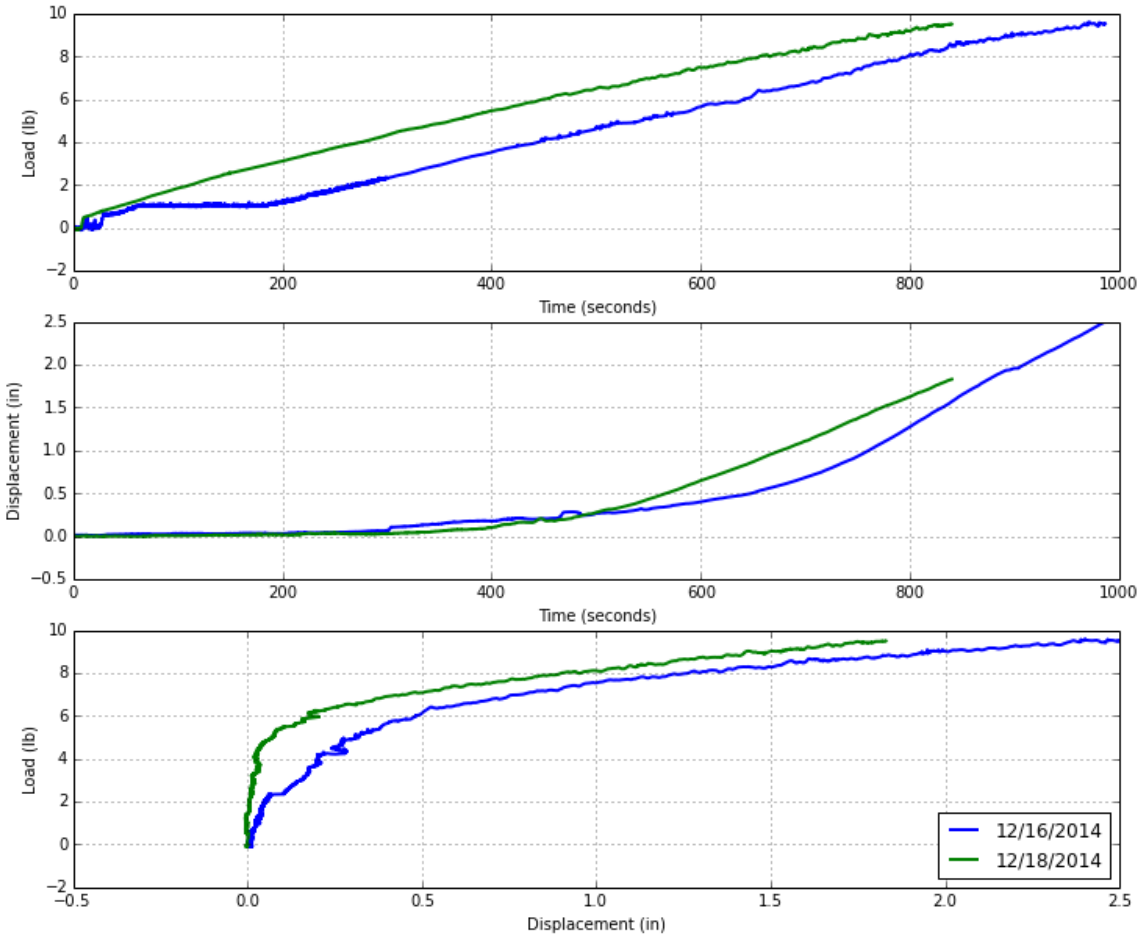

Figure 3.65: Static load tests, overconsolidated Gulf of Mexico clay, D=2-inches, embedment = 8D, load eccentricity = 5D, target lateral displacement = D

3.8.2 Cyclic Lateral Load Tests

Two cyclic load tests with a target tilt of 0.5° were done on a 2-inch diameter pile. These tests were carried out 01/12/2015 and 01/13/2015, which was approximately four weeks after the static tests. The results from these tests are shown in Figure 3.66 and Figure 3.67. The load-displacement cycles in Figure 3.66 show that the pile translated laterally during the test. This unintended translation was due to the counter-weight attached to the pile not being completely balanced when the test was initiated. Despite this error, the lateral load curves are still considered usable if this translation is subtracted (i.e., the secant stiffness values are considered).

The test on 01/12/2015 was done 15-20 minutes after installation of the pile. The test on 01/13/2015 was done on the same pile after it had had approximately 24-hours of setup time.

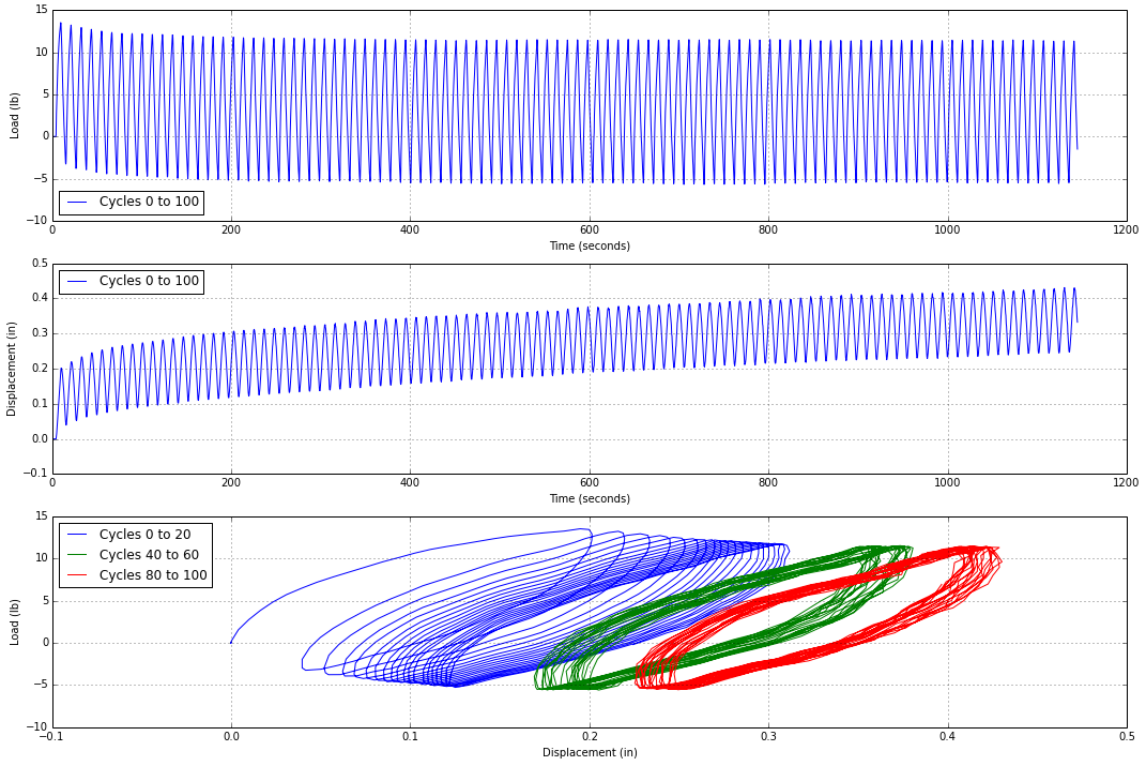

Figure 3.66: Cyclic load test results, diameter=2-inch, embedment = 8D, load eccentricity = 5D, target tilt angle = 0.5°, overconsolidated Gulf of Mexico clay bed (Test 1, 1 hour after installation, 1/12/2015)

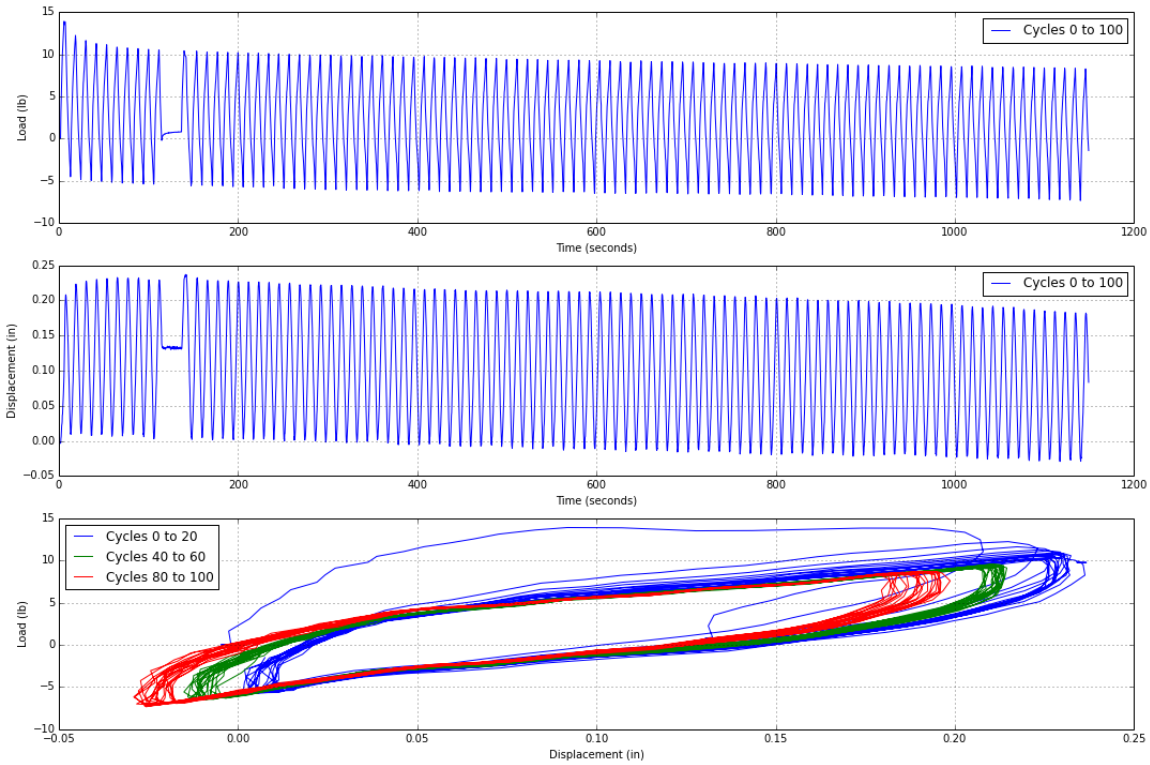

Figure 3.67: Cyclic load test results, diameter=2-inch, embedment = 8D, load eccentricity = 5D, target tilt angle = 0.5°, overconsolidated Gulf of Mexico clay bed (Test 2, 1-day after installation, 1/13/205)

4 NUMERICAL MODELING

A series of numerical modeling studies were conducted to explore the effect of pile diameter and slenderness on the lateral response under static loading. The following models were developed and implemented:

1. Two-dimensional finite element method modeling with ABAQUS and KeyCreator in clay
2. Three-dimensional finite element method modeling with ABAQUS in clay
3. Three-dimensional finite element method modeling with ABAQUS in sand

Details of each soil type and how the test beds were prepared are given in the following sections.

Three different software namely, LPILE, KEYCREATOR, and ABAQUS, were used to carry out the numerical modeling component of this study.

LPILE is a finite-difference code by Ensoft Inc. that has been specially designed to carry p-y analyses of laterally loaded piles. It has a built-in database of p-y curves for a variety of soil types and is the widely used in the civil engineering industry.

KEYCREATOR Analysis is a general purpose and multi-physics finite element analysis program that provides fast and accurate true-multi-physic results, coupled with the simplicity and speed of Direct CAD Modeling. The program allows FEA analysts the ability to handle large complex problems with both computation speed and accuracy. KeyCreator Analysis uses a novel mesh generation technology called Sefea (Strain Enriched Finite Element Analysis), which is an advanced solving technique that allows the user to obtain accurate results from coarse low order elements. Sefea Technology speeds up processing time and reduces the memory requirements without compromising results.

ABAQUS is a software suite for finite element analysis and computer-aided engineering, originally released in 1978. The Abaqus FEA product suite from Dassault Systems offers powerful and complete solutions for both routine and sophisticated engineering problems covering a vast spectrum of industrial applications. Abaqus is widely-accepted FEA software in both academic and industrial fields for handling nonlinear and large deformation engineering problems, and it provides special functions for handling geo-static stresses for the geotechnical engineering applications.

4.1 2-D FINITE ELEMENT MODELING IN CLAY

Preliminary finite element method analyses have been performed to investigate the possible effect of pile diameter from a fundamental perspective. KeyCreator and ABAQUS were used by Ensoft Inc. to carry out 2-D FE analysis of laterally loaded piles and the results were compared with those from LPILE.

There are two recognized failure modes for laterally loaded piles. The first is under plain strain conditions where there is a flow around failure mode that occurs at deep layers in two dimensions. The second is the wedge type failure mode that occurs near the ground surface in three dimensions. The study started with the two dimensional flow around failure mode.

Figure 4.1 shows the model used in FE analysis. ‘B’ is the diameter of the pile and ‘A’ is the distance to the boundary of the soil continuum in the FE model. KeyCreator and ABAQUS models showed that the distance to the boundary of the modelled soil continuum affects the shape of the predicted p-y curves.

Figure 4.2 shows how the model with a closer boundary (mesh width three times the pile diameter or A/B = 3) has a stiffer p-y curve than the model with a farther boundary (mesh width 15 times the pile diameter or A/B = 15). This effect can be explained by the observing how the soil moves in each model when the pile is loaded.

Slip line theory says that the soil should flow around the pile as it moves in plain strain conditions. This does happen in the models where A/B = 3 but not in the models where A/B = 15. In both the A/B = 3 and A/B = 15 cases, KeyCreator models showed that gaps form behind the pile. The difference is that the soil shows an indication of moving into that gap in the A/B = 3 case but it did not show that indication in the A/B = 15 case. The closer boundary forces the soil to move like the theory predicts, while the farther boundary allows the soil to compress in front of the pile. The results from KeyCreator were verified by ABAQUS for the A/B = 3 case and is shown in Figure 4.3. As can be seen, the vector plot from ABAQUS clearly indicate that the soil is moving into the gap behind the pile (when A/B = 3).

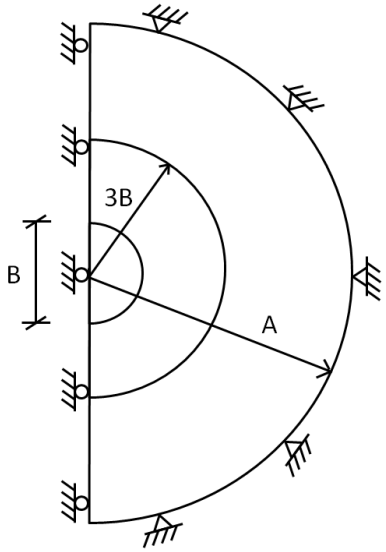

E_{soil} = 1500 psi

v_{soil} = 0.45

c = 10 psi

ϕ = 0°

$E_{pile} = 1000E_{soil}$

v_{pile} = 0.3

Mesh refinement:

at the pile-soil interface = B/120

in the 3B soil face = B/16

Figure 4.1: 2D FE Model

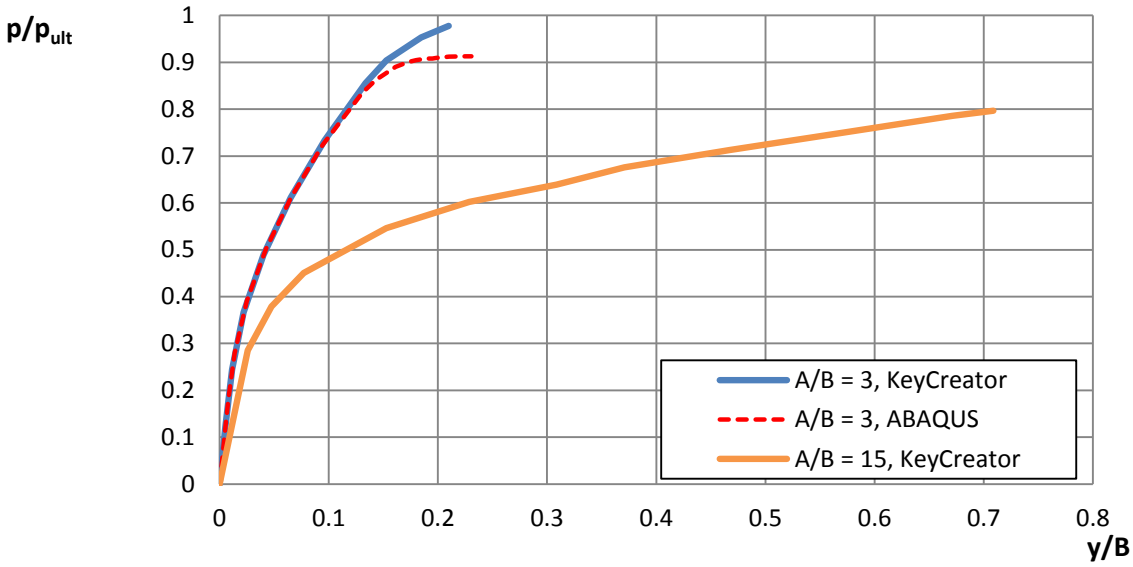

Figure 4.2: Effect of A/B on normalized 'p-y' Curves (Pult = 9SuB, A = Width of Mesh, B = Pile Diameter, Su=1440psf)

Figure 72 and 73: Explain why A/B = 3 was chosen. It would be nice to add a ABAQUS result for the A/B=15 case in Figure 73.

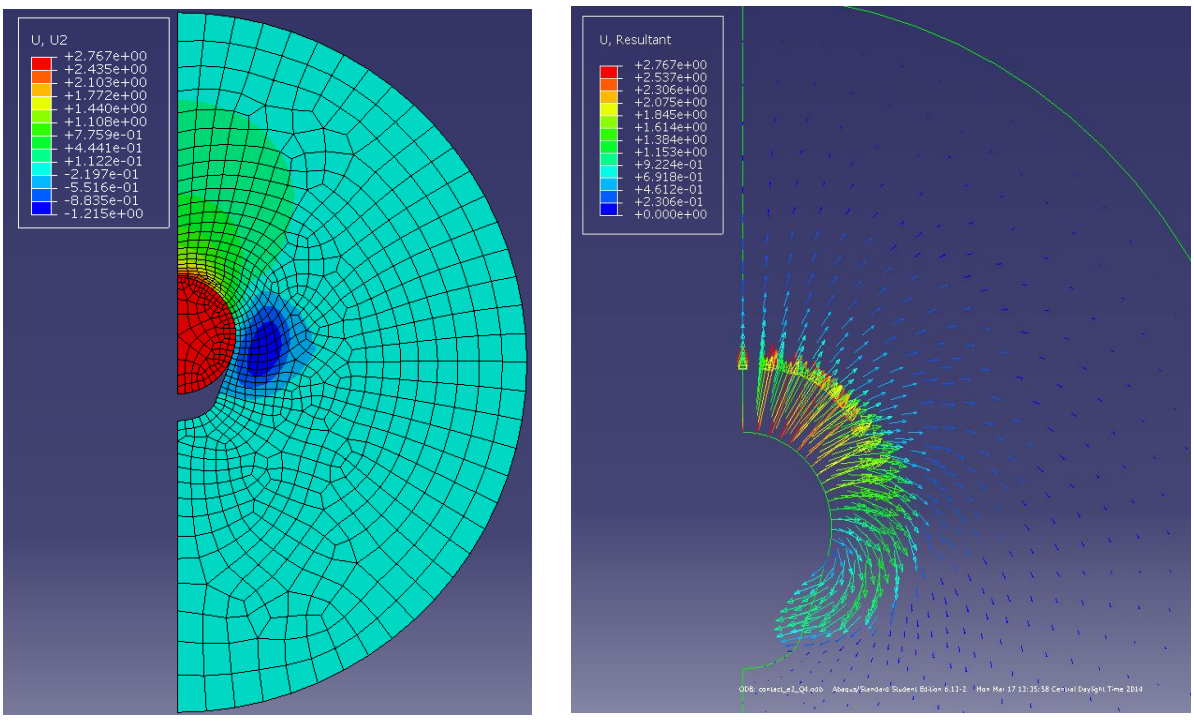

Figure 4.3: Contour and Vector Plots from ABAQUS (Width of Mesh 3 Times the Pile Diameter of 1 foot)

P-y curves from KeyCreator were compared with the semi-empirical p-y curves used in LPILE which are based on the "Stiff Clay without Free Water" model proposed by Reese (1975). It can be seen that the 2D FE model predicts p-y curves with lower stiffness than those by Reese (1975) for all three pile

diameters considered. Figure 4.4 shows that for both models p_{ult} increases with diameter. Figure 4.5 shows that the effect of pile diameter vanishes when the p-y curves are normalized.

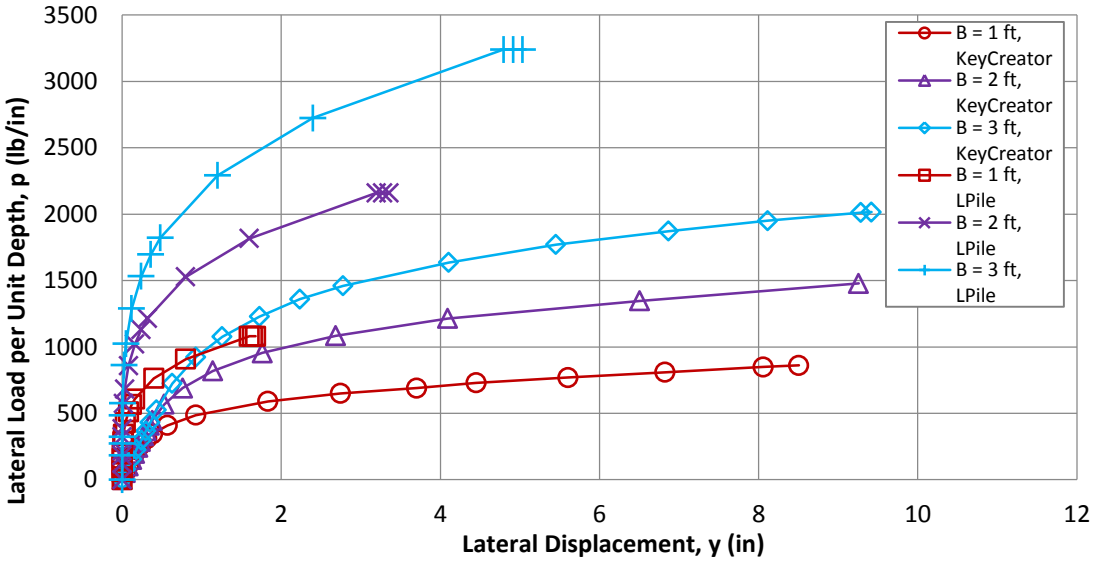

Figure 4.4: Comparison of p-y curves (A/B = 15)

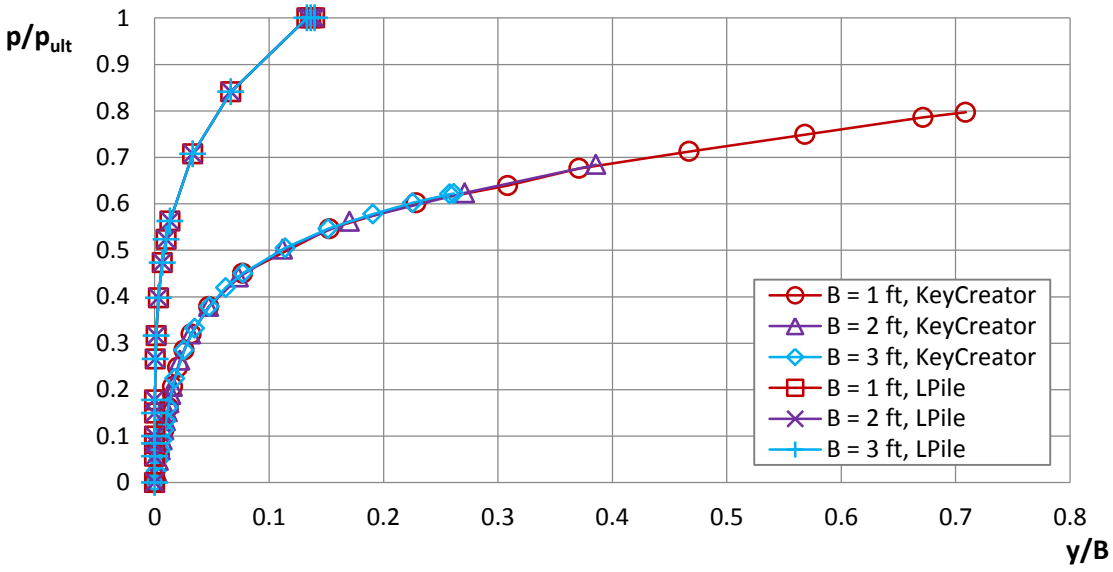

Figure 4.5: Comparison of Normalized p-y Curves (A/B = 15)

4.2 3-D FINITE ELEMENT MODELING IN CLAY

Three dimensional numerical modeling was required to investigate the soil-pile interaction near the ground surface or mudline. At shallow depths, failure of the soil mass follows a 3-D wedge mechanism and plane strain conditions do not apply.

Half models of laterally loaded piles were analyzed in the finite element software, ABAQUS, with diameters of 36 in, 72 in, and 144 in. The piles extended 10 diameters into the soil with an additional 0.5 diameter hemisphere below the shaft of the pile, and the piles extended one diameter above the soil. The soil extended 4 diameters below the tip of the pile shaft (or 3.5 diameters below the tip of the hemisphere). Horizontally, the soil extended 10 diameters from the edge of the pile with 8-node linear brick elements and then extended another 10.5 diameters with infinite elements.

The top 7 diameters of soil had cohesion yield stress equal to 10-psi (1440-psf), submerged unit weight equal to 0.0362-pci (62.6-pcf), Young's modulus equal to 1500-psi (i.e. $150S_u$), and Poisson's ratio equal to 0.45. The bottom 7 diameters of soil had the same soil properties except for cohesion yield stress equal to 20-psi (2880-psf), so that the soil could hold its own weight.

The piles were modeled as solids and had bending stiffness values equal to 2.637×10^8 kip-in^2, 4.219×10^9 kip-in^2, and 6.751×10^{10} kip-in^2 for the 36-in, 72-in, and 144-in pile diameter models respectively. The piles had a unit weight equal to 0.0751-pci (130-pcf) and Poisson's ratio equal to 0.3.

The soil-pile interface had a friction coefficient of 0.35. Gravity was present in the simulation, and the initial state of stress was considered in a geostatic step. The loading was displacement controlled with displacements applied to the pile in the horizontal direction 12-in above the mud line. A screenshot of the mesh for the 36 in diameter pile model is shown in Figure 4.6.

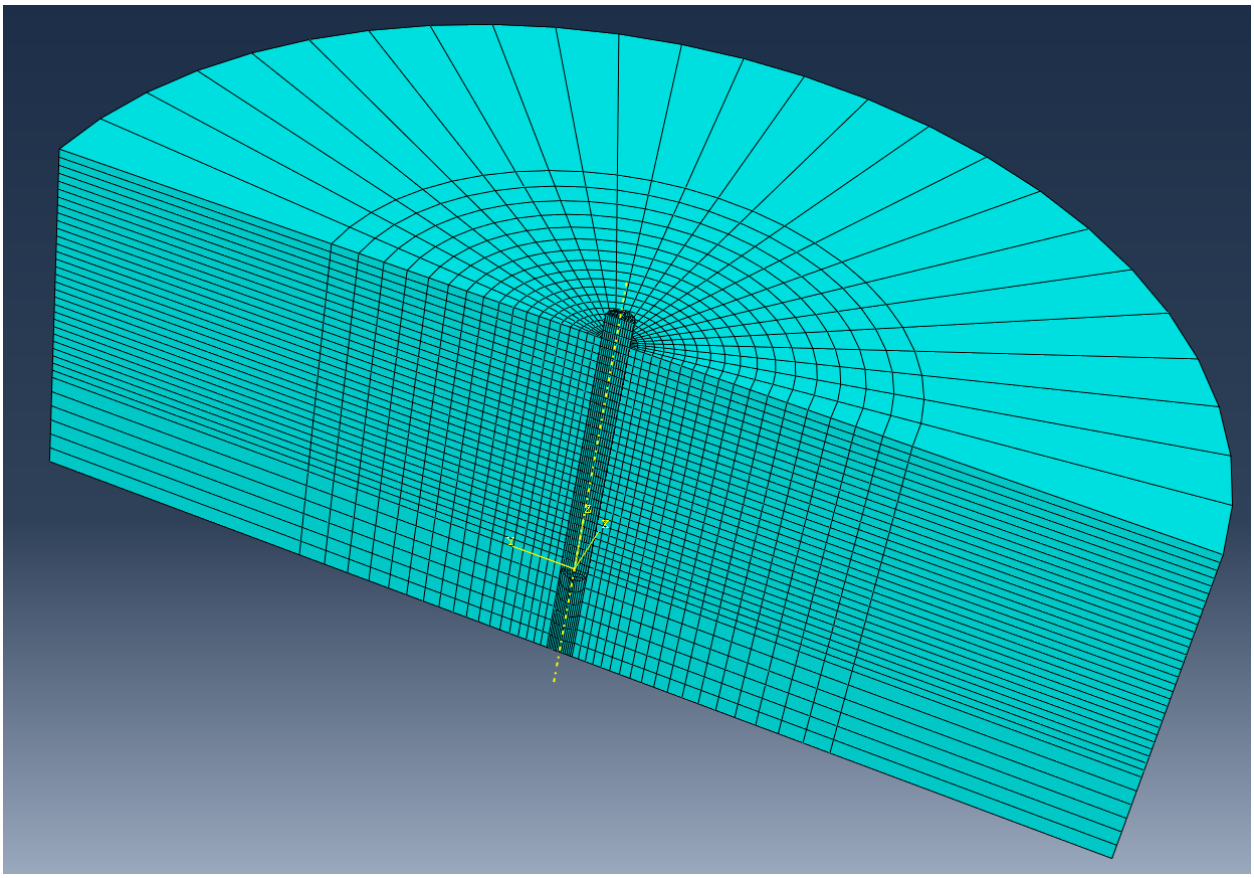

Figure 4.6: Pile model in ABAQUS

Piles were also analyzed in ABAQUS for a normally consolidated soil profile representative of Gulf of Mexico clay. The same three diameters were considered, 36 in, 72 in, and 144 in.

The piles were modeled as solids with an elastic modulus of 3090432 psi, which is equivalent to a steel pipe pile with thickness equal to the diameter divided by 72. The piles had a Poisson's ratio equal to 0.3. The pile was modeled with 8-node linear brick elements.

The piles extended 10 diameters into the soil. The piles had hemispherical tips, the length of which was included in the 10 diameter embedment. The piles extended one diameter above the soil. The soil extended 4 diameters below the hemispherical tip of the pile. Horizontally, the soil extended 10 diameters from the center of the pile with 8-node linear brick elements and then extended another 10 diameters with infinite elements.

The soil was modeled with 26 soil layers each half a diameter thick, except for the layer starting at the depth of the hemisphere. That layer was 1.5 diameters thick in order to accommodate a structured mesh. The normally consolidated clay considered had a cohesion increasing with depth according to the equation shown below.

$$c = 150psf + \left(\frac{8psf}{ft}\right)x$$

where x is depth. With a submerged unit weight of 32 pcf, the "c/p" ratio was 0.25. To model this profile with discrete layers, soil parameters were entered for a layer based of the depth at the middle of the layer. The soil throughout its depth had a Poisson's ratio of 0.475 and a void ratio of 2.3.

A piecewise linear model was implemented for the soil material based on Von Mises plasticity. This particular plasticity in ABAQUS allows for a tabular entry of a normal stress-normal strain curve for each soil layer. The stress-strain curves used in this study were based on the following relationship from Kondner (1963), Duncan and Chang (1970), and Hardin and Drnevich (1972).

$$\frac{G}{G_{max}} = \frac{1}{1 + \frac{\gamma}{\gamma_{ref}}}$$

where γ is shear strain, γ_{ref} equals the cohesion divided by Gmax, and Gmax is given by

$$\frac{\mathrm{G_{max}}}{\mathrm{p'_r}} = \frac{\mathrm{B}}{(1+\mathrm{e})^{2.4}} \left(\frac{\mathrm{p'}}{\mathrm{p'_r}}\right)^{0.5}$$

where B = 20,000, $\mathrm{p'_r}$ = 20.9 psf, e is the void ratio, and p' is the confining stress. The lateral earth pressure coefficient was taken as 1 so the confining stress was equal to the effective stress. This equation for G_{max} comes from Vardanega and Bolton (2013).

The soil-pile interface had a friction coefficient of 0.35. Gravity was present in the simulation, and the initial state of stress was considered in a geostatic step. The loading was displacement controlled with displacements applied to the center of the pile at the ground line.

Please refer to Section 5.2.2 for the results from these models and the discussion.

4.3 3-D Finite Element Modeling in Sand

Half models of laterally loaded piles in non-cohesive soils were analyzed in the finite element software, ABAQUS, with diameters of 36 in, 72 in, and 144 in. The piles extended 10 diameters into the soil with an additional 0.5 diameter hemisphere below the shaft of the pile, and the piles extended one diameter above the soil. The soil extended 4 diameters below the tip of the pile shaft (or 3.5 diameters below the tip of the hemisphere). Horizontally, the soil extended 10 diameters from the edge of the pile with 8-node linear brick elements and then extended another 10.5 diameters with infinite elements.

The piles were modeled as solids and had an elastic modulus of 3199679 psi. The piles had a unit weight equal to 0.0470 pci and a Poisson's ratio equal to 0.3.

The soil was cohesionless with friction angle equal to 35 degrees, dilation angle equal to 5 degrees, submerged unit weight equal to 0.0333 pci, and Poisson's ratio equal to 0.35. The Young's modulus increased with depth as shown in Table 4.1 (Duncan & Chang, 1970). The deepest soil layer for each model extended from 2 ft above the pile tip to the bottom boundary. The 36 in diameter model had 11 layers, the 72 in diameter model had 21 layers, and the 144 in diameter model had 41 layers.

The soil-pile interface had a friction coefficient of 0.35. Gravity was present in the simulation, and the initial state of stress was considered in a geostatic step. The loading was displacement controlled with

displacements applied to the pile in the horizontal direction 12 in above the ground line. The mesh looked to identical to that shown in Figure 4.6.

These analyses were performed in a computer lab at the University of Texas. The approximate analysis run times were 2.5 hr, 6 hr, and 8 hr for the 36 in, 72 in, and 144 in diameter models, respectively. The intensity of the computation is related to the number of nodes in the model, the soil-pile contact definition, and the nonlinearity of the soil material. At the conclusion of each analysis, values for several output variables were collected and processed at specific nodal locations for each time step to generate load-displacement graphs and p-y curves.

The results from the ABAQUS models were compared with LPILE results employing the API sand p-y criteria. The pile head load versus the pile head displacement curves are shown in Figure 4.7. For the 36 in and 72 in diameter models, the ABAQUS and LPILE results match very well. For the 144 in diameter model, ABAQUS had more pile head displacement at the same level of loading. This indicates that the API sand p-y criteria can result in a stiffer pile response for large size piles. This preliminary finding is consistent with literature published overseas based on FEM studies. When LPILE was run for the 144 in diameter model with the Reese p-y criteria for sand, there was closer agreement with ABAQUS.

In Figure 4.8, the pile head load is divided by the maximum pile head load, and the pile head displacement is divided by the maximum pile head displacement. The three different diameter curves from ABAQUS coincide on this normalized graph. The shape of the load-displacement curve appears independent of diameter.

For all three diameters, p-y curves derived from ABAQUS are compared to API sand p-y curves at a depth of one diameter in Figure 4.9. All three diameters show very good agreement between the two procedures. Although, the ABAQUS p-y curve for the 144 in diameter model does have slightly larger displacements than the API p-y curve. Since ABAQUS p-y curves for all three diameters had reached ultimate at this depth, a normalized plot is shown in Figure 4.10. The resistance, p, was divided by the maximum resistance, p_{ult}, and the displacement, y, was divided by diameter, b. The curves for all diameters fall very close together demonstrating that the shape function is independent of diameter at this depth.

Figure 4.11 and Figure 4.12 compare p-y curves from ABAQUS and the API definition for the three piles at depths of two diameters and three diameters, respectively. Agreement between ABAQUS and API p-y curves at these depths is not as good. At a depth of two diameters, the API p-y curve for the 72 in diameter pile is stiffer than the ABAQUS p-y curve, and the API p-y curve for the 144 in diameter pile is much stiffer than the ABAQUS p-y curve. This trend is even more pronounced at a depth of three pile diameters. It may be that the initial modulus of subgrade reaction, k, should be a function of diameter. The ultimate soil resistance is also lower for the API p-y curves. Continued effort will focus on these differences between API p-y curves and ABAQUS generated p-y curves.

While discrepancies between API p-y curves and ABAQUS generated p-y curves at depth/diameter ratios greater than two did not seem to adversely affect the pile head load versus pile head displacement comparison in Figure 4.7, p-y curves at lower depths could be more influential than they were in our case.

Table 4.1: Young's modulus changing with depth

Layer	Top of Layer	Bottom of Layer	E
	in	in	psi
1	0	12	2031
2	12	48	5059
3	48	84	7911
4	84	120	10126
5	120	156	12019
6	156	192	13707
7	192	228	15249
8	228	264	16681
9	264	300	18024
10	300	336	19294
11	336	372	20504
12	372	408	21662
13	408	444	22774
14	444	480	23846
15	480	516	24882
16	516	552	25886
17	552	588	26862
18	588	624	27811
19	624	660	28736
20	660	696	29639
21	696	732	30521
22	732	768	31384
23	768	804	32230
24	804	840	33059
25	840	876	33872
26	876	912	34671
27	912	948	35456
28	948	984	36227
29	984	1020	36987
30	1020	1056	37735
31	1056	1092	38471
32	1092	1128	39197
33	1128	1164	39913
34	1164	1200	40619
35	1200	1236	41316
36	1236	1272	42004
37	1272	1308	42683
38	1308	1344	43355
39	1344	1380	44018
40	1380	1416	44674
41	1416	1452	45323

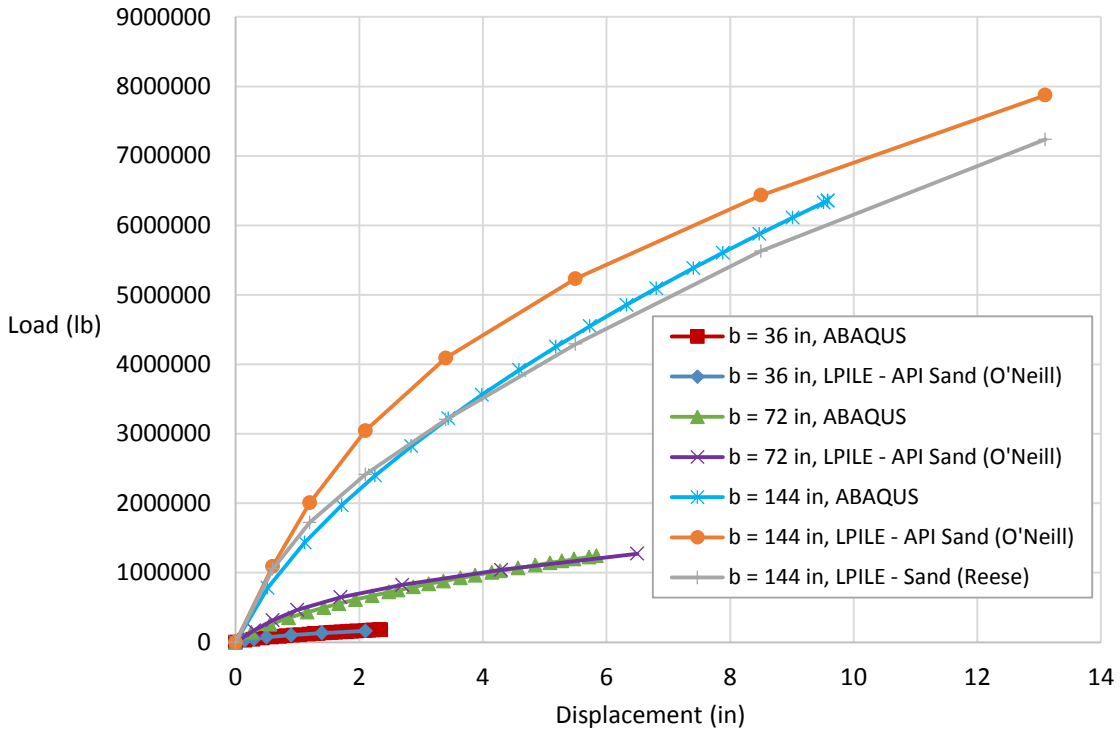

Figure 4.7: Load versus displacement at the pile head from ABAQUS models compared with LPILE results

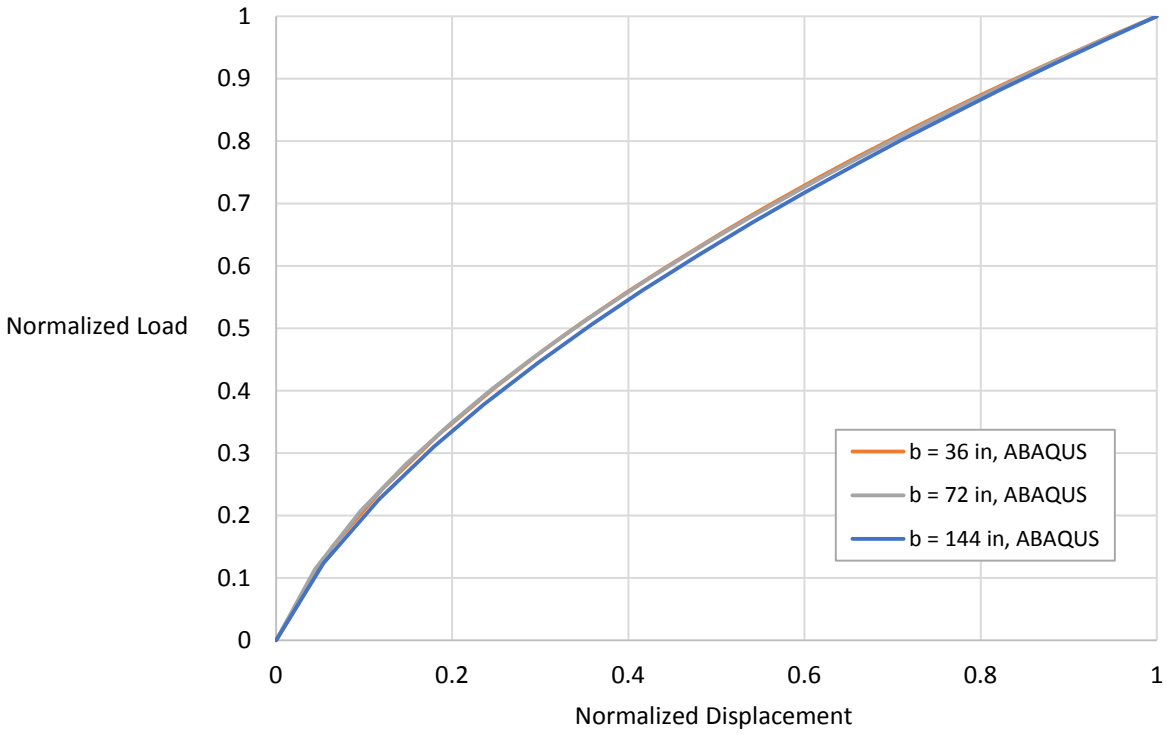

Figure 4.8: Normalized load versus normalized displacement, ABAQUS model results

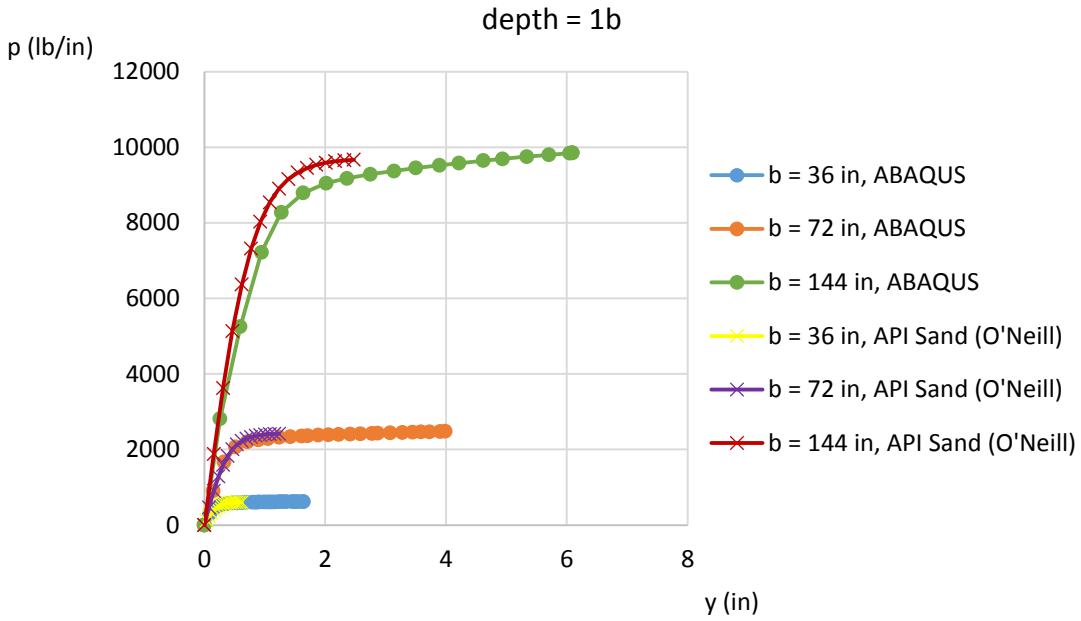

Figure 4.9: P-y curves at a depth of one pile diameter, comparison of ABAQUS results with API model

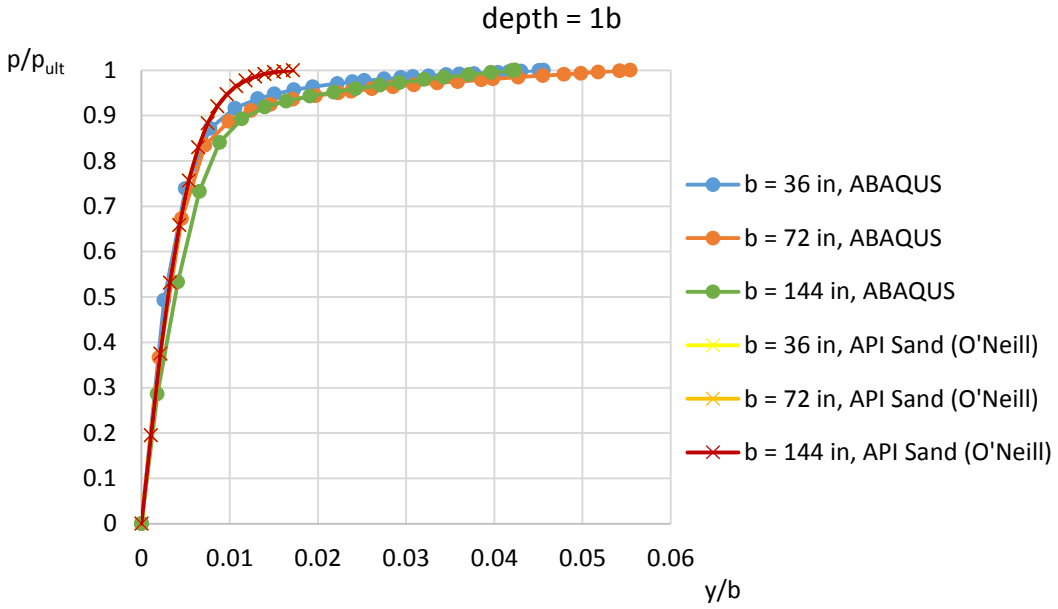

Figure 4.10: Normalized p-y curves at a depth of one pile diameter

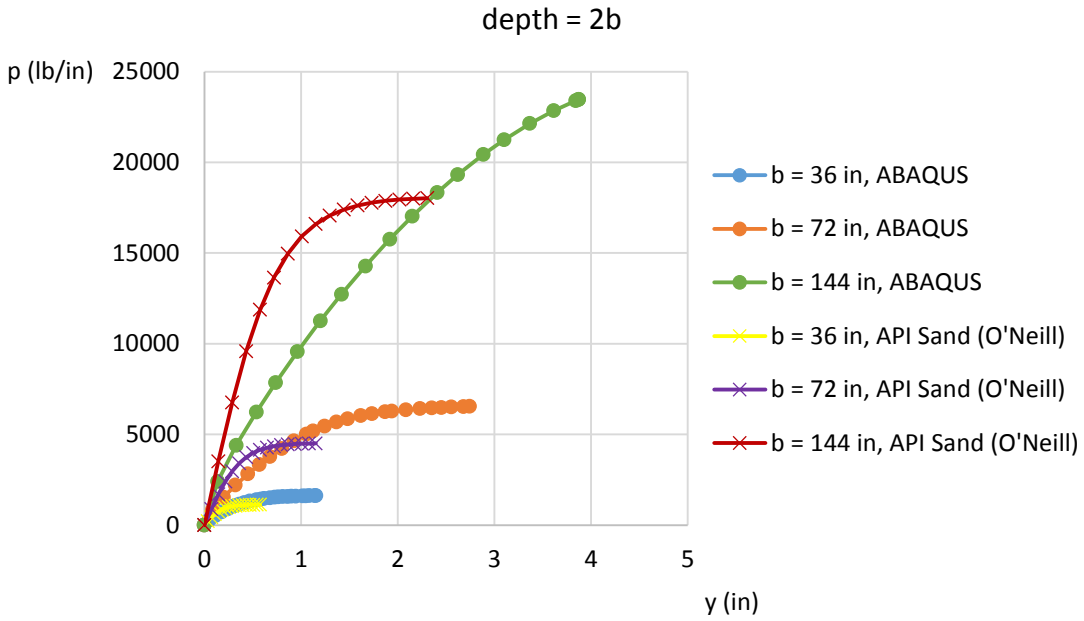

Figure 4.11: P-y curves at a depth of two pile diameters, comparison of ABAQUS results with API model

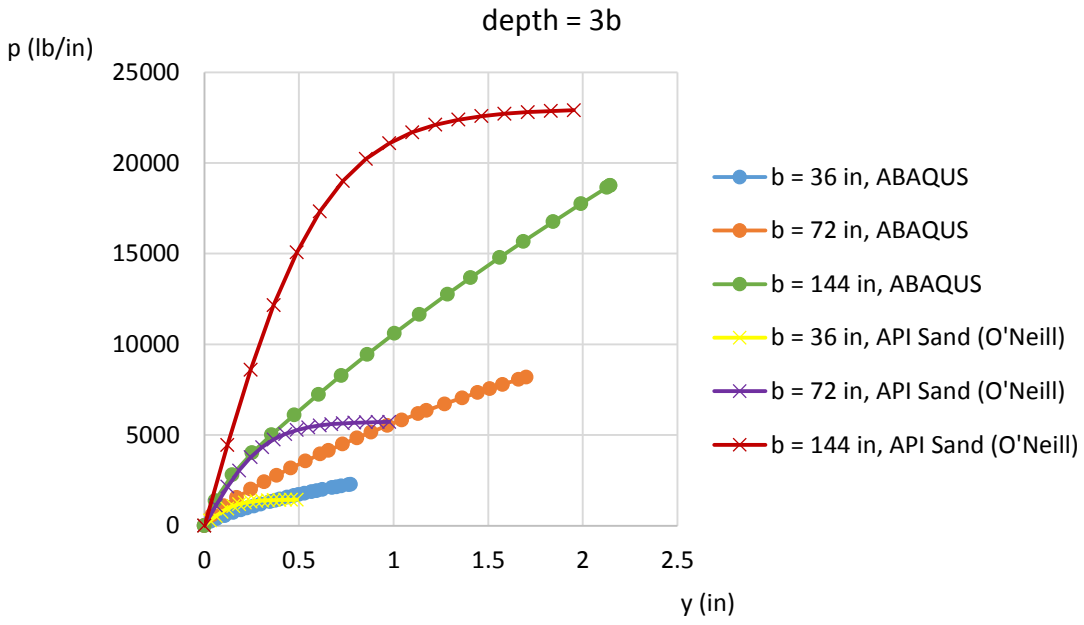

Figure 4.12: P-y curves at a depth of three pile diameters, comparison of ABAQUS results with API model

5 DISCUSSION

5.1 LATERAL CAPACITY OF PILES

The static/monotonic laboratory test and the field test results consistently show that the p-y curves proposed by Matlock (1970) and recommended for the design of offshore piles in API RP 2A/2GEO predict a softer lateral response than is measured. The degree to which the Matlock (1970) curves under-predict the lateral stiffness depends on whether a gap forms in the soil behind the pile at the mudline.

5.1.1 Modification to Matlock (1970) p-y Curves

Figure 5.1 shows an example model test result for static loading compared to the behavior predicted using LPILE with the Matlock (1970) p-y curves. It can be seen that Matlock (1970) p-y curves tend to underestimate the lateral resistance. Previous researchers have made this same observation (e.g., Murff and Hamilton 1993 and Jeanjean 2009) and proposed modifications to the Matlock p-y curves. The p-y model proposed by Jeanjean (2009) was also used to predict the lateral response with LPILE and compare it to measurements (Figure 5.1). In order to expedite the LPILE analyses, an approximate version of the Jeanjean (2009) p-y curves was implemented by using p-multipliers to convert the Matlock (1970) p-y curves. The p-y curves were developed using the "idealized" undrained shear strength profile based on the undisturbed S_u profile measured by T-bar tests. P-multipliers used to convert the Matlock (1970) p-y curves to an approximate version of the Jeanjean (2009) curves were calculated by comparing the N_p profiles according both models (Figure 5.2). A range ε_{50} values from 0.005 to 0.02 were used to establish the p-y curves in these comparisons (Figure 5.1); the value of 0.02 is most appropriate for a normally consolidated to moderately overconsolidated clay.

The model test results consistently show that the Matlock (1970) p-y curves predict a softer lateral response at the pile head than is measured (Figure 5.1 and Figure 5.3 to Figure 5.8). The model test with the pressure sensor readings provides direct evidence that the measured p-y curves at different depths are stiffer than those predicted by Matlock (1970). The load versus displacement curve from a static load test on a 4-in diameter pile instrumented with a tactile pressure sensor is shown in Figure 5.9 (a). The lateral load on this pile was applied at height of 5D above the mudline, and the lateral displacement was measured at two locations to calculate the displacement at any point along its length (Figure 5.9 (b)). P-y curves were derived by plotting the measured net soil pressure acting on a 1-inch segment along the length of the pile (Figure 5.10). The Matlock (1970) curves with $\varepsilon_{50} = 0.02$ underestimate the lateral soil resistance at depths of 8-in (2D), 12-in (3D), and 16-in (4D). Matlock (1970) p-y curve matches reasonably closely with the measured curve at depth of 4-in (1D); this result is not surprising as N_p in this case was much higher than three since the soil profile had a very low undrained shear strength near mudline and it increased with depth. Figure 5.11 shows the distribution of the soil stress around the circumference of the model pile.

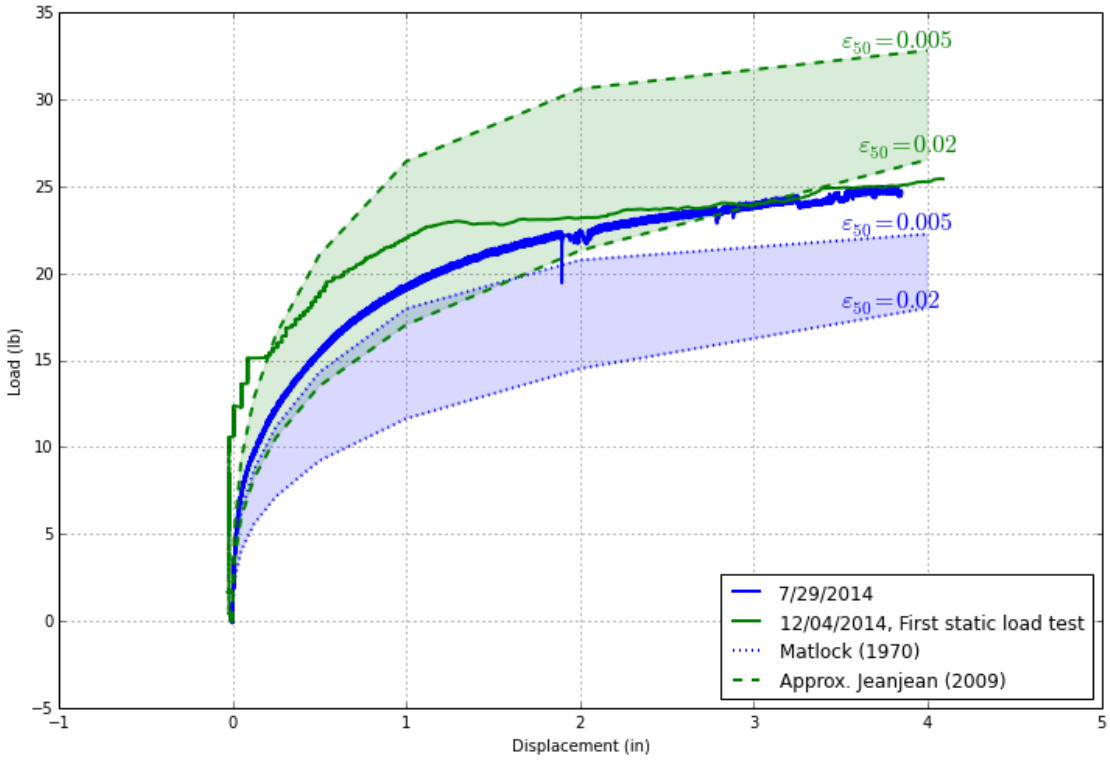

Figure 5.1: Comparison of monotonic lateral load test results with LPILE analyses, normally consolidated to moderately overconsolidated kaolinite, D = 4-inches (no gap formed)

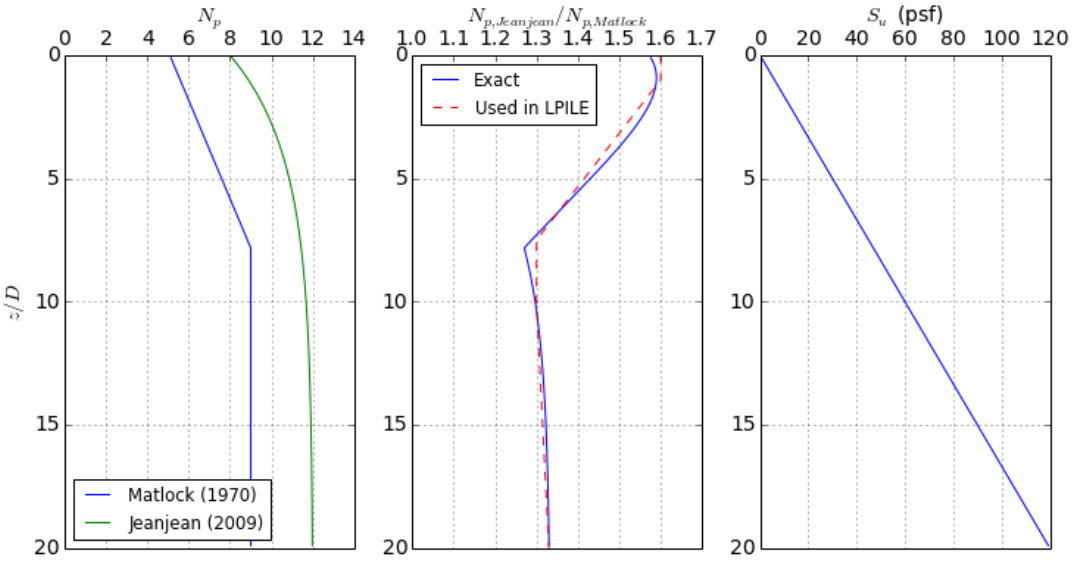

Figure 5.2: Calculation of p-multipliers to convert Matlock (1970) to approximate Jeanjean (2009) in LPILE, based on the idealized undrained shear strength profile and D=4-in

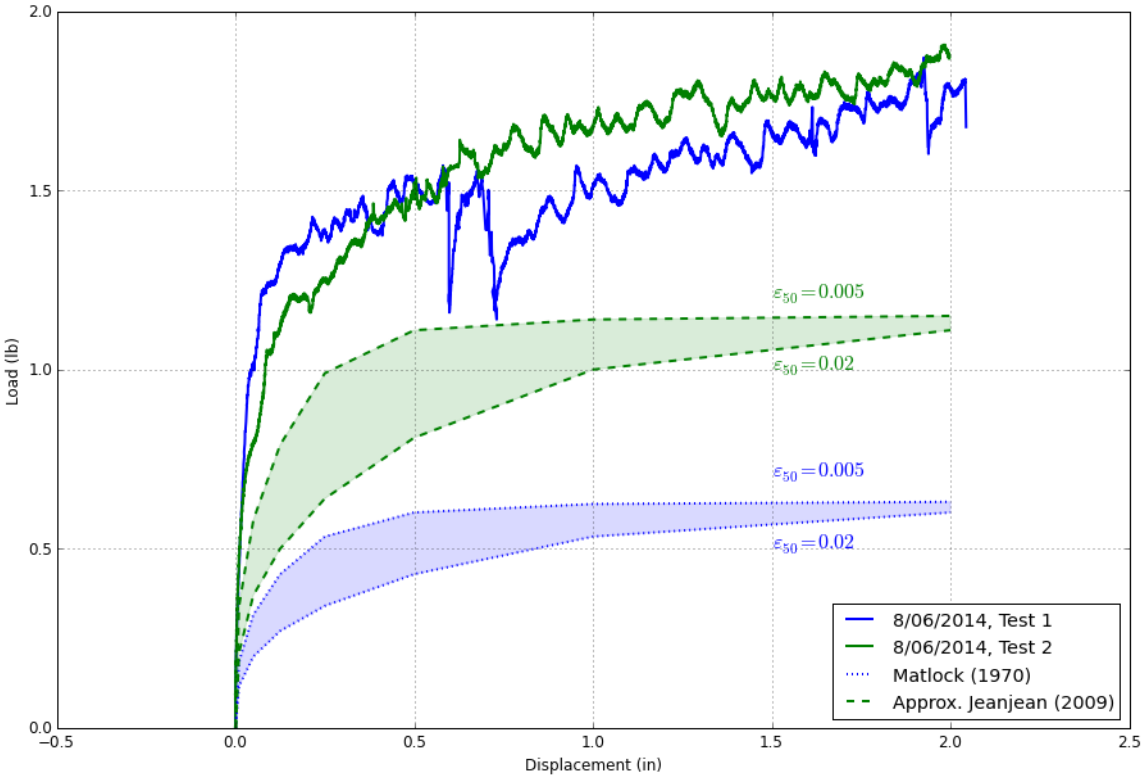

Figure 5.3: Comparison of test results with available p-y models using LPILE, heavily overconsolidated kaolinite (Su = 10-psf), D = 1-inch (no gap formed)

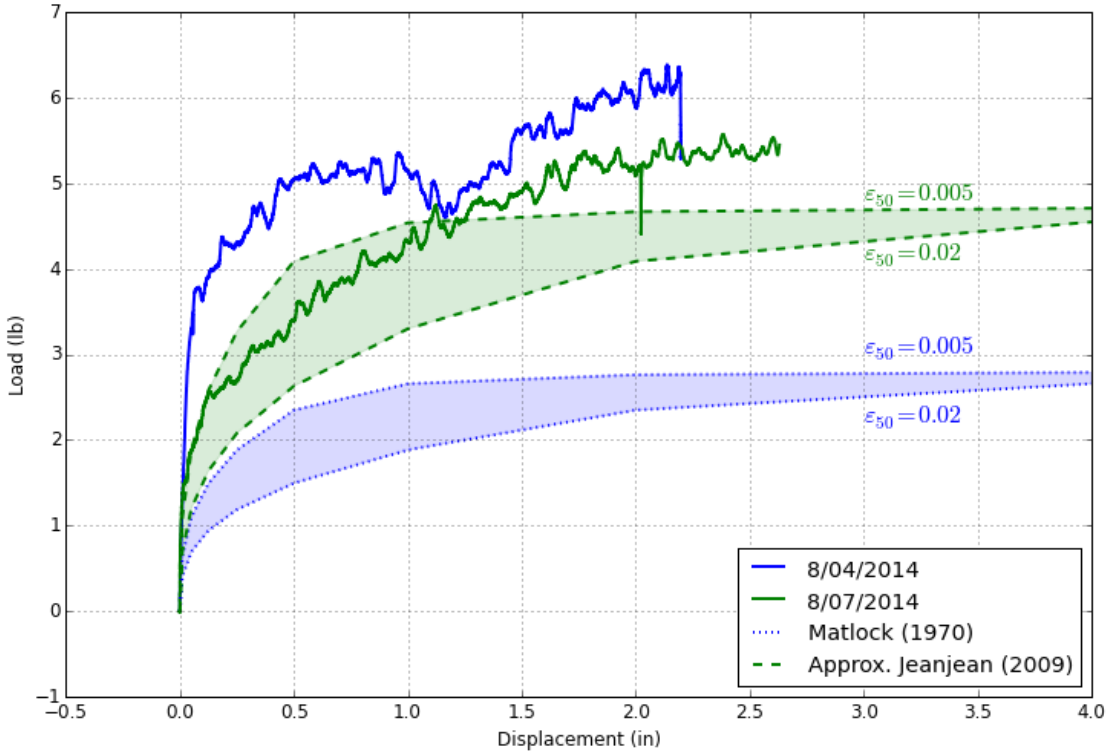

Figure 5.4: Comparison of test results with available p-y models using LPILE, heavily overconsolidated kaolinite (Su = 10-psf), D = 2-inches (no gap formed)

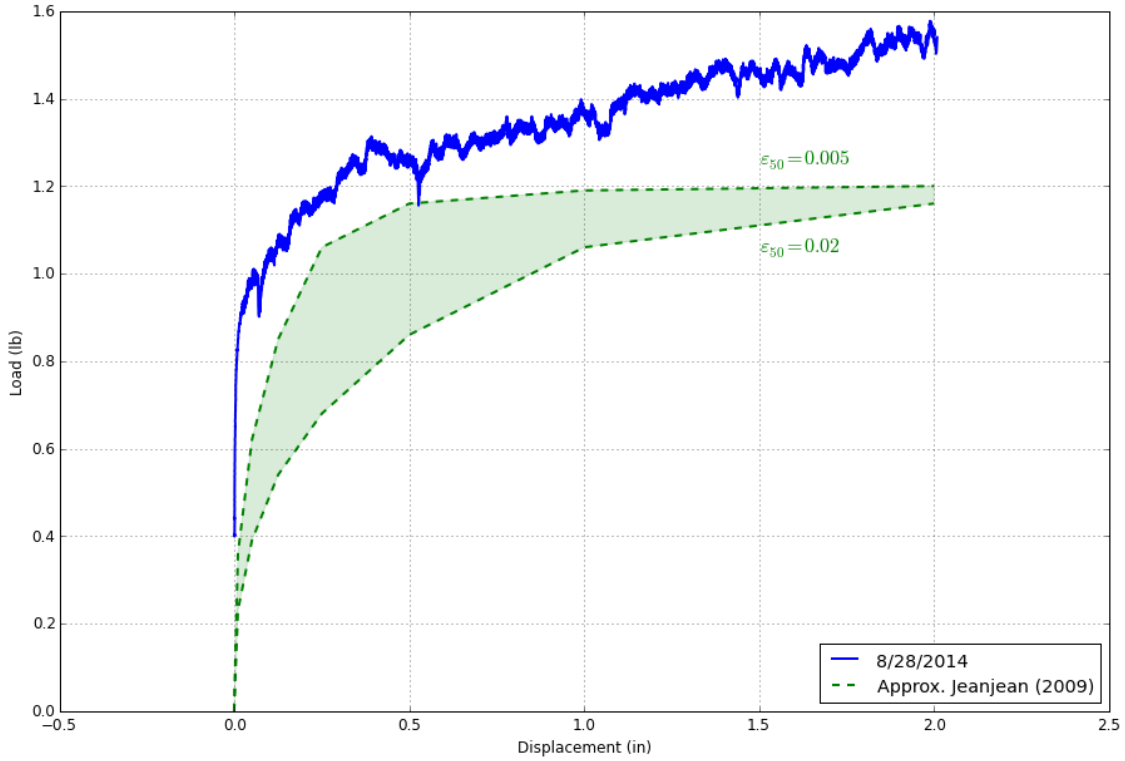

Figure 5.5: Comparison of test results with available p-y models using LPILE, heavily overconsolidated kaolinite (Su = 8-psf), D = 1-inch (no gap formed)

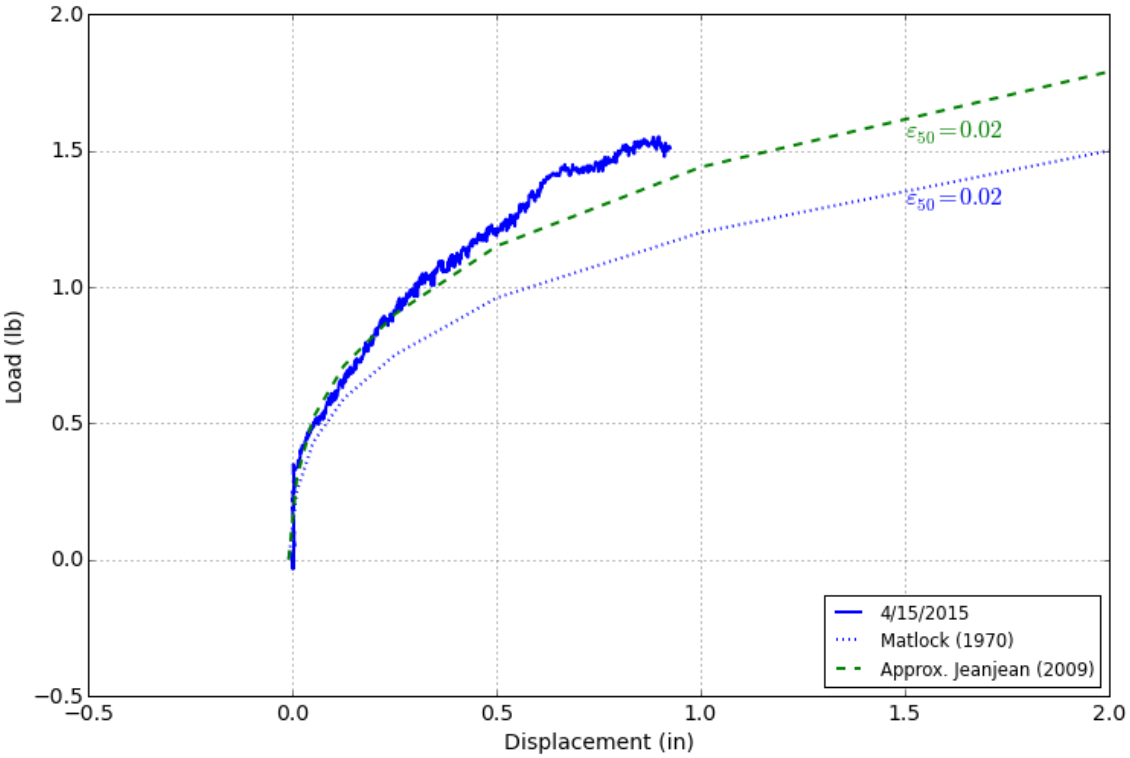

Figure 5.6: Comparison of monotonic lateral load test results with LPILE analyses, normally consolidated Gulf of Mexico clay bed, D = 2-inches (no gap formed)

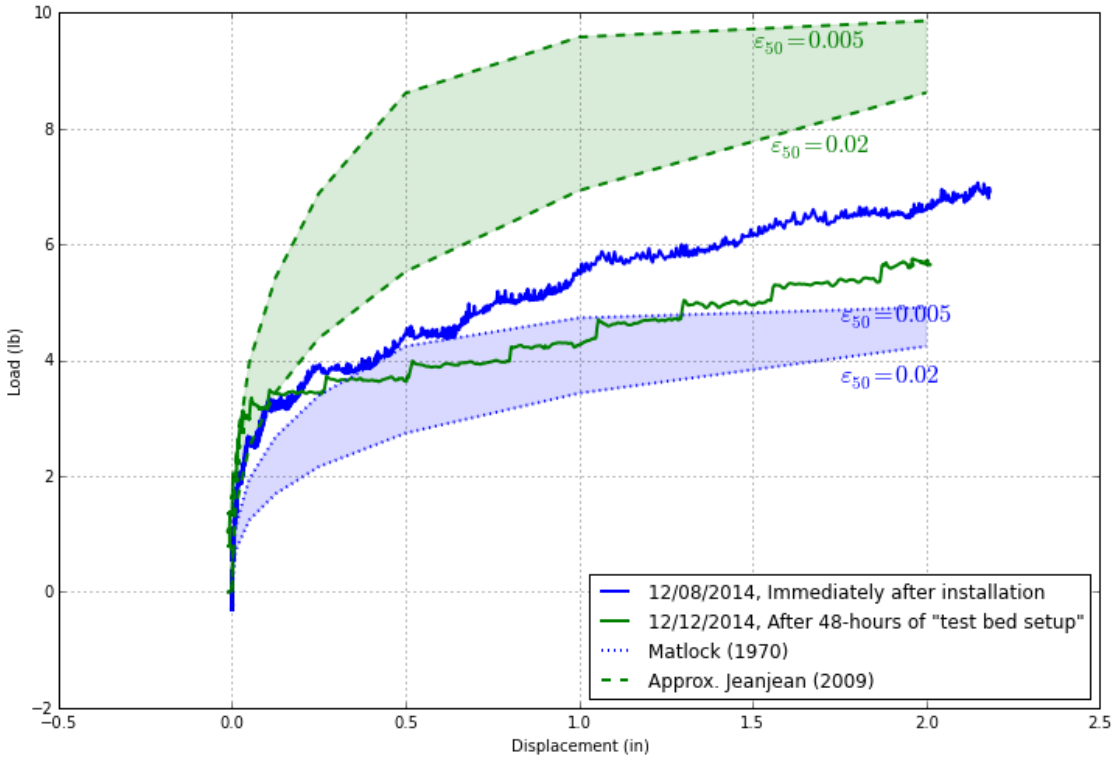

Figure 5.7: Comparison of test results with available p-y models using LPILE, heavily overconsolidated kaolinite clay bed with stiff top crust, D = 2-inches (gap formed)

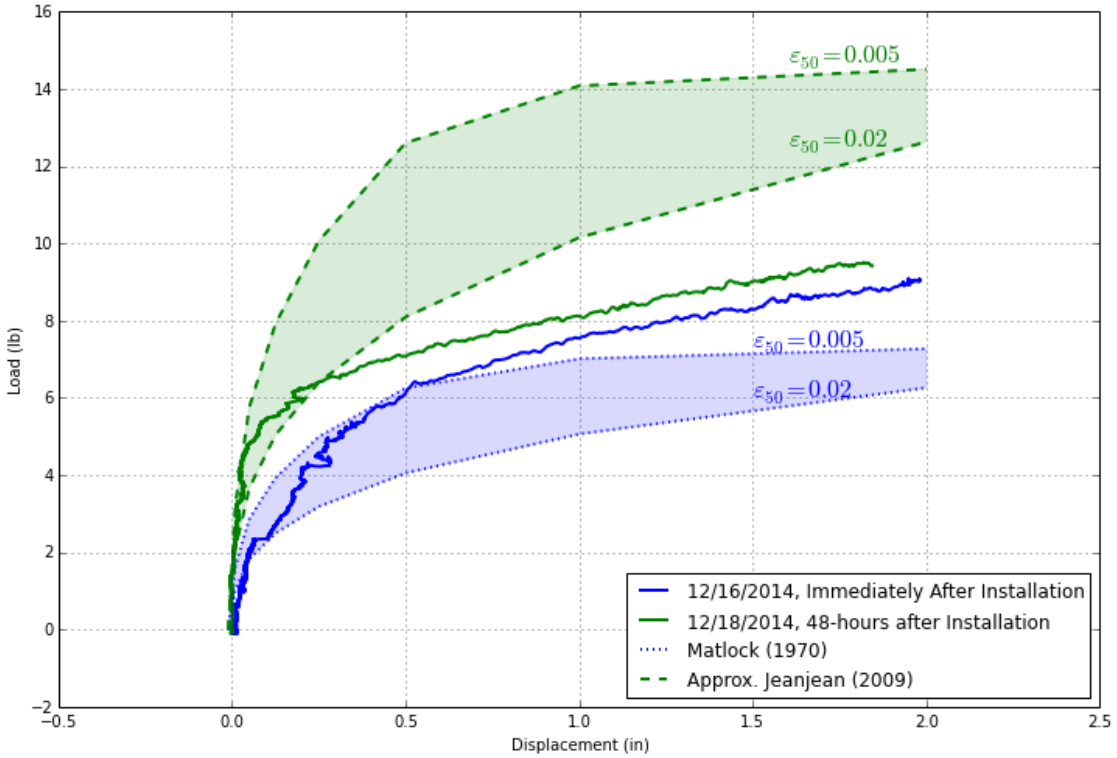

Figure 5.8: Comparison of test results with available p-y models using LPILE, heavily overconsolidated Gulf of Mexico clay bed, D = 2-inches (gap formed)

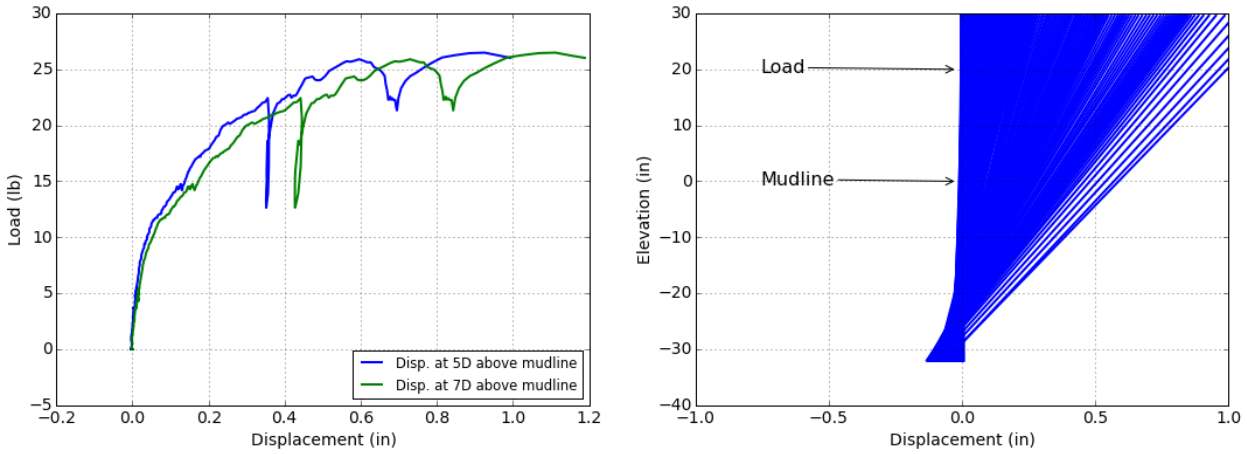

(a) *(b)*

Figure 5.9: Static load test on model pile instrumented with tactile pressure sensor, D=4-inches, normally consolidated to moderately overconsolidated kaolinite, (a) Load versus displacement curves at pile head and 2D above pile head, (b) profile of the pile as the test progressed

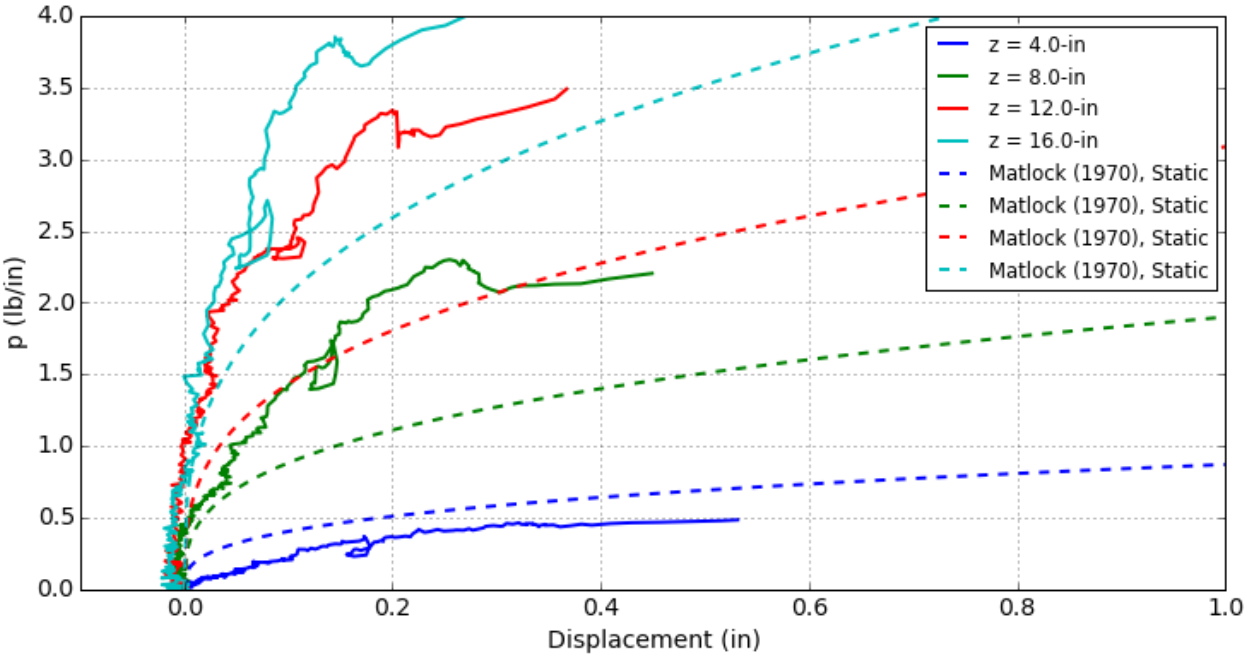

Figure 5.10: P-y curves measured using tactile pressure sensor, D=4-inches

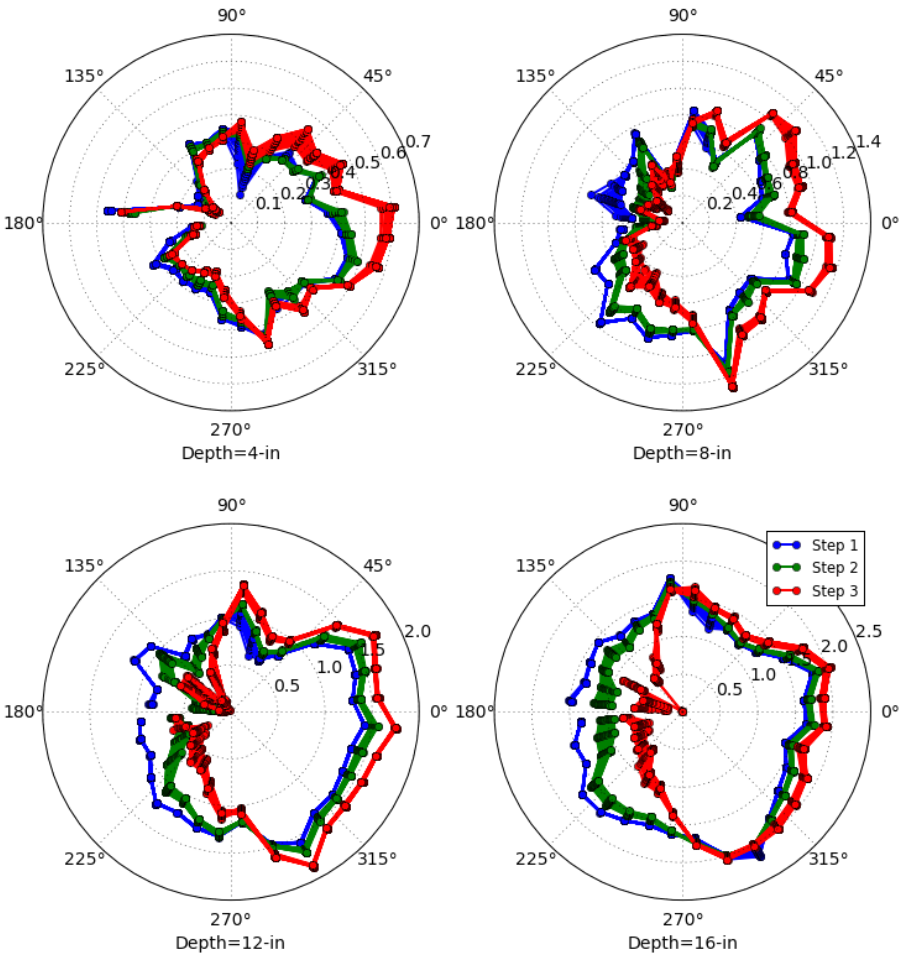

Figure 5.11: Stress distribution along the circumference of the pile, at various depth, D=4-inches (unit of stress = psi; loading direction is 0 degrees)

As with the laboratory model tests, the field tests compiled in the lateral load test database also consistently show that the Matlock (1970) p-y curves under-predict the lateral resistance (Figure 5.12 to Figure 5.16). It is interesting to note that even the Sabine River test, which was used as the basis for the Matlock (1970) p-y curves, shows a measured lateral resistance that is greater than that predicted with the Matlock (1970) curves.

For both the laboratory model tests and the field tests, the p-y curves proposed by Jeanjean (2009) with $\varepsilon_{50} = 0.02$ generally provide a better match to the measured results; this conclusion is particularly true when a gap does not form behind the pile.

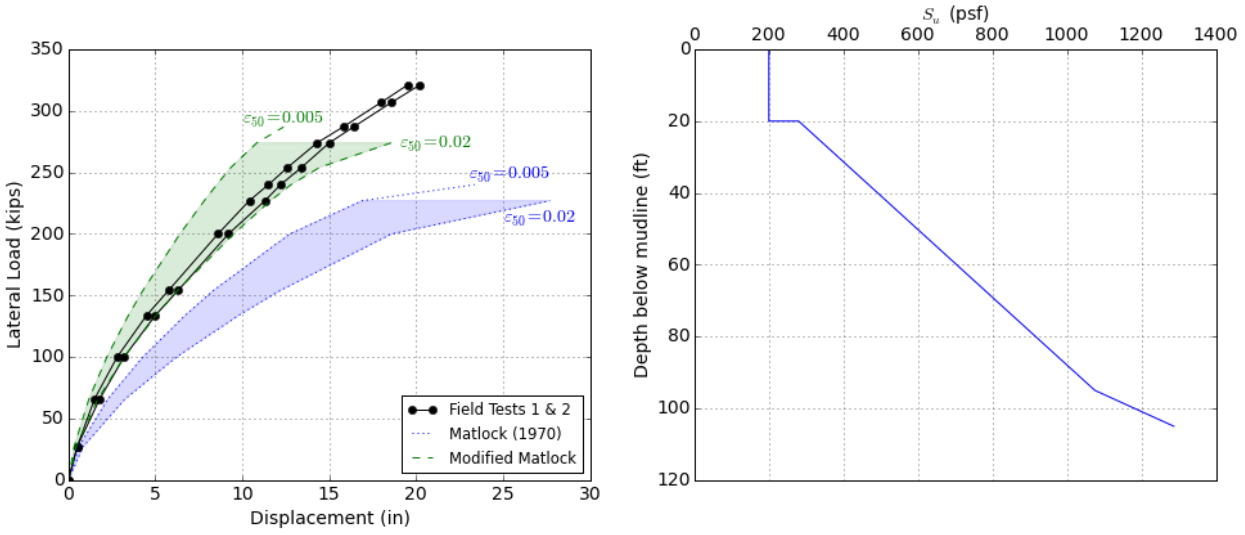

(a) *(b)*

Figure 5.12: (a) Comparison of New Orleans tests (LCR&A, 2010) with LPILE analyses using Matlock (1970) and approx. Jeanjean (2009) p-y curves, D=54-in, (b) Insitu undrained shear strength profile (formation of gap not documented)

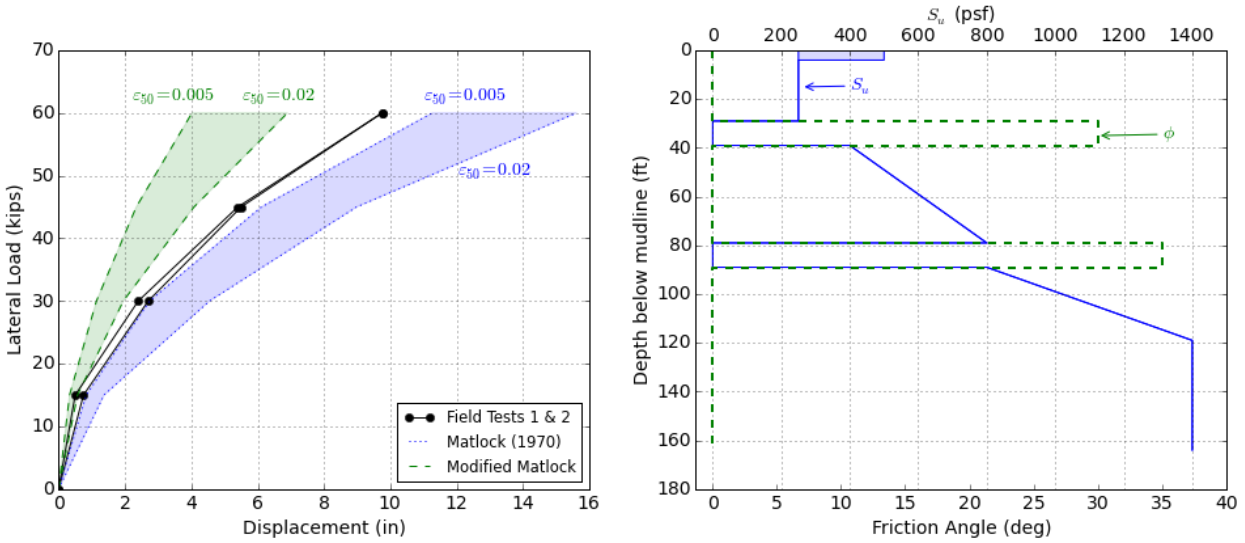

(a) *(b)*

Figure 5.13: (a) Comparison of New Orleans tests (LCR&A, 2009) with LPILE analyses using Matlock (1970) and approx. Jeanjean (2009) p-y curves, D=24-in, (b) Insitu undrained shear strength profile (formation of gap not documented)

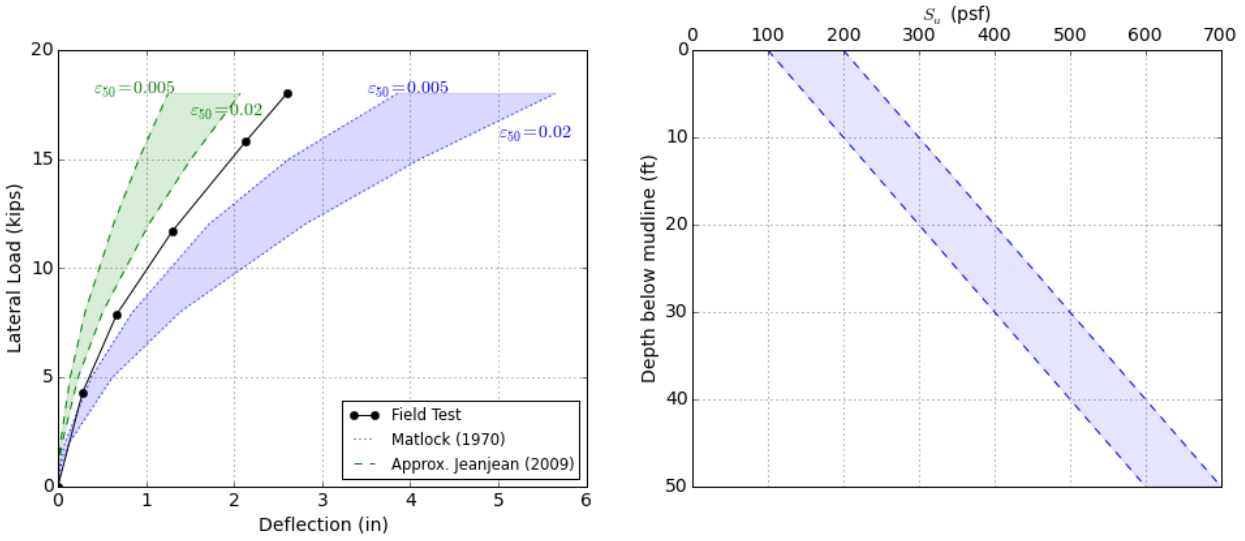

(a) *(b)*

Figure 5.14: (a) Comparison of Sabine River test result with LPILE analyses using Matlock (1970) and approx. Jeanjean (2009) p-y curves, D=12.75-in, (b) Insitu undrained shear strength profile (gap formed)

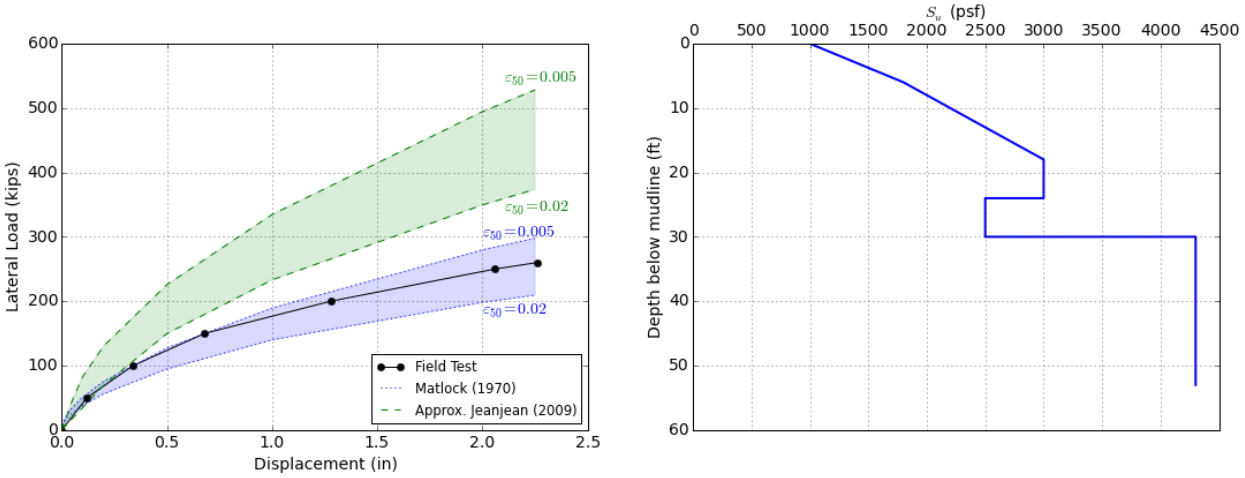

(a) *(b)*

Figure 5.15: (a) Comparison of test results from O'Neill & Dunnavant (1984) with p-y analyses using Matlock (1970) and approx. Jeanjean (2009) p-y curves, D=48-in, (b) Insitu undrained shear strength profile (gap formed)

Note: The undrained shear strength profile at this site was highly non-uniform so, calculating p-multipliers in LPILE to approximate the Jeanjean (2009) p-y curves was not simple. Therefore, a custom written finite-difference code that directly implemented approximate Jeanjean (2009) p-y curves was used instead of LPILE to obtain the results shown in Figure 5.15.

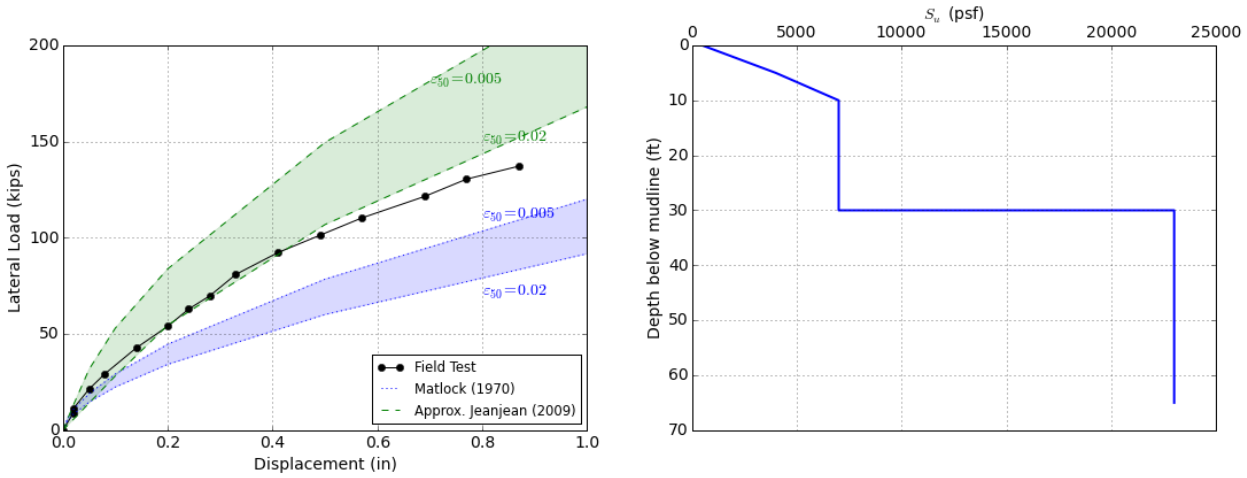

(a) *(b)*

Figure 5.16: (a) Comparison of test results from Reese et al. (1975) with p-y analyses using Matlock (1970) and approx. Jeanjean (2009) p-y curves, D=25.5-in, (b) Insitu undrained shear strength profile (gap formed)

5.1.2 Effect of Gap Forming behind Pile

The laboratory model tests and field tests in which a gap forms on the backside of the pile show relatively less lateral resistance compared to those when a gap does not form (e.g., Figure 5.1 versus Figure 5.7). A clear illustration of the effect of the gap on the lateral resistance is shown in Figure 5.17 and Figure 5.18; in this test, a gap formed at a lateral displacement of 0.9 inches or 0.45 times the diameter and the lateral resistance subsequently dropped in response.

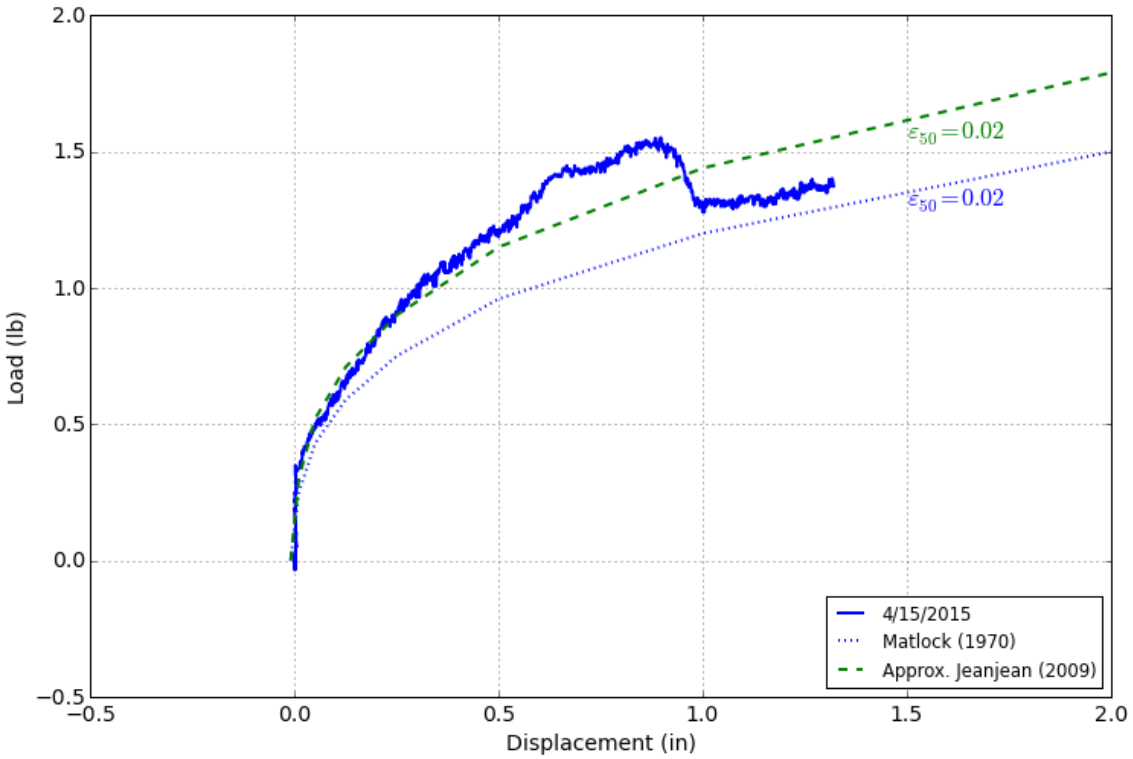

Figure 5.17: Comparison of monotonic lateral load test results with LPILE analyses, D = 2-inches, normally consolidated Gulf of Mexico clay bed, after gap was created

Figure 5.18: Creation of a gap behind the 2-inch diameter pile during monotonic load test, normally consolidated Gulf of Mexico clay bed

A gap formed behind the pile during the tests as a result of the stiff crust as can be seen in Figure 5.19. The first test (12/08/2014) in the clay bed with a stiff crust was done immediately after installation and the second test (12/12/2014) was done on the same pile after an additional 2-days of "test bed setup" time. The test with a longer "test bed setup" time had a more brittle response and a distinct bend-over point corresponding to the initiation of the gap can be seen in the load-displacement (Figure 5.7).

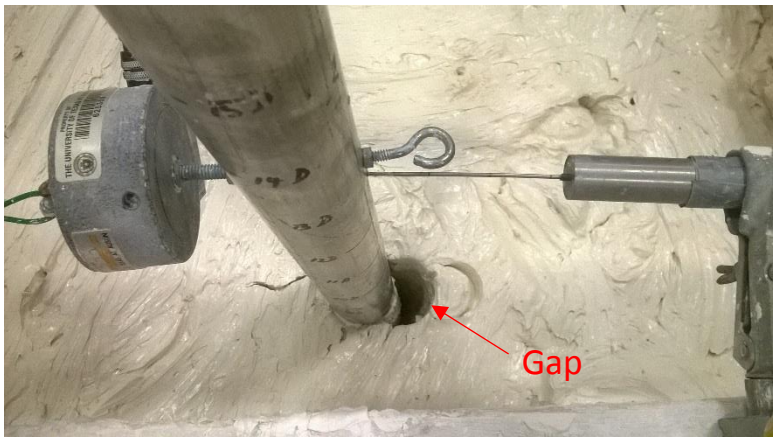

Figure 5.19: Creation of a gap behind the pile, D = 2-in, heavily overconsolidated kaolinite with a stiff top crust

There are no field tests on laterally loaded piles in which it was specifically reported that a gap did not form during loading. Based on the lab test results, the most likely scenario for a field test without gapping would be that of a pile installed in a clay bed with an undrained shear strength profile that increases with depth and with relatively low value at the mudline. The field test on the 54-in diameter pile carried out in New Orleans by Lymon C. Reese & Associates in 2010 is a good candidate for representing a case with no gap; the undrained shear strength profile at this location is close to normally consolidated at the mudline (the ground surface was under approximately 8 feet of water). This field test result is very similar to the laboratory model tests in which a gap did not form, with the measured lateral response being close to that predicted by the Jeanjean (2009) p-y curves with $\varepsilon_{50} = 0.02$ (Figure

5.12). An interesting comparison for this test is a companion test on a 24-in diameter pile in which a softer lateral response was measured (Figure 5.13). Unlike the 54-in diameter pile test in New Orleans, this site was not under water resulting in a much drier and stiffer top crust, which in turn could have led to gapping.

When gapping occurs, the lateral response is still consistently stiffer than that predicted using the Matlock (1970) p-y curves. However, the Matlock (1970) p-y curves provide a reasonable lower bound on the lateral resistance.

At present, we do not have a simple or general way to predict whether a gap will form. It depends on (1) the strength of the soil relative to the overburden stress (i.e., the overconsolidation ratio), (2) the stiffness of the soil as stress is relieved by the pile moving away, (3) the magnitude of the lateral displacement of the pile, and (4) the three-dimensionality of the shearing zone in the soil at the vicinity of the pile (meaning that the pile diameter may be important). Others have similarly acknowledged the importance of a gap forming without being able to provide general or clear guidance about whether it will happen. Murff & Hamilton (1993) assumed that a gap was created behind the pile when they proposed their model for calculating lateral bearing capacity factors (N_p). They "conservatively" assumed that a gap formed behind the pile to derive their upper-bound plasticity solution but, stated that it is possible for suction to develop on the back side of the pile and increase the soil resistance in the wedge failure region. However, they did not provide any guidance on how to predict whether gapping would occur or not. A similar problem was encountered in the failure of I-walls in New Orleans levees during hurricane Katrina. The formation of a gap behind the I-wall when it was laterally loaded was identified as a key contributor to its failure (Brandon et al., 2008). However, the investigators were "unable to predict with a high degree of reliability" whether or not a gap will form at any particular location behind an I-wall.

5.2 EFFECT OF PILE DIAMETER

Both laboratory model tests results and numerical analyses indicate that the effect of pile diameter is appropriately accounted for in normalizing the p-y curves by the pile diameter, as is proposed by Matlock (1970) and is the current standard of practice. We believe this conclusion about the p-y curves scaling with diameter is valid for any L/D ratio. However, for very small L/D ratios (e.g., $L/D < 1$), the following additional factors need to be considered:

- the resistance mobilized in the soil at and around the tip will become significant; and
- the interaction between the lateral resistance on the side of the pile and the resistance at the tip of the pile may affect the p-y curves near the tip.

Therefore, the simplest way to qualify this conclusion is that it applies to any L/D ratio provided that the lateral resistance at the tip of the pile is relatively small or negligible. In our testing with L/D ratios as small as eight, this tip resistance and its interaction with the side resistance was not significant (at least until very large pile head displacements).

5.2.1 Laboratory Test Results

Figure 5.20 shows the normalized results from the lateral load test to failure on all three piles by dividing the displacement by the diameter of the pile and dividing the load by the ultimate load. The ultimate load for this particular analysis was defined as the load carried by the pile at a displacement of 1D where D is the pile diameter.

The normalized load-displacement curves coincide very closely but it should be noted that the method of normalizing that we have chosen forces the curves to coincide at $y = 0$ and $y = D$. Therefore, any difference due to diameter effects will only appear in the form of a divergence in the middle portion of the curve. The difference in the middle portion of the curves in Figure 5.20 is very small and could easily be due to experimental errors.

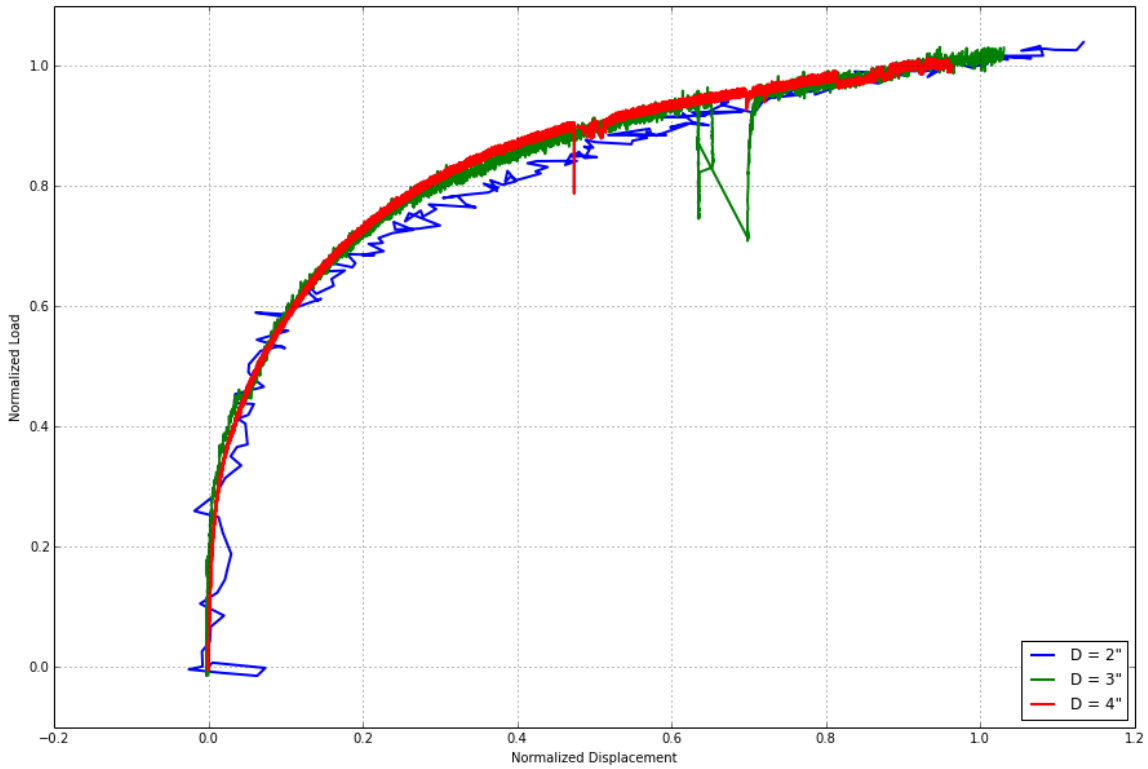

Figure 5.20: Normalized monotonic lateral load tests

One of the concerns we had was whether defining the ultimate lateral capacity of a pile based on an arbitrarily selected lateral displacement was satisfactory. To address this concern we used a second method where the ultimate lateral capacity of a pile obtained by fitting in a hyperbolic curve of the form shown below, to the measured data.

$$P = a \tanh by^c \qquad (1)$$

$$P - Lateral\ load\ at\ pile\ head \qquad y - lateral\ displacement \qquad a, b, c - Fitting\ parameters$$

Note: This form of curve was proposed by Dunnavant & O'Neill (1989) for p-y curves and later used by O'Neill, Reese, & Cox (1990) and Jeanjean (2009).

Figure 5.21(a) shows the load-displacement curves measured at the pile head (5D above the mudline) for each of the models. Figure 5.21(b) shows the three normalized load-displacement curves. Notice that the curves are not forced to coincide at $y = D$. Despite this extra degree of freedom, the curves are still very close together with little or no discernible difference in shape. This led us to conclude that the pile diameter effect was sufficiently accounted by both procedures of normalizing.

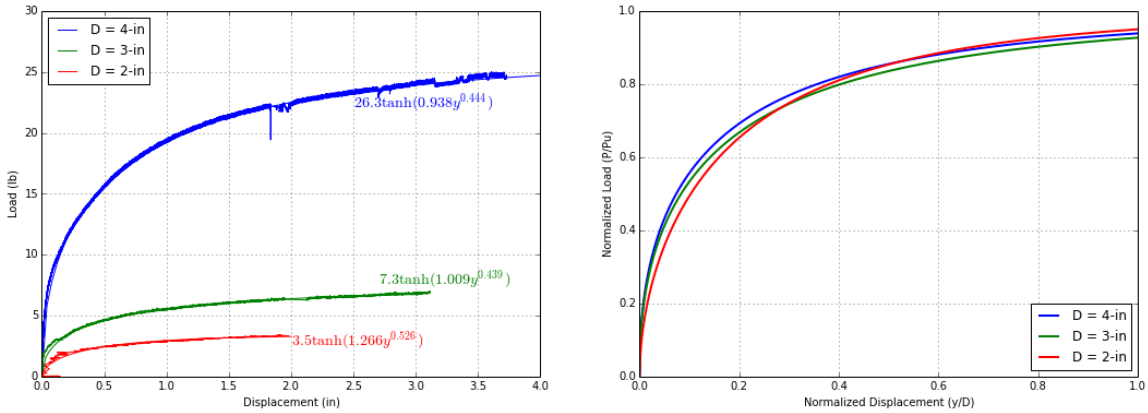

(a) (b)

Figure 5.21: Load versus displacement curves, normally to moderately overconsolidated kaolin clay bed

Figure 5.22 shows a plot of normalized load-displacement curves of all the monotonic tests done in the overconsolidated soil bed. While there is relatively greater variation in the measured curves (presumably due to the small loads with small diameter piles), the general conclusion is the same as that for the normally to moderately overconsolidated test bed.

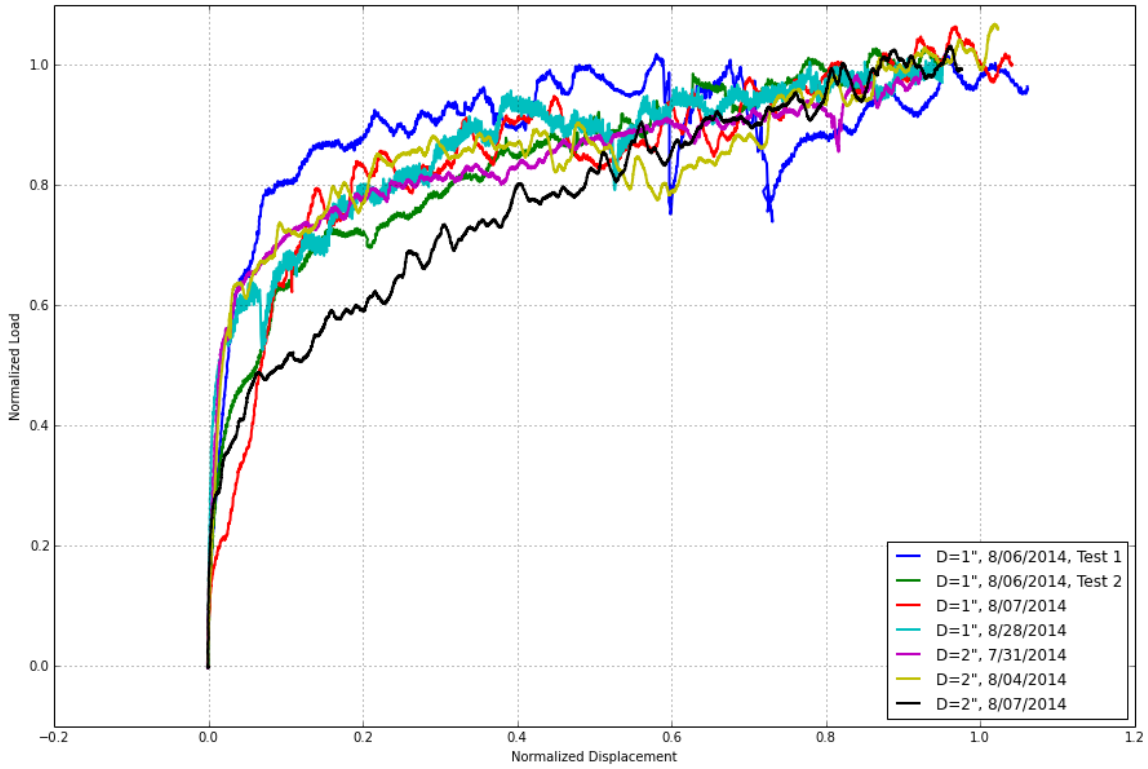

Figure 5.22: Normalized monotonic lateral load tests (overconsolidated soil bed)

5.2.2 3-D Numerical Modelling in Clay

5.2.2.1 Constant Shear Strength Profile versus Depth

The results from the 3-D ABAQUS models were compared with LPILE results with the Matlock (1970) p-y model. The load versus displacement curves from numerical models of three full-scale piles are shown in Figure 5.23. The LPILE results using Matlock (1970) are slightly different from the ABAQUS results. According to Figure 5.23, Matlock (1970) estimates a higher initial stiffness and a lower ultimate capacity compared to the ABAQUS. However, these differences are consistent for all three pile diameters which lead us to conclude that Matlock (1970) is able to reasonably account for large changes in the pile diameter.

The load and the displacement at the pile head from the ABAQUS models were normalized by dividing by $P_{ultimate}$ and pile diameter respectively. The normalized curves (shown Figure 5.24) coincide with each other perfectly, showing that this method of normalizing is able to sufficiently account for any pile diameter effects.

Further evidence to support this conclusion is provided in Figure 5.25 and Figure 5.26, which show p-y curves from depths of two and three pile diameters respectively, for all three piles that were modelled. The differences in initial stiffness and ultimate value seen between the load versus displacement curves from LPILE and ABAQUS are also seen in the p-y curves but, they are consistent across all three pile diameters.

Figure 5.27 shows the normalized p-y curves from ABAQUS at a depth of one pile diameter.

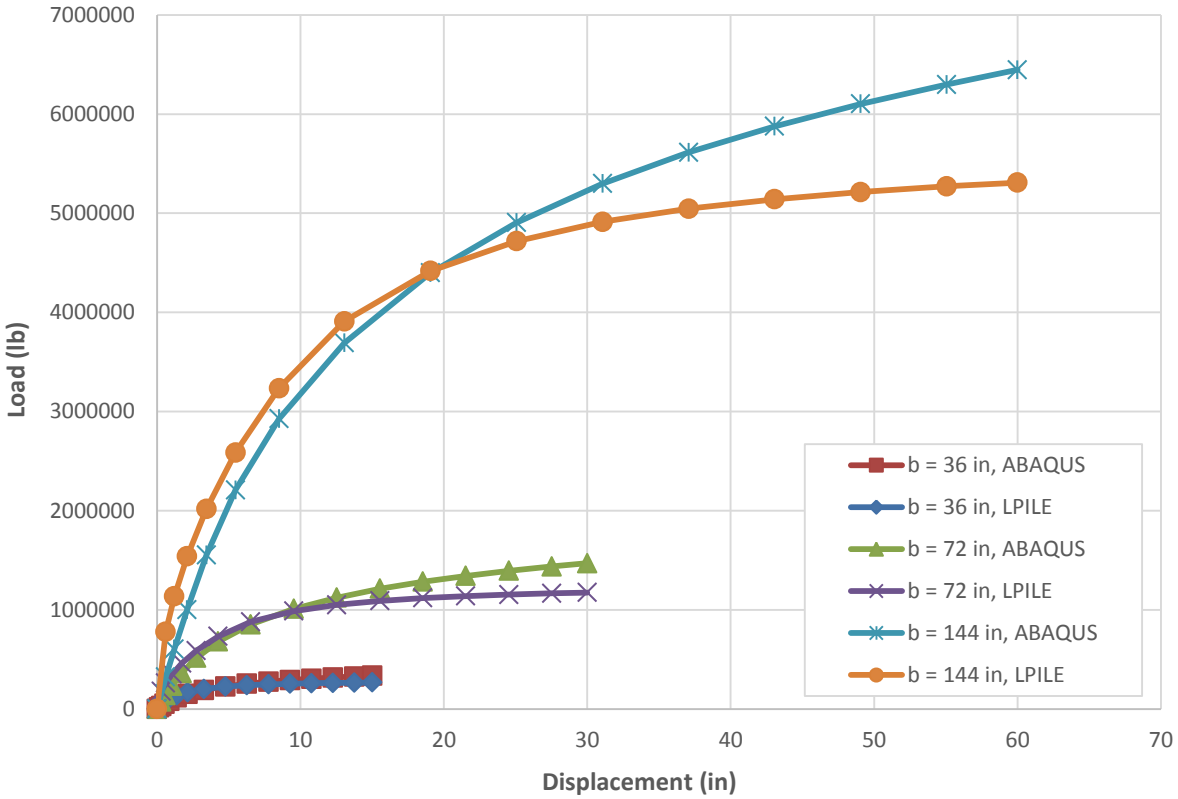

Figure 5.23: Load versus displacement at the pile head from ABAQUS models compared with LPILE results

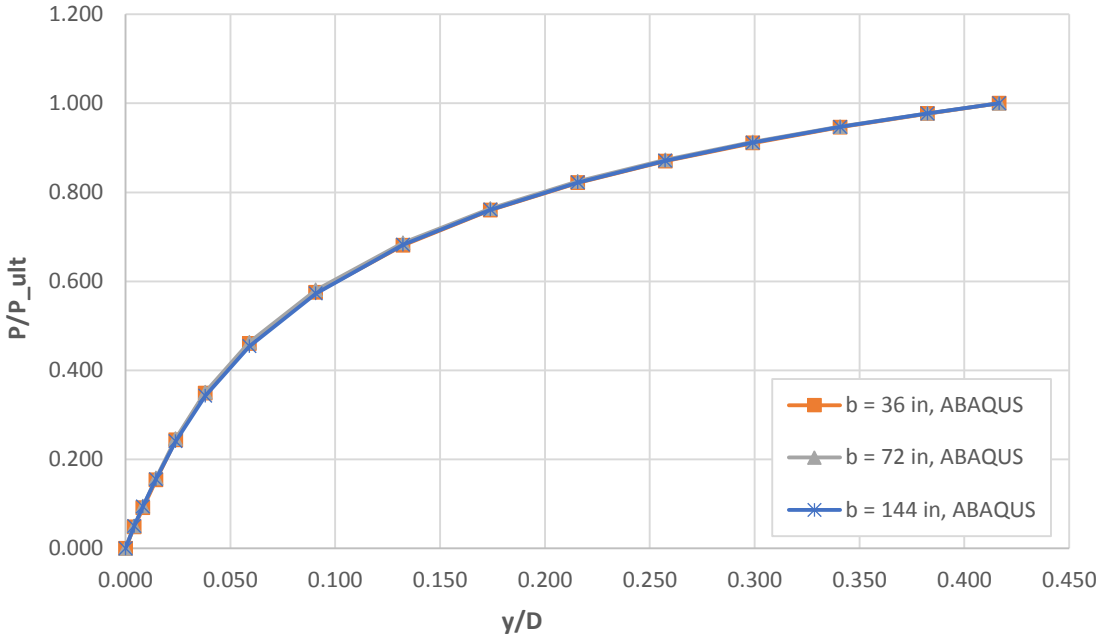

Figure 5.24: Normalized load versus normalized displacement, ABAQUS model results

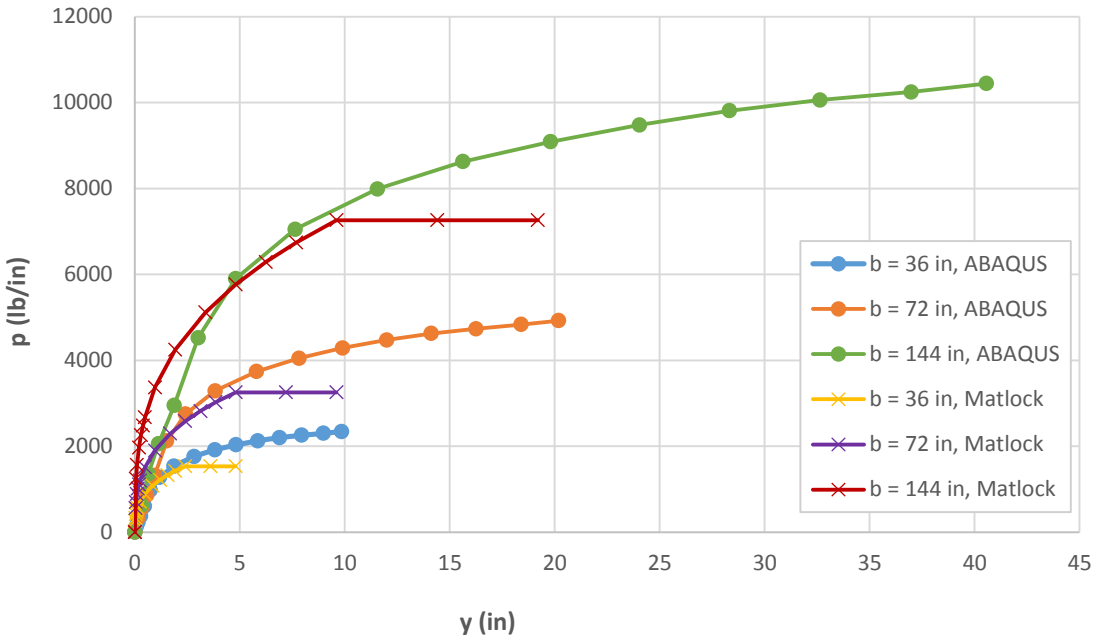

Figure 5.25: P-y curves at a depth of two pile diameters, comparison of ABAQUS results with Matlock (1970) model

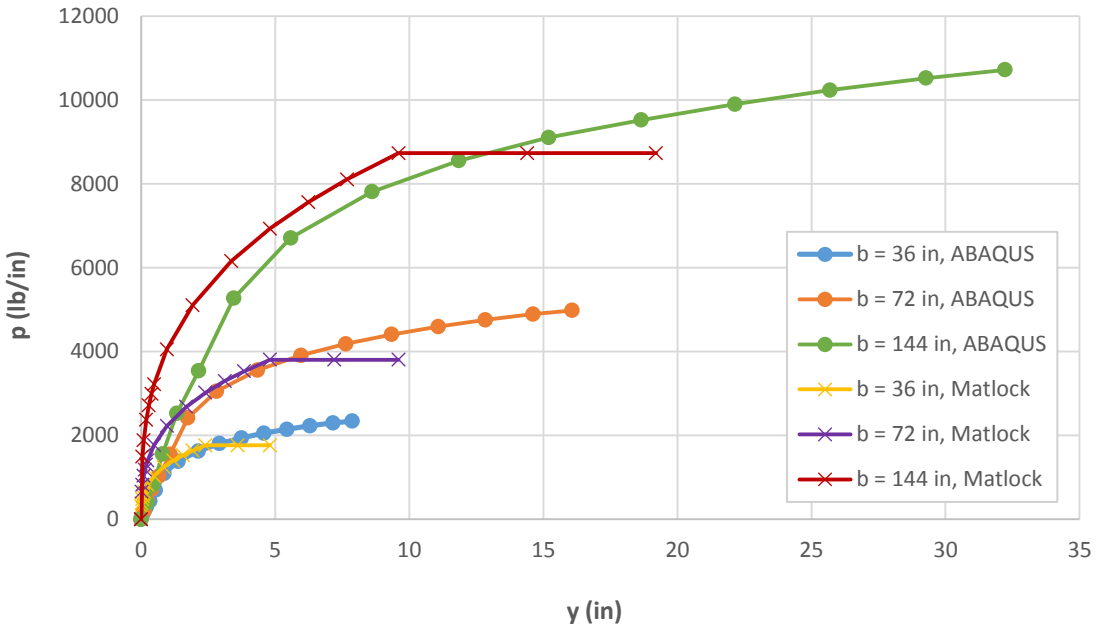

Figure 5.26: P-y curves at a depth of three pile diameters, comparison of ABAQUS results with Matlock (1970) model

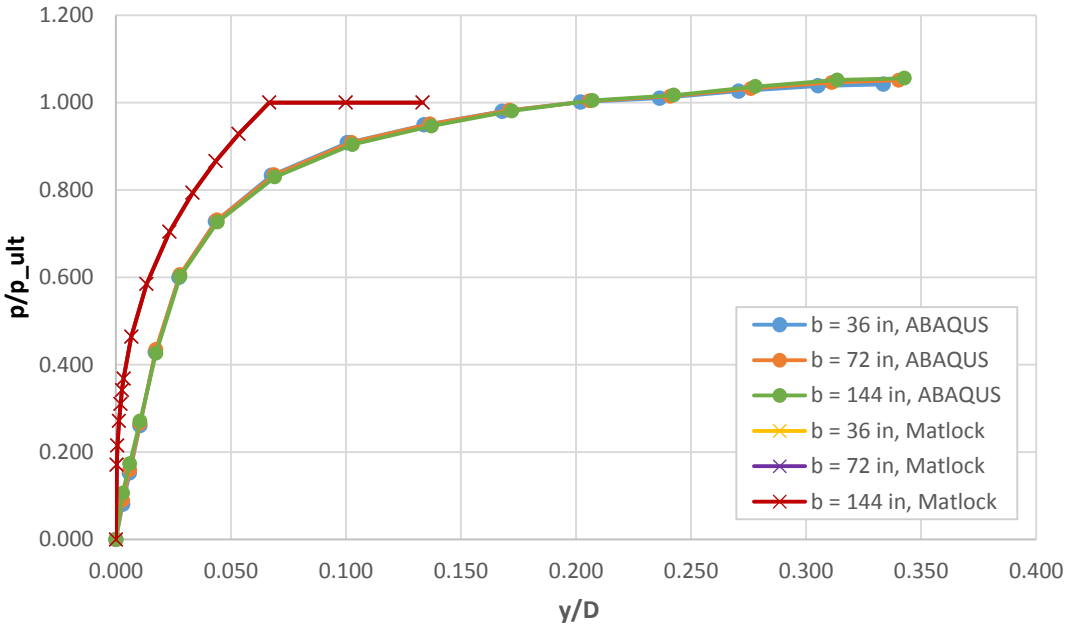

Figure 5.27: Normalized p-y curves at a depth of 1D

5.2.2.2 Increasing Shear Strength Profile versus Depth

Figure 5.28, Figure 5.29, Figure 5.30, and Figure 5.31 show that the diameter affect is adequately accounted for by normalization, as was the case for the other soil profiles. In the Normalized Load versus Normalized Displacement graph, displacement is normalized by diameter, and the load is normalized for the load at a normalized displacement of 0.7. In the normalized p-y curve graphs, p_{ult} is equal to p at a normalized displacement of 0.7

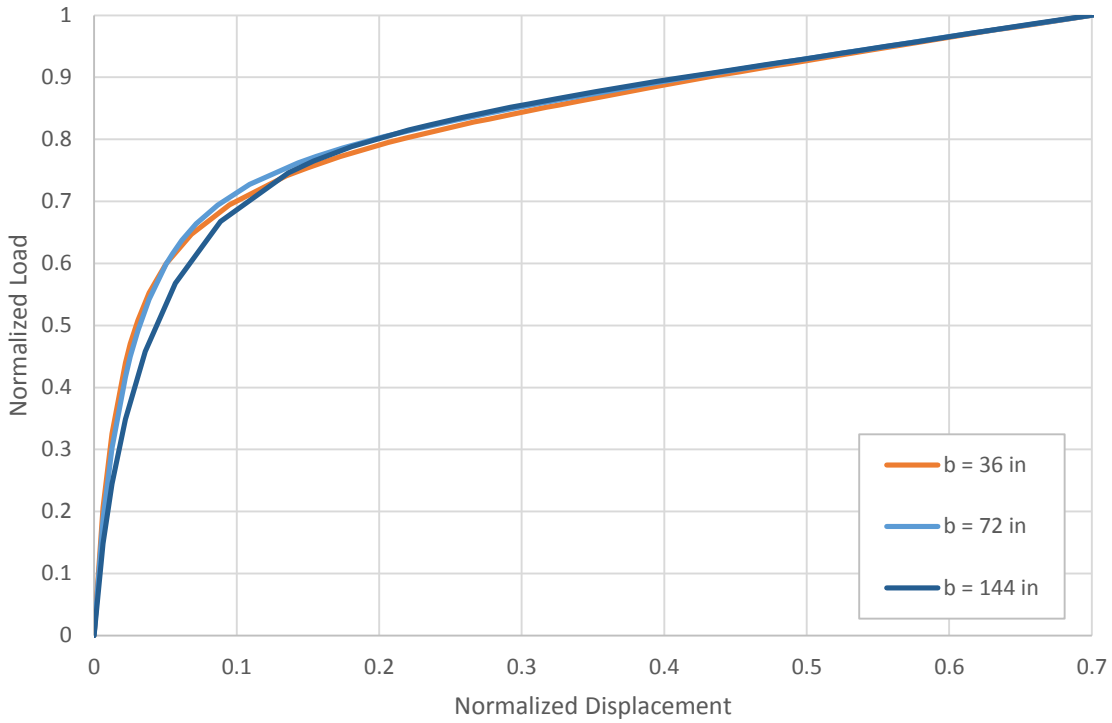

Figure 5.28: Normalized load versus displacement at the pile head

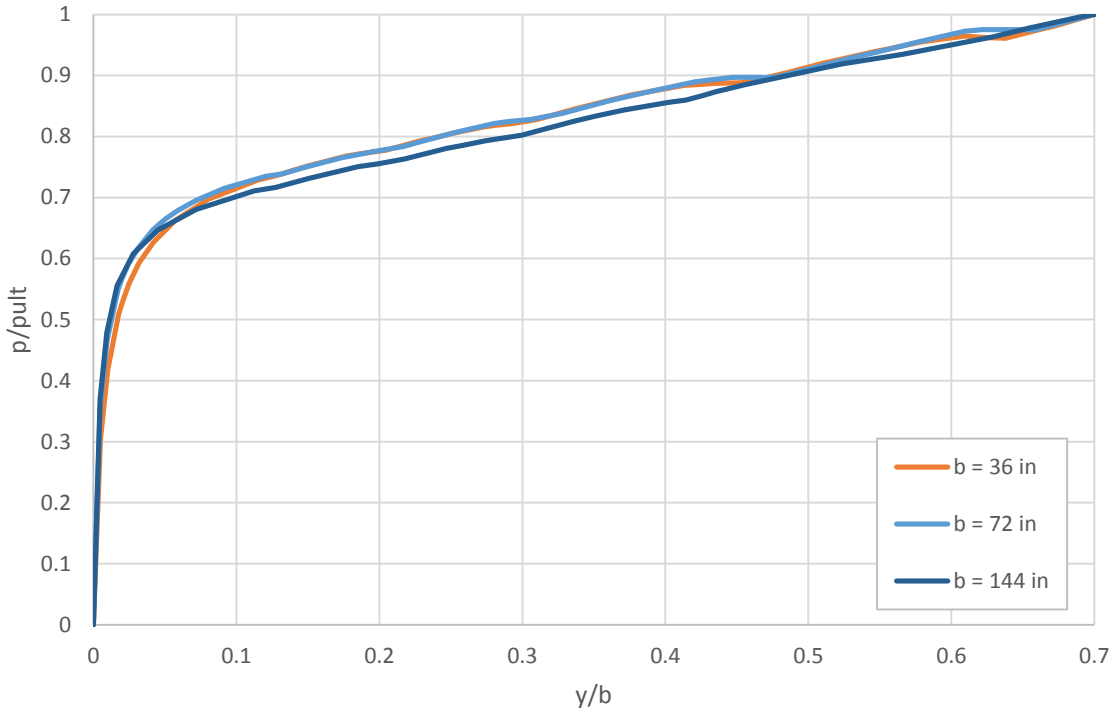

Figure 5.29: Normalized p-y curves, Depth =1b

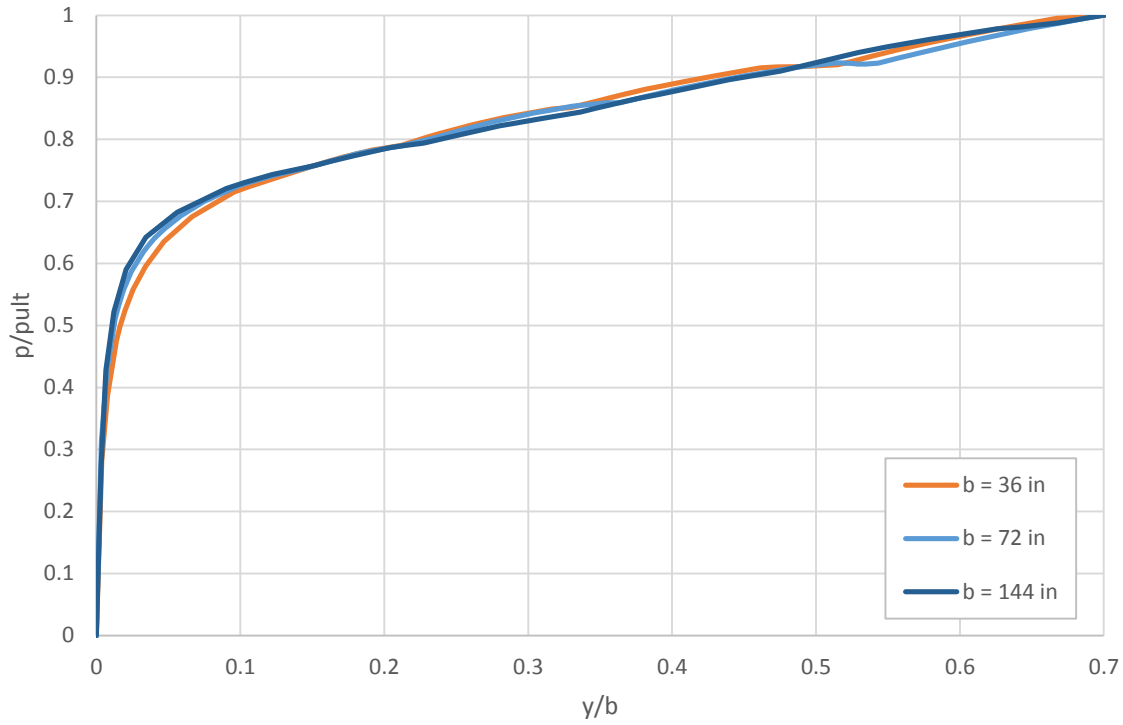

Figure 5.30: Normalized p-y curves , Depth = 2b

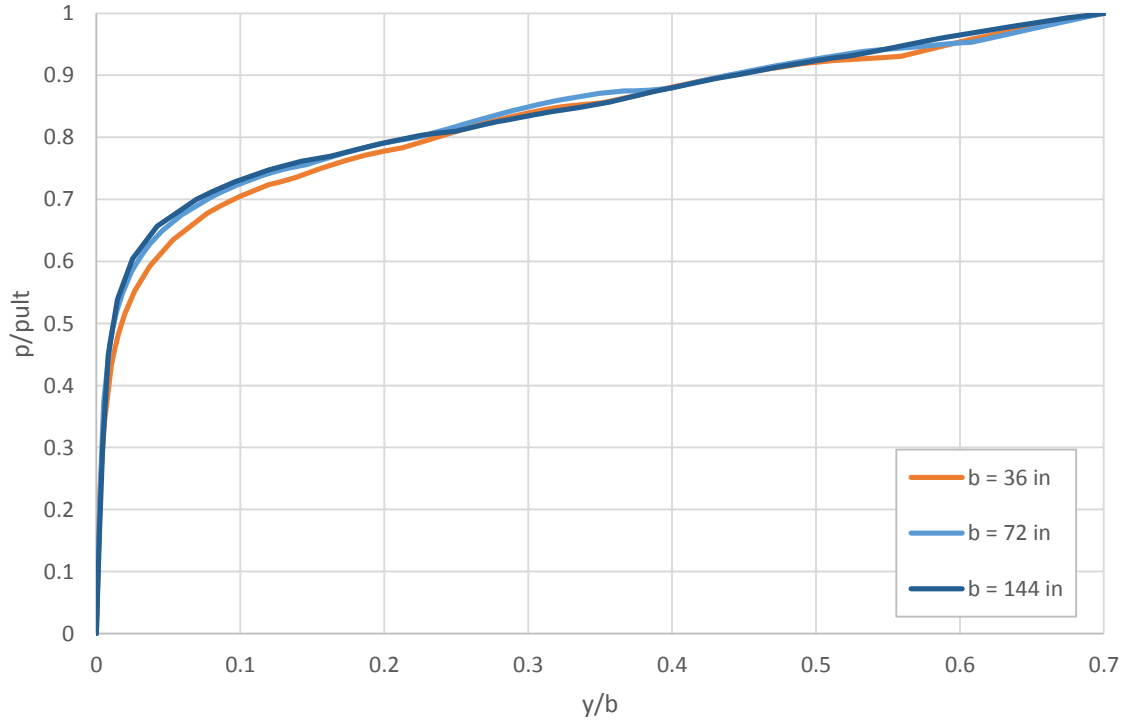

Figure 5.31: Normalized p-y curves , Depth = 3b

5.3 EFFECT OF CYCLIC LOADING

One-way cyclic loading in normally consolidated to overconsolidated clay reduces the initial secant stiffness by up to about 30 percent in the about first 100 cycles of loading. The ultimate lateral capacity after cyclic loading is not affected by the cyclic loading.

5.3.1 Reduction in Stiffness

In all model tests with cyclic loading, changes in stiffness occurred in the first 100 cycles and then stabilized (Figure 5.32 to Figure 5.42). This result is consistent with both model tests (e.g., Jeanjean 2009) and field tests in the database (Matlock & Tucker 1961 and Reese et al. 1975) in the lateral load database.

In nearly all model tests, the secant stiffness decreased between 20 and 30 percent in the first 100 cycles of loading (Figure 5.32 to Figure 5.42). This behavior was seemingly independent of the pile diameter, observed in both normally consolidated and overconsolidated clay, and observed in both kaolinite and Gulf of Mexico marine clay. There were several tests in which a slight increase in stiffness was observed with cyclic loading (Figure 5.32 to Figure 5.34); however, these results were attributed to settlement of the pile during cyclic loading caused by having lifted the pile after installation to align it with the loading system. This increase in stiffness was not observed when these tests were repeated with better control on the installation depth (Figure 5.35 to Figure 5.37).

This reduction in the secant stiffness of 20 to 30 percent is consistent with the model tests and field tests in the data base. Jeanjean (2009) observed a reduction in the secant stiffness of about 30 percent in model tests (note that this reduction is not reported but can be calculated from the data they do report). Lake Austin and Sabine River field tests by Matlock showed that the pile capacity at moderate displacements ($\approx 0.2D$) had decreased by approximately 1/3rd (i.e 33%) during post-cyclic monotonic loading. There were no discernible changes in the response of the pile for displacements less than about $0.02D$. The field tests in Manor, TX by Reese also showed an approximately 33% difference between the initial and post-cyclic responses. This drop took place at a much small lateral displacement of about $0.04D$. The clay at this site was stiffer than at Lake Austin and Sabine River, and seems to have degraded at smaller displacement amplitudes. Field tests in Houston, TX by Dunnavant and O'Neill showed post-cyclic drop in capacity of: 1) about 40% for a 10.75-in diameter pile at a displacement of $0.3D$, 2) about 20% for a 48-in pile at a displacement of about $0.02D$.

The reduction in secant stiffness observed in the model tests is presumably a limiting case (for one-way cyclic loading) since the cyclic load amplitudes ranged from 50 to 90 percent of the ultimate capacity. If the lateral displacement amplitudes are very low, then the degree of degradation may be less than 30%. If the shear strains do not exceed the elastic limit of the soil then, no degradation should occur. Matlock (1970) estimated this elastic limit as a lateral displacement less than $3y_{50}$.

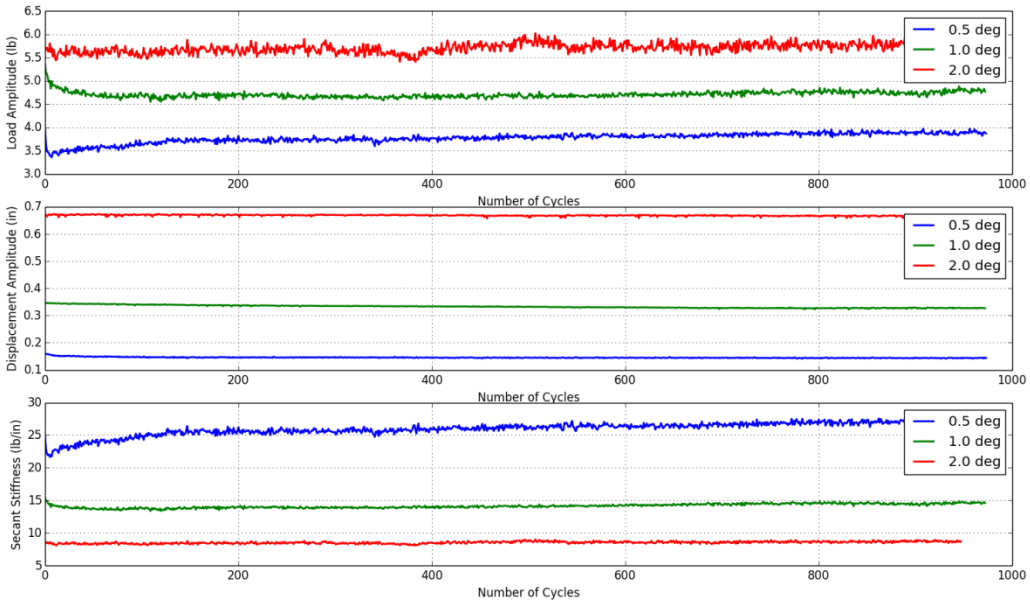

Figure 5.32: Variation of load amplitude, displacement amplitude, and secant stiffness of pile response versus number of load cycles, normally consolidated to moderately overconsolidated kaolinite, D = 2-inches

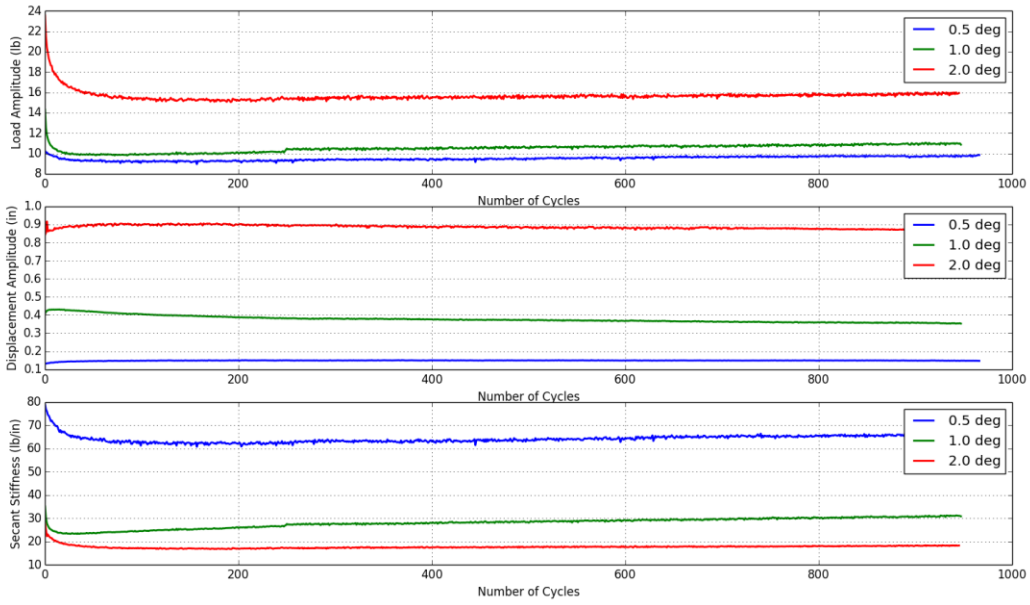

Figure 5.33: Variation of load amplitude, displacement amplitude, and secant stiffness of pile response versus number of load cycles, normally consolidated to moderately overconsolidated kaolinite, D = 3-inches

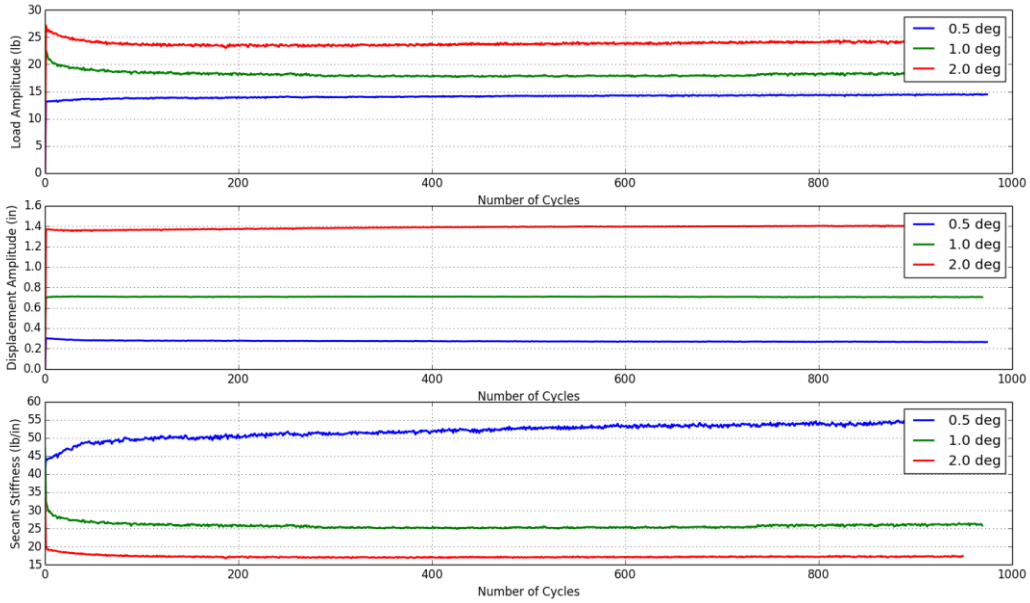

Figure 5.34: Variation of load amplitude, displacement amplitude, and secant stiffness of pile response versus number of load cycles, normally consolidated to moderately overconsolidated kaolinite, D = 4-inches

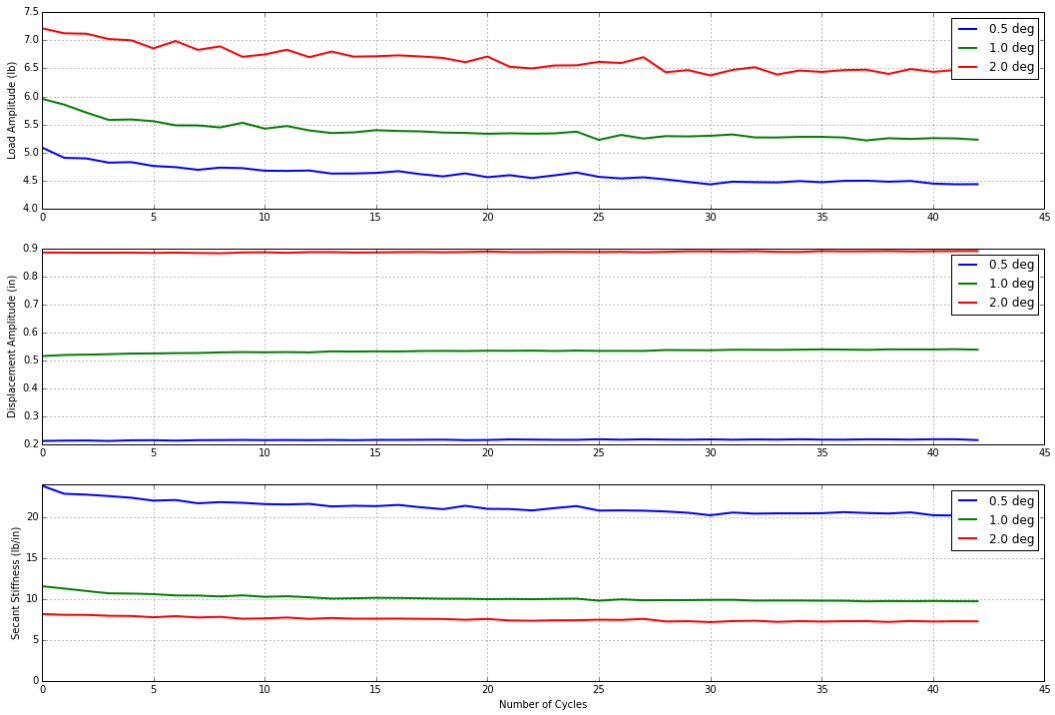

Figure 5.35: Variation of load amplitude, displacement amplitude, and secant stiffness of pile response versus number of load cycles, normally consolidated to moderately overconsolidated kaolinite, D = 2-inches, repeat test

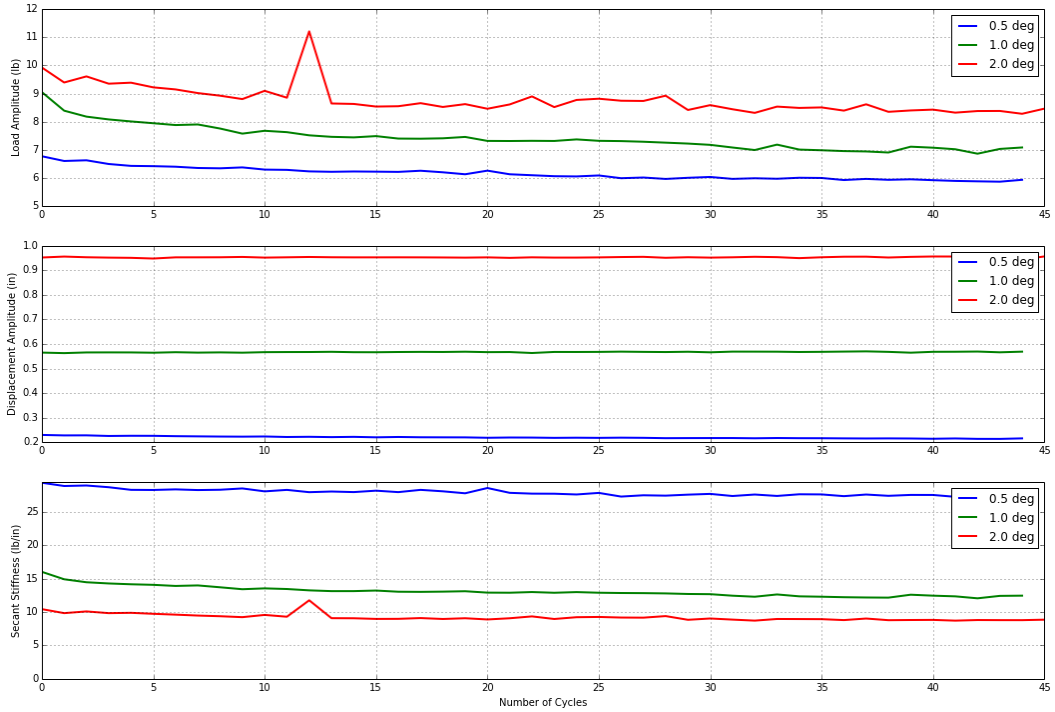

Figure 5.36: Variation of load amplitude, displacement amplitude, and secant stiffness of pile response versus number of load cycles, normally consolidated to moderately overconsolidated kaolinite, D = 3-inches, repeat test

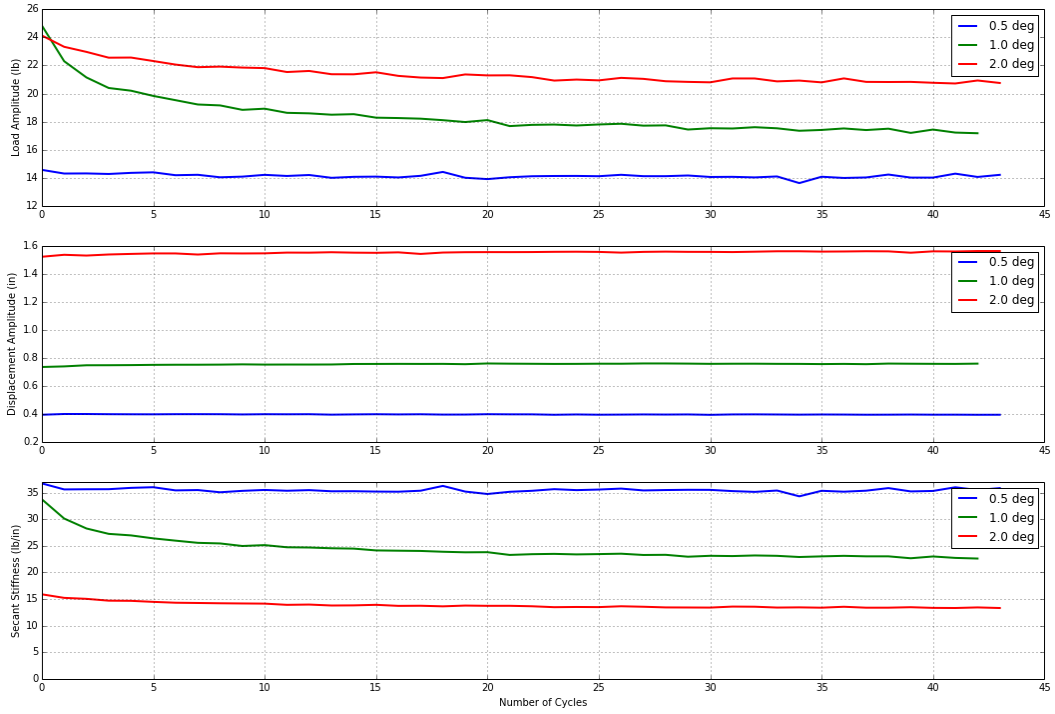

Figure 5.37: Variation of load amplitude, displacement amplitude, and secant stiffness of pile response versus number of load cycles, normally consolidated to moderately overconsolidated kaolinite, D = 4-inches, repeat test

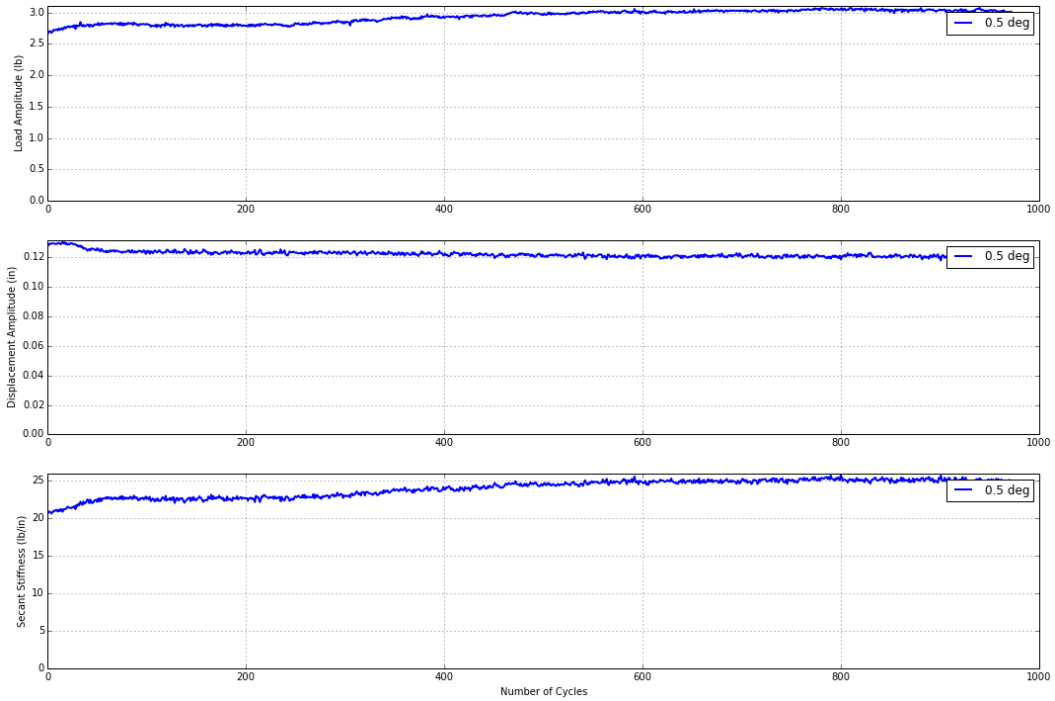

Figure 5.38: Variation of load amplitude, displacement amplitude, and secant stiffness of pile response versus number of load cycles, heavily overconsolidated kaolinite, D = 1-inches

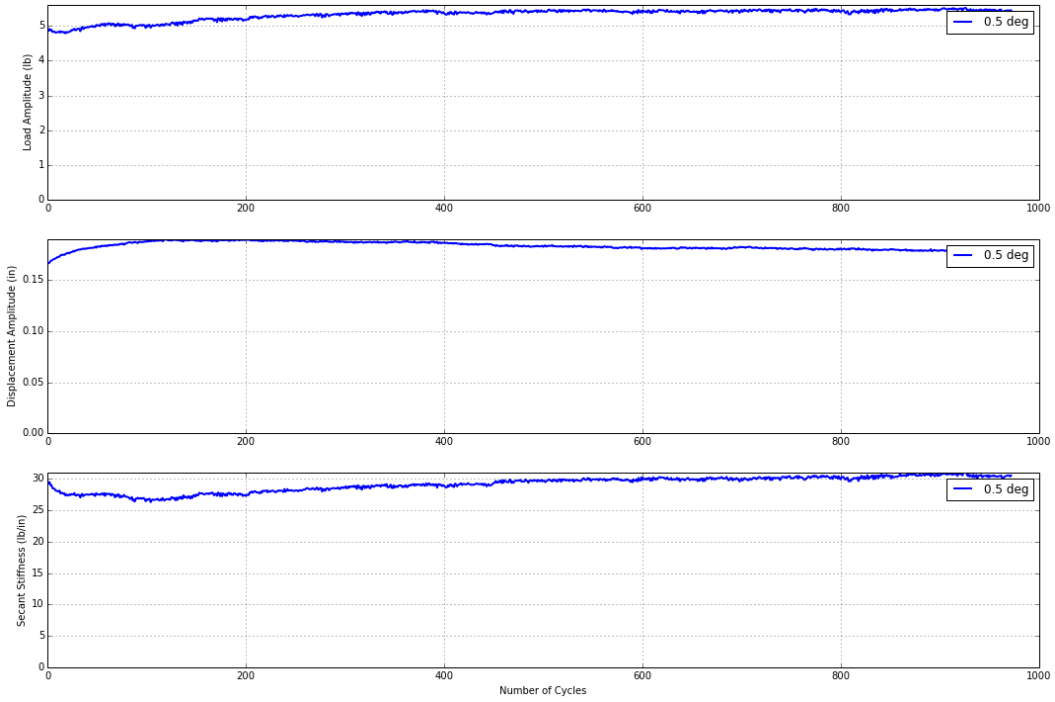

Figure 5.39: Variation of load amplitude, displacement amplitude, and secant stiffness of pile response versus number of load cycles, heavily overconsolidated kaolinite, D = 2-inches

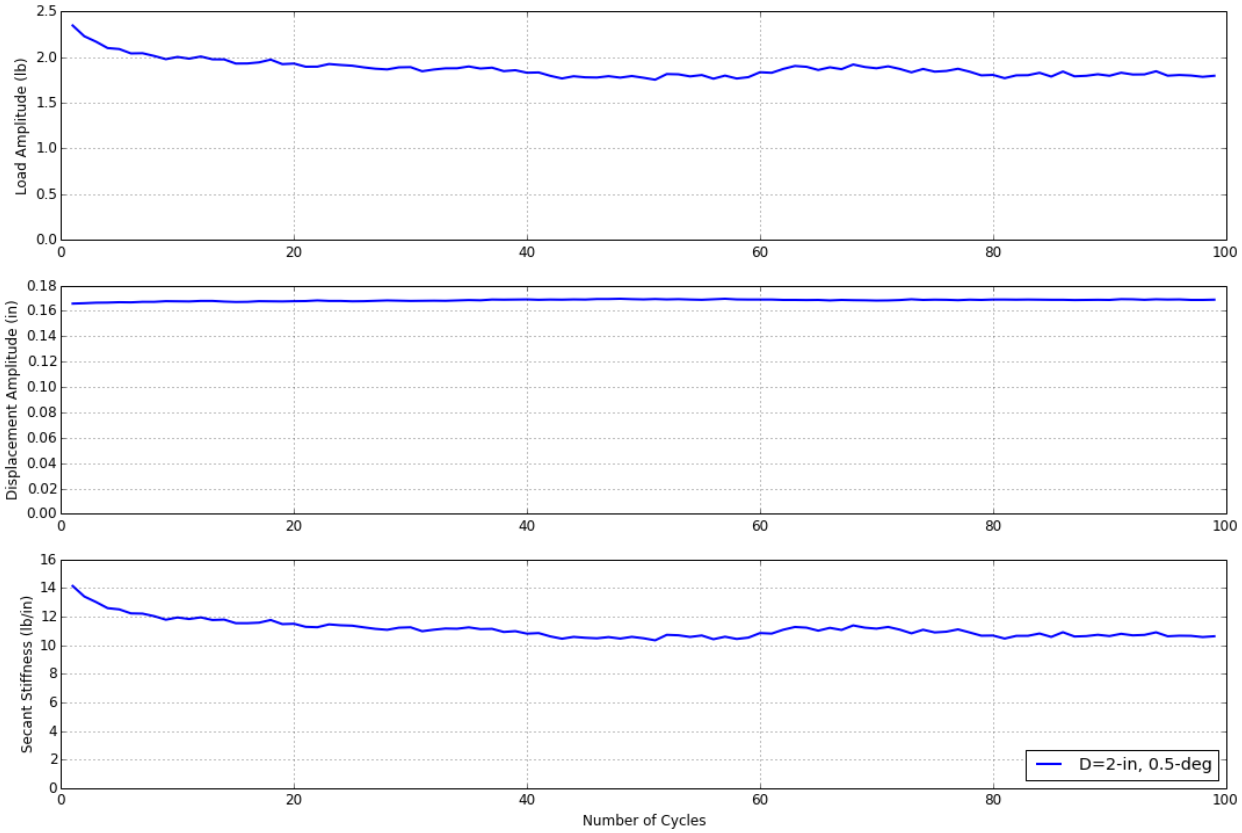

Figure 5.40: Variation of load amplitude, displacement amplitude, and secant stiffness of pile response versus number of load cycles, normally consolidated Gulf of Mexico clay, D = 2-inches

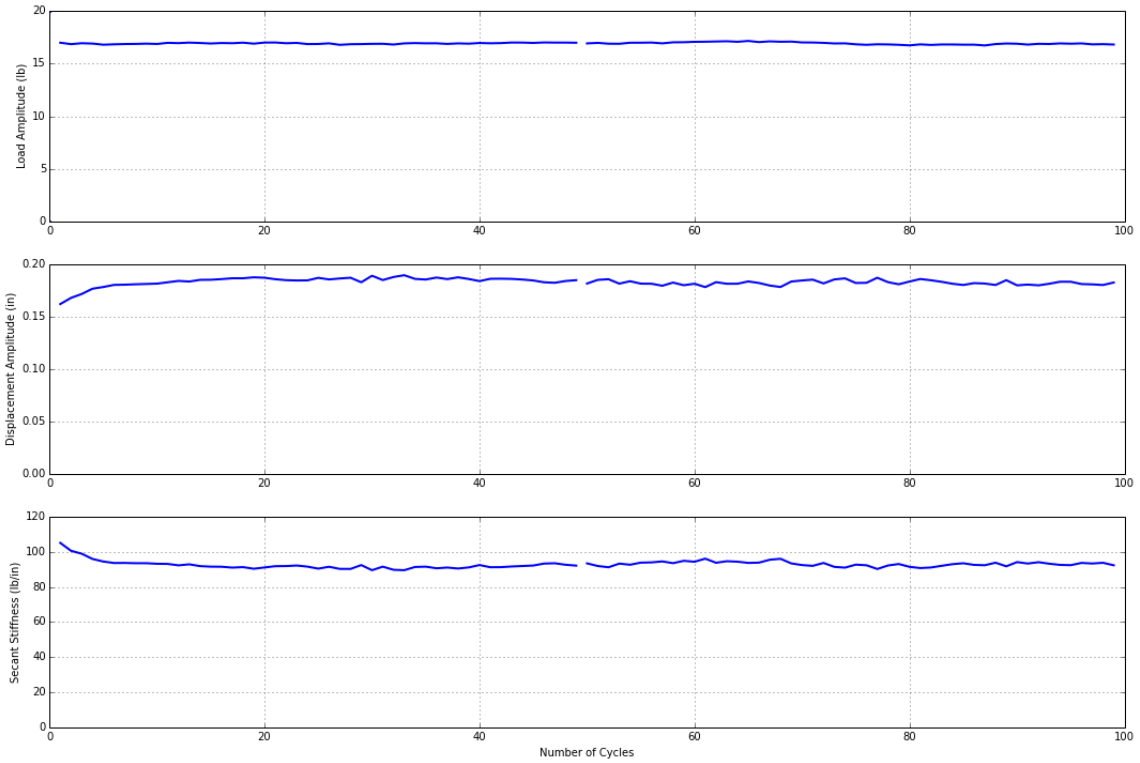

Figure 5.41: Variation of load amplitude, displacement amplitude, and secant stiffness of pile response versus number of load cycles, overconsolidated Gulf of Mexico clay, D = 2-inches

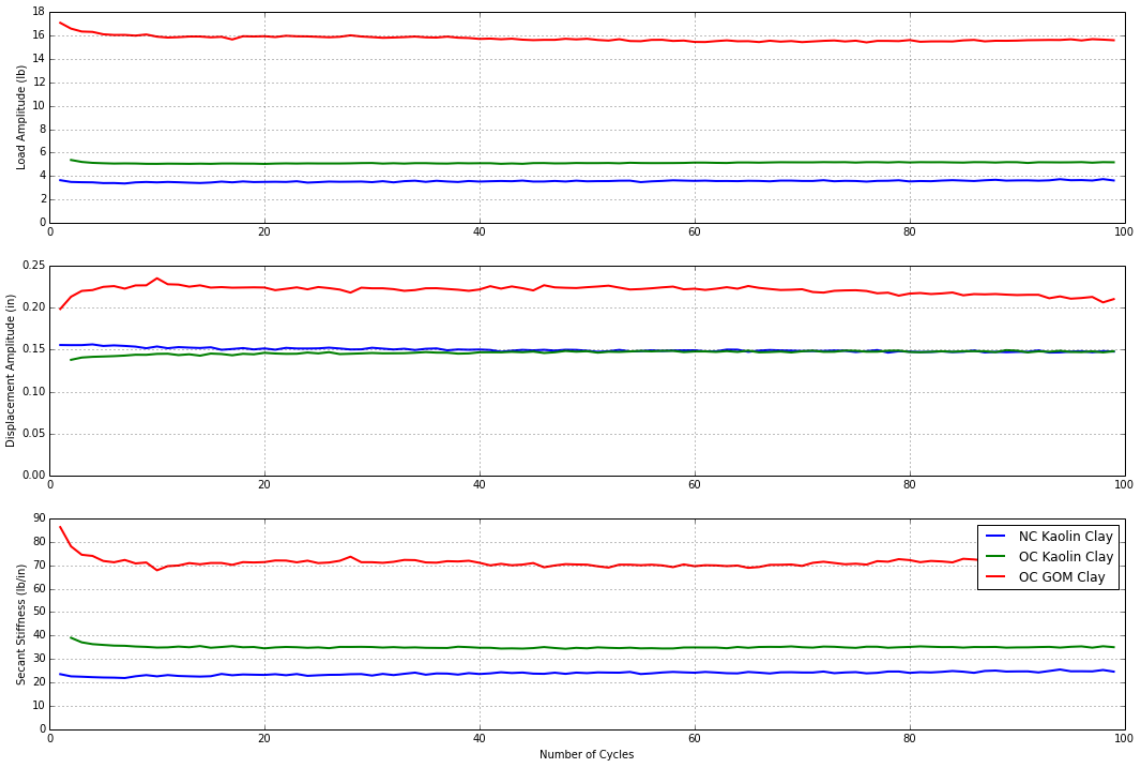

Figure 5.42: Variation of load amplitude, displacement amplitude, and secant stiffness of pile response versus number of load cycles, all soil beds, D = 2-inches

5.3.2 Ultimate Pile Capacity after Cyclic Loading

After the cyclic loading of piles, the same piles were subjected to static or monotonic loading to determine their post-cyclic lateral capacities. The results from two such tests are shown in Figure 5.43. Figure 5.43 (a) is based on a displacement controlled test subsequent to 1000-cycles of one-way displacement of amplitude corresponding to 0.5° of tilt. Figure 5.43 (b) is based on a load controlled test subsequent to 50 cycles of one-way displacement of amplitude corresponding to 2.0° of tilt. In both cases, the cyclic loading has caused the load-displacement response to soften. However, this does not have a significant effect on the ultimate lateral capacity which is regained after a sufficient amount of lateral displacement. This result is consistent with the observations by Hamilton & Murff (1995), Jeanjean (2009) and Zhang et al (2011), who all observed that the ultimate static/monotonic capacity of a laterally loaded pile was regained even after being subject to cyclic loads although it might larger displacement to achieve it.

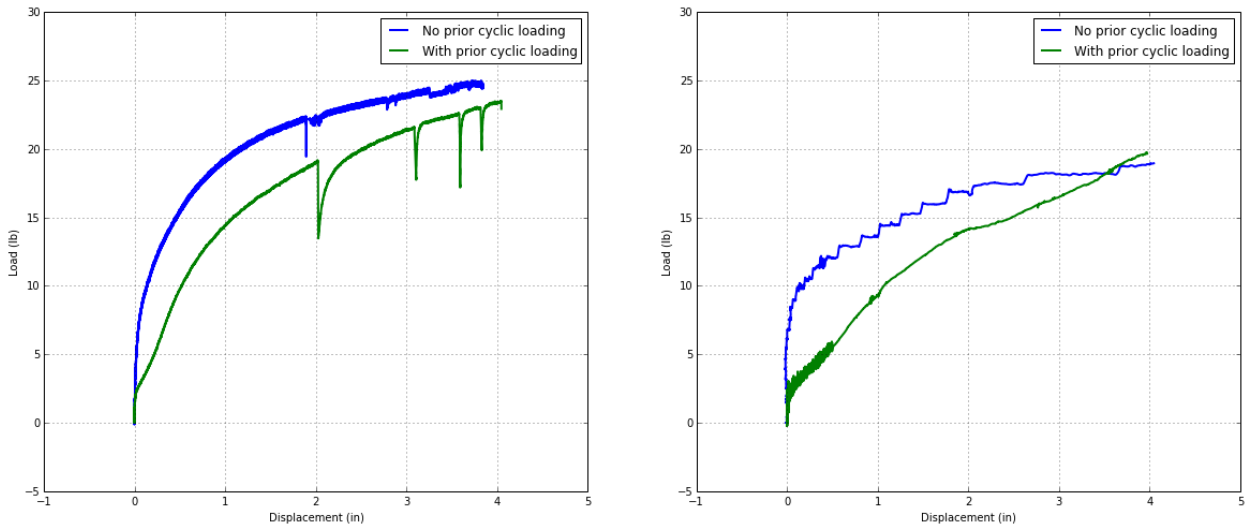

(a) (b)

Figure 5.43: Effect of prior cyclic loading on monotonic load versus displacement curves, D=4-in, normally to moderately overconsolidated kaolin clay, (a) displacement controlled (b) load controlled

Note: It is unlikely that the original ultimate capacity will be exceeded even though this is the case in Figure 5.43 (b). This behavior can be explained by the fact that the loading rate in the first load controlled test had larger load steps (which can be seen in the plot) which in turn resulted in softer response at higher loads.

6 CONCLUSIONS AND RECOMMENDATIONS

The following conclusions about laterally loaded monopiles in clay are drawn based on our analysis of the laboratory, numerical modeling, and field test results:

1. Numerical modeling and model-scale testing with rigid piles of different diameters indicate that the form of the Matlock (1970) p-y curves, in which the lateral displacement is normalized by pile diameter and lateral soil resistance is normalized by the ultimate resistance, appropriately captures the effect of pile diameter. For very small L/D ratios (say less than one), the p-y curves near the tip may be affected by interaction with the soil resistance mobilized around the tip.
2. Field and model testing indicate that the Matlock (1970) p-y models consistently underestimate the lateral resistance when used to analyze laterally loaded piles in normally to moderately overconsolidated clays. This observation applies to small (2 inch) and large (54 inch) diameter piles. It even applies to the Sabine River tests (Matlock and Tucker 1961) that formed the basis of the Matlock (1970) p-y models.
3. An approximate version of the Jeanjean (2009) p-y model, in which the Matlock (1970) p-y curves are scaled by p-multipliers calculated at various depths, generally provides a reasonable match to measured lateral displacements at the pile head when a relatively large strain at one-half the undrained shear strength is assumed, i.e., ε_{50}= 0.02. This result applies both to small scale model tests in kaolinite and large-scale field tests in high-plasticity clay provided that a gap does not form behind the pile.
4. The creation of a gap on the backside of the pile can lead to a reduction in the stiffness of the pile response and the ultimate lateral capacity. The creation of a gap is related both to the overconsolidation ratio and the magnitude of lateral displacement; as the overconsolidation ratio near the ground surface increases and the magnitude of lateral displacement increases, the potential for a gap increases. The Matlock (1970) p-y models provide a lower bound estimate for the response of a laterally loaded pile if a gap forms.
5. Field and model testing show that cyclic loading causes the secant stiffness of the lateral pile-soil response to degrade by up to 20 to 30 percent when the cyclic load amplitudes are 50 to 90 percent of the ultimate lateral capacity. The stiffness degradation occurs within the first 100 cycles, after which the stiffness is reasonably constant. Smaller or no degradation may occur if the lateral loading is a smaller percentage of the ultimate lateral capacity.
6. Model testing shows that the ultimate lateral capacity of the pile is not significantly affected by the previous cyclic loading.

For design of laterally loaded monopiles in clay, it is recommended that the following guidance be provided:

1. The form of the p-y curves for static loading in API RP 2GEO be adjusted using a bearing capacity factor of 8 versus 3 at the mudline and 12 versus 9 at depth for a normally consolidated to moderately overconsolidated clay (i.e., one in which a gap is not likely to form).
2. For cyclic loading in normally consolidated and overconsolidated clay, the currently recommended reduction in stiffness in API RP 2GEO (2011) be applied to the adjusted static p-y curves.

3. For lateral capacity checks under extreme environmental loading conditions after cyclic loading, the ultimate lateral resistance be represented by the ultimate lateral resistance for the adjusted static p-y curves.
4. The design of wind turbine structures be checked by both increasing and decreasing lateral stiffness of the soil that is predicted by the p-y curves in order to account for possible variations in the natural frequency of the structure.

7 REFERENCES

API, R. 2GEO (2011) Geotechnical and foundation design considerations. *American Petroleum Institute, Washington, DC, USA*.

Brandon, T. L., Wright, S. G., & Duncan, J. M. (2008). Analysis of the Stability of I-Walls with Gaps between the I-Wall and the Levee Fill. *Journal of Geotechnical and Geoenvironmental Engineering*.

Doherty, P., & Gavin, K. (2011). Laterally loaded monopile design for offshore wind farms

Duncan, J. M., and Chang, C.-Y. (1970). "Nonlinear analysis of stress and strain in soils." *J. Soil. Mech. and Found. Div*., 96(5), 1629-1653.

Dunnavant, T. W., & O'Neill, M. W. (1989). Experimental p-y Model for Submerged, Stiff Clay. *Journal of Geotechnical Engineering*, *115*(1), 95-114.

El-Sherbiny, R.M. (2005). Performance of Suction Caisson Anchors in Normally Consolidated Clay. PhD thesis, The University of Texas at Austin.

Hamilton, J. M., & Murff, J. D. (1995, January). Ultimate lateral capacity of piles in clay. In *Offshore Technology Conference*. Offshore Technology Conference.

Hardin, B. O., and Drnevich, V. P. (1972). "Shear modulus and damping in soils: Design equations and curves." *J. Soil Mech. and Found. Div*., 98(7), 667-691.

Isenhower, W. M., & Wang, S. T. (2013). Technical manual for LPILE, *Ensoft, Inc., Austin, Texas*.

Jeanjean, P. (2009, January). Re-assessment of py curves for soft clays from centrifuge testing and finite element modeling. In *Offshore Technology Conference*. Offshore Technology Conference.

Kondner, R. L. (1963). "Hyperbolic stress-strain response: Cohesive soils." *J. Soil Mech. and Found. Div*., 89(1), 115-143.

Lam, Ignatius Po (2009). Diameter Effects on p-y Curves. Deep Marine Foundations: A Perspective on the Design and Construction of Deep Marine Foundation. *Deep Foundations Institute*. 27-41

Lam, I. P., & Martin, G. R. (1986). Seismic Design for Highway Bridge Foundations. FHWA Report No. FHWA/RD-86/102

LCR&A (2009). Report of studies of Harvey canal lateral pile load test and of soil springs for West Closure Complex. Technical report, *Lymon C. Reese & Associates.*

LCR&A. (2010) Report of lateral load tests and field-derived p-y curves on piles at West Closure Complex. Technical report, *Lymon C. Reese & Associates.*

Leblanc, C., Byrne, B. W., & Houlsby, G. T. (2010). Response of stiff piles to random two-way lateral loading. *Geotechnique*, *60*(9), 715-721.

Matlock, H., & Reese, L. C. (1962). Generalized solutions for laterally loaded piles. *Transactions of the American Society of Civil Engineers*, *127*(1), 1220-1247.

Matlock, H, and Tucker RL. (1961). Lateral-load Tests of an Instrumented Pile at Sabine, Texas. *A Report to the Shell Development Company.*

Matlock, H. (1970). Correlations for design of laterally loaded piles in soft clay. *Offshore Technology in Civil Engineering's Hall of Fame Papers from the Early Years*, 77-94

McClelland, B., & Focht, J. A. (1958). Soil modulus for laterally loaded piles. *Transactions of the American Society of Civil Engineers*, *123*(1), 1049-1063.

Murff, J. D., & Hamilton, J. M. (1993). P-ultimate for undrained analysis of laterally loaded piles. *Journal of Geotechnical Engineering*, *119*(1), 91-107.

O'Neill, M. W., Reese, L. C., & Cox, W. R. (1990, January). Soil behavior for piles under lateral loading. In *Offshore Technology Conference*. Offshore Technology Conference.

Randolph, M. F., & Houlsby, G. T. (1984). The limiting pressure on a circular pile loaded laterally in cohesive soil. *Geotechnique*, *34*(4), 613-623.

Reese, L. C., Cox, W. R., & Koop, F. D. (1975, January). Field testing and analysis of laterally loaded piles in stiff clay. In *Offshore Technology Conference*. Offshore Technology Conference.

Reese, L. C., & Welch, R. C. (1975). Lateral loading of deep foundations in stiff clay. *Journal of the Geotechnical engineering division*, *101*(7), 633-649.

Senanayake, A., Rendon, E., Wang, S. T., Gerkus, H., Stevens, R. F., & Gilbert, R. B. (2015, May). Design of Large Diameter Monopiles under Lateral Loads in Normally to Moderately Overconsolidated Clay. In *Offshore Technology Conference*. Offshore Technology Conference.

Soderberg, L. O. (1962). Consolidation theory applied to foundation pile time effects. *Geotechnique*, *12*(3), 217-225.

Stevens, J. B., & Audibert, J. M. E. (1979, January). Re-examination of py curve formulations. In *Offshore Technology Conference*. Offshore Technology Conference.

Stevens, R. F., Soosainathan, L., Rahim, A., Saue, M., Gilbert, R., Senanayake, A. I., Rendon, E., Gerkus, H., Wang, S.T., & O'Connell, D. P. (2015, May). Design Procedures for Marine Renewable Energy Foundations. In *Offshore Technology Conference*. Offshore Technology Conference.

Stewart, D. P., & Randolph, M. F. (1994). T-bar penetration testing in soft clay. *Journal of Geotechnical Engineering*, *120*(12), 2230-2235.

Vanka, S.K.R. (2004). Laboratory tests to estimate strength profile of normally consolidated kaolinite. *Master's thesis, The University of Texas at Austin*.

Vardanega, P. J., and Bolton, M. D. (2013). "Stiffness of Clays and Silts: Normalizing Shear Modulus and Shear Strain." *Journal of Geotechnical and Geoenvironmental Engineering,* 139(9), 1575-1589.

Zhang, C., White, D., & Randolph, M. (2010). Centrifuge modeling of the cyclic lateral response of a rigid pile in soft clay. *Journal of Geotechnical and Geoenvironmental Engineering*.

A. APPENDIX – DATABASE OF LATERAL LOAD TESTS

The compiled database is contained in spreadsheet “Pile Database.xlsx” and the contents of the database are shown Table A.1.

Table A.1: Contents of Pile Test Database

Worksheet	Field/ Lab	Cyclic Loading	Location	Soil	Diameter (in)	Length (ft)	L/D	Type	Source
58	L	Y	University of Western Australia (Lab Test at 50g)	Clay (Kaolinite)	23.6	9.8	5	Aluminum Tube	Zhang, White, and Randolph (2011)
59	L	Y	University of Western Australia (Lab Test at 50g)	Clay (Kaolinite)	23.6	9.8	5	Aluminum Tube	Zhang, White, and Randolph (2011)
60	L	Y	University of Western Australia (Lab Test at 50g)	Clay (Kaolinite)	23.6	9.8	5	Aluminum Tube	Zhang, White, and Randolph (2011)
61	L	Y	University of Western Australia (Lab Test at 50g)	Clay (Kaolinite)	23.6	9.8	5	Aluminum Tube	Zhang, White, and Randolph (2011)
73	L	Y	Cambridge University, UK (Lab Test at 49g)	Clay (Kaolinite)	25.6	18.6	9	Aluminum Tube	Hamilton & Murff (1995)
74	L	N	Cambridge University, UK (Lab Test at 49g)	Clay (Kaolinite)	26	59.1	27	Aluminum Tube	Hamilton & Murff (1995)
62	L	Y	C-CORE Centrifuge Lab (48g)	Clay (Kaolinite)	36	66	22	Steel Pipe	Jeanjean (2009)
63	L	Y	C-CORE Centrifuge Lab (48g)	Clay (Kaolinite)	36	66	22	Steel Pipe	Jeanjean (2009)
64	L	Y	C-CORE Centrifuge Lab (48g)	Clay (Kaolinite)	36	66	22	Steel Pipe	Jeanjean (2009)
65	L	Y	C-CORE Centrifuge Lab (48g)	Clay (Kaolinite)	36	66	22	Steel Pipe	Jeanjean (2009)
75	L	Y	Cambridge University, UK (Lab Test at 49g)	Clay (Kaolinite)	48.8	34.7	9	Aluminum Tube	Hamilton & Murff (1995)
76	L	Y	Cambridge University, UK (Lab Test at 49g)	Clay (Kaolinite)	48.8	35.2	9	Aluminum Tube	Hamilton & Murff (1995)

Worksheet	Field/ Lab	Cyclic Loading	Location	Soil	Diameter (in)	Length (ft)	L/D	Type	Source
66	L	Y	UT Austin	Clay (NC, Kaolinite)	12	1	1	Steel Suction Caisson	Chen & Gilbert (Unpublished)
67	L	Y	UT Austin	Clay (OC, Kaolinite)	6	0.5	1	Steel Suction Caisson	Chen & Gilbert (Unpublished)
13	F	N	Japan	Clay (Soft)	12	17.0	17	Steel Pipe Pile	Reese & Van Impe (2001), Meyer & Reese (1979)
6	F	Y	Lake Austin	Clay (Soft)	12.75	42	40	Steel Pipe Pile	Matlock (1970)
7	F	Y	Sabine River	Clay (Soft)	12.75	42	40	Steel Pipe Pile	Matlock (1970)
45	F	N	California ?	Clay (Soft)	12.75	16.7	16	Steel Pipe Pile	Meyer & Reese (1979)
46	F	N	California ?	Clay (Soft)	12.75	16.7	16	Steel Pipe Pile	Meyer & Reese (1979)
47	F	N	California ?	Clay (Soft)	16	26.7	20	Steel Pipe Pile	Meyer & Reese (1979)
48	F	N	California ?	Clay (Soft)	16	26.7	20	Steel Pipe Pile	Meyer & Reese (1979)
5	F	N	Jefferson Parish, Louisiana	Clay (Soft)	24	160	80	Steel Pipe Pile	USACE, Ensoft (2004)
31	F	N	Spring Villa Geotechnical Test Site, Auburn, Alabama	Clay (Soft)	36	37	12	RC Drilled Shaft	Anderson, Townsend & Grajales (2003)
43	F	N	Puerto Nuevo, Puerto Rico	Clay (Soft)	48	68	17	Steel Pipe Pile	Anderson, Townsend & Grajales (2003)
44	F	N	Puerto Nuevo, Puerto Rico	Clay (Soft)	48	48	12	Steel Pipe Pile	Anderson, Townsend & Grajales (2003)

Worksheet	Field/ Lab	Cyclic Loading	Location	Soil	Diameter (in)	Length (ft)	L/D	Type	Source
2	F	N	Jefferson Parish, Louisiana	Clay (Soft)	54	124	28	Steel Pipe Pile	USACE, Ensoft (2010)
3	F	N	Jefferson Parish, Louisiana	Clay (Soft)	54	124	28	Steel Pipe Pile	USACE, Ensoft (2010)
1	F	N	New Orleans, Louisiana	Clay (Soft)	66	70	13	Prestressed Concrete Pile	USACE, Ensoft (2009)
4	F	N	Jefferson Parish, Louisiana	Clay (Soft, Stiff), Sand	24	160	80	Steel Pipe Pile	USACE, Ensoft (2004)
53	F	Y	Houston, TX	Clay (Stiff)	10.75	38.7	43	Steel Pipe Pile	O'Neill & Dunnavant (1984)
52	F	N	Southern California	Clay (Stiff)	24	15.5	8	RC Drilled Shaft	Meyer & Reese (1979), Bhushan et al (1978)
8	F	Y	Austin/Manor, TX	Clay (Stiff)	25.25	49	23	Steel Pipe Pile	Reese, Cox, & Koop (1975)
10	F	Y	Houston, TX	Clay (Stiff)	30	42	17	RC Drilled Shaft with Steel Pipe Core	Reese & Welch (1975)
54	F	Y	Houston, TX	Clay (Stiff)	48	37.5	9	Steel Pipe Pile	Dunnavant & O'Neill (1985)
50	F	N	Southern California	Clay (Stiff)	48	15	4	RC Drilled Shaft	Meyer & Reese (1979), Bhushan et al (1978)
51	F	N	Southern California	Clay (Stiff)	48	15.5	4	RC Drilled Shaft	Meyer & Reese (1979), Bhushan et al (1978)

Worksheet	Field/ Lab	Cyclic Loading	Location	Soil	Diameter (in)	Length (ft)	L/D	Type	Source
49	F	N	Ontario, Canada	Clay (Stiff)	60	38	8	RC Drilled Shaft	Meyer & Reese (1979)
56	F	Y	Houston, TX	Clay (Stiff)	72	39.5	7	RC Drilled Shaft	Dunnavant & O'Neill (1985)
23	F	N	California	Clay (Stiff)	96	62	8	RC Drilled Shaft	UFlorida Database, Caltrans
69	F	N	Incheon, South Korea	Clay, Silt, Weathered Rock	40	84	25	Steel Pipe Pile	Jeong et al. (2007) ISOFPE
70	F	N	Incheon, South Korea	Clay, Silt, Weathered Rock	40	84	25	Steel Pipe Pile	Jeong et al. (2007) ISOFPE
71	F	N	Incheon, South Korea	Clay, Silt, Weathered Rock	40	84	25	Steel Pipe Pile	Jeong et al. (2007) ISOFPE
72	F	N	Incheon, South Korea	Clay, Silt, Weathered Rock	94.5	147.6	19	Drilled Shaft	Jeong et al. (2007) ISOFPE
11	F	N	Alcacer do Sol	Layered Clay and Sand	47.2	131.2	33	RC Drilled Shaft	Portugal & Seco e Pinto (1993), Reese & Van Impe (2001)
27	F	N	Century Freeway, California	Layered Clay and Sand	48	51	13	RC Drilled Shaft	UFlorida Database, Caltrans, Naramore & Feng (1990)
28	F	N	Century Freeway, California	Layered Clay and Sand	50.4	50	12	RC Drilled Shaft	UFlorida Database, Caltrans, Naramore & Feng (1990)
30	F	N	Daytona Bridge	Layered Clay and Sand	72	93	16	RC Drilled Shaft	UFlorida Database, FDOT

Worksheet	Field/ Lab	Cyclic Loading	Location	Soil	Diameter (in)	Length (ft)	L/D	Type	Source
26	F	N	Century Freeway, California	Layered Clay and Sand	96	56	7	RC Drilled Shaft	UFlorida Database, Caltrans, Naramore & Feng (1990)
29	F	N	Century Freeway, California	Layered Clay and Sand	97.2	59	7	RC Drilled Shaft	UFlorida Database, Caltrans, Naramore & Feng (1990)
24	F	N	Fuller Warren, FL	Marl (Very Dense Clayey, Silty, Fine Sand)	72	35	6	RC Drilled Shaft	UFlorida Database, Castelli & Fan (2002)
25	F	N	Fuller Warren, FL	Marl (Very Dense Clayey, Silty, Fine Sand)	72	35	6	RC Drilled Shaft	UFlorida Database, Castelli & Fan (2002)
68	L	Y	UT Austin	Sand	6	0.5	1	Steel Suction Caisson	Chen & Gilbert (Unpublished)
9	F	Y	Mustang Island, TX	Sand	24	69	35	Steel Pipe Pile	Cox, Reese, & Grubs (1974)
38	F	Y	Houston, TX	Sand	24	100	50	Steel Pipe Pile	Little & Briaud (1988)
57	F	N	Roosevelt Bridge, FL	Sand	30	48	19	Prestressed Concrete Pile	Ruesta & Townsend (1997), Anderson, Townsend, & Grajales (2003)
39	F	Y	Houston, TX	Sand	36	97	32	RC Drilled Shaft	Little & Briaud (1988)

Worksheet	Field/ Lab	Cyclic Loading	Location	Soil	Diameter (in)	Length (ft)	L/D	Type	Source
40	F	Y	Houston, TX	Sand	42	128	37	RC Drilled Shaft	Little & Briaud (1988)
41	F	Y	Houston, TX	Sand	42	128	37	RC Drilled Shaft	Little & Briaud (1988)
42	F	Y	Houston, TX	Sand	42	128	37	RC Drilled Shaft	Little & Briaud (1988)
21	F	N	Skyway Bridge Site	Sand	48	51	13	RC Drilled Shaft	UFlorida Database, FDOT
22	F	N	Skyway Bridge Site	Sand	48	51	13	RC Drilled Shaft	UFlorida Database, FDOT
18	F	N	Onslow, NC	Sand	48	57	14	RC Drilled Shaft	UFlorida Database, NCDOT
19	F	N	New Bern, NC	Sand	48	44	11	RC Drilled Shaft	UFlorida Database, NCDOT
17	F	N	Oregon Inlet, NC	Sand	54	71	16	RC Drilled Shaft	Keaney & Batts (2007), UFlorida Database
12	F	N	Florida	Sand	56	26	6	Steel Pipe Pile	Davis (1977), Reese & Van Impe (2001)
16	F	N	Oregon Inlet, NC	Sand	66	106	19	Prestressed Concrete Pile	Keaney & Batts (2007), UFlorida Database
20	F	N	Nevada	Sand	96	32	4	RC Drilled Shaft	UFlorida Database
14	F	N	Kuwait	Sand (Cemented)	11.8	16.4	17	RC Drilled Shaft	Ismael (1990)

Worksheet	Field/ Lab	Cyclic Loading	Location	Soil	Diameter (in)	Length (ft)	L/D	Type	Source
15	F	N	Kuwait	Sand (Cemented)	11.8	9.84	10	RC Drilled Shaft	Ismael (1990)
36	F	N	Naselle, WA	Sand (Silty)	18	75	50	Steel Pipe Pile	FHWA, Kramer (1991)
37	F	N	Naselle, WA	Sand (Silty)	18	77	51	Steel Pipe Pile	FHWA, Kramer (1991)
32	F	N	Boston	Sand (Silty)	48	173	43	Drilled Shaft with Casing	FHWA Database
34	F	N	Boston	Sand (Silty)	48	156	39	Drilled Shaft with Casing	FHWA Database
33	F	N	Boston	Sand (Silty)	54	171	38	Drilled Shaft with Casing	FHWA Database
35	F	N	Boston	Sand (Silty)	54	144	32	Drilled Shaft with Casing	FHWA Database
55	F	Y	Houston, TX	Sand, Clay	10.75	38.7	43	Steel Pipe Pile	Dunnavant & O'Neill (1985)

B. APPENDIX – SUMMARY OF MODEL TESTS

A summary of all the tests conducted so far (including those that were reported in previous reports) are provided in tabular format as follow:

Table B.1 – Table B.*3*	All tests conducted in the normally to moderately overconsolidated kaolinite clay bed
Table B.*4*	All tests conducted in the heavily oversonsolidated kaolinite clay bed
Table B.*5*	All tests conducted in the normally to moderately overconsolidated kaolinite clay bed with lateral soil pressure measurements.
Table B.6	All tests conducted in the heavily overconsolidated kaolinite clay bed with a stiff top crust.
Table B.*7*	All tests conducted in the heavily overconsolidated Gulf of Mexico clay bed.
Table *B.8*	All tests conducted in the normally consolidated Gulf of Mexico clay bed.

Table B.1: Summary of preliminary tests done in normally to moderately overconsolidated kaolin clay bed

Date	Filename	Diameter (in)	Embedment (D)	Moment Arm (D)	Target Tilt (deg)	Target Disp (in)	Rate of Lateral Disp (in/s)	Motor Speed (rpm)	Final Vertical Settlement (mm)	Cumulative Vertical Settlement (mm)
5/1/14 11:53	M4_0.5_1000_10_9D_test1.txt	4	8	9.0	0.5	0.506	0.101	16	30	30
5/2/14 11:41	M4_1.0_1000_10_9D_test1.txt	4	8	9.0	0.5	0.506	0.101	16	25	55
5/5/14 11:11	M4_2.0_1000_10_9D_test2.txt	4	8.40	8.6	2.0	2.024	0.405	209	41	96
5/6/14 10:28	M4_lateral_failure_test1.txt	4	9.27	7.7		8.000	0.100	52		96
5/27/14 16:33	M4_0.5_1000_10_5D_test1.txt	4	8	5.0	0.5	0.366	0.073	12	4	4
5/28/14 8:39	M4_1.0_1000_10_5D_test1.txt	4	8.05	4.9	1.0	0.733	0.147	76	7	11
5/28/14 11:55	M4_2.0_1000_10_5D_test1.txt	4	8.14	4.9	2.0	1.466	0.293	151	11	22
5/29/14 10:22	M4_5D_lateral_failure_test1.txt	4	8.29	4.7		8.000	0.058	30		22
5/29/14 11:58	M4_5D_lateral_failure_test2.txt	4	8.29	4.7		8.000	0.058	30		22
5/9/14 0:00	M3_0.5_1000_10_5D_test1.txt	3	8	5.00	0.5	0.288	0.058	30	15	15
5/12/14 11:33	M3_0.5_1000_10_5D_test2.txt	3	8.20	4.80	0.5	0.288	0.058	30	6	21
5/12/14 15:46	M3_1.0_1000_10_5D_test1.txt	3	8.28	4.72	1.0	0.576	0.115	59	5	26
5/13/14 10:52	M3_2.0_1000_10_5D_test1.txt	3	8.34	4.66	2.0	1.152	0.230	119	21	47
5/13/14 14:12	M3_lateral_failure_test1.txt	3	8.62	4.38	-	6.000	1.200	619	25	72
5/14/14 10:15	M3_1.0_1000_10_13D_test3.txt	3	8.94	4.06	1.0	0.576	0.115	59	0	72
5/15/14 10:29	M3_0.5_1000_10_13D_test4.txt	3	8.94	4.06	0.5	0.288	0.058	30	0	72
5/16/14 12:12	M3_lateral_failure_test2.txt	3	8.94	4.06	-	6.000	0.058	30		72
5/29/14 12:35	M3_lateral_failure_test3.txt	3	8.00	5.00	-	6.000	0.058	30		
5/19/14 11:24	M2_0.5_1000_10_13D_test1.txt	2	8.5	4.50	0.5	0.183	0.037	19	1	1
5/19/14 14:16	M2_1.0_1000_10_13D_test1.txt	2	8.01	4.99	1.0	0.366	0.073	38	0	1
5/20/14 8:11	M2_2_1000_10_13D_test3.txt	2	8.01	4.99	2.0	0.733	0.147	76	0	1
5/26/14 13:13	M2_lateral_failure_2014_05_26.txt	2	8.01	4.99		4.000	0.058	30		1

Table B.2: Summary of additional tests done in the normally to moderately overconsolidated kaolin clay bed, with a load eccentricity of 5D

Date	Filename	Diameter (in)	Moment Arm (D)	Target Tilt (deg)	Target Disp (in)	Rate of Lateral Disp (in/s)	Motor Speed (rpm)	Final Vertical Settlement (mm)	Cumulative Vertical Settlement (mm)
6/11/14 15:04	M4_0.5_50_10_5D_test1.txt	4	5.0	0.5	0.384	0.077	40	0	
6/11/14 15:17	M4_1.0_50_10_5D_test1.txt	4	5.0	1.0	0.768	0.154	79	0	
6/11/14 15:31	M4_2.0_50_10_5D_test1.txt	4	5.0	2.0	1.535	0.307	158	0	
6/12/14 11:53	M4_0.5_50_10_5D_test2.txt	4	5.0	0.5	0.384	0.077	40	0	
6/12/14 12:09	M4_1.0_50_10_5D_test2.txt	4	5.0	1.0	0.768	0.154	79	0	
6/13/14 10:49	M4_0.5_50_10_5D_test3.txt	4	5.0	0.5	0.384	0.077	40	0	
6/5/14 13:39	M3_lateral_failure_test4.txt	3	5				30		
6/10/14 14:57	M3_0.5_50_10_5D_test1.txt	3	5.0	0.5	0.288	0.058	30	0	
6/10/14 15:07	M3_1.0_50_10_5D_test2.txt	3	5.0	1.0	0.576	0.115	59	0	
6/10/14 15:20	M3_2.0_50_10_5D_test1.txt	3	5.0	2.0	1.152	0.230	119	0	
6/11/14 10:40	M3_lateral_2in_test1	3	5.0			0.058	30		
6/11/14 12:06	M3_lateral_2in_1rpm_test2.txt	3	5.0			0.002	1		
6/13/14 11:39	M2_0.5_50_10_5D_test1.txt	2	5.0	0.5	0.192	0.038	20	0	
6/13/14 12:25	M2_1.0_50_10_5D_test1.txt	2	5.0	1.0	0.384	0.077	40	0	
6/13/14 12:43	M2_2.0_50_10_5D_test1.txt	2	5.0	2.0	0.768	0.154	79	0	
6/13/14 14:23	M2_lateral_2in_1rpm_test1.txt	2	5.0			0.002	1		
6/17/14 11:32	M2_lateral_2in_1rpm.txt	2	5.0			0.002	1		

Table B.3: Summary of tests done in normally to moderately overconsolidated kaolin clay bed, with the load applied at the mudline

Date	Filename	Diameter (in)	Embedment (D)	Moment Arm (D)	Target Tilt (deg)	Target Disp (in)	Rate of Lateral Disp (in/s)	Motor Speed (rpm)	Final Vertical Settlement (mm)
7/19/14 13:11	M4_0.5_1000_10s_0D_test1_edited.txt	4	8.0	0.0	0.5	0.209	0.042	22	
7/28/14 12:54	M4_0.5_1000_10_0D_test2.txt	4	8.0	0.0	0.5	0.209	0.042	22	1
Not Done	M4_1.0_1000_10_0D_test1.txt	4	8.0	0.0	1.0	0.419	0.084	43	
Not Done	M4_2.0_1000_10_0D_test1.txt	4	8.0	0.0	2.0	0.838	0.168	86	
7/14/14 11:19	M3_1.0_30_10s_0D_test1.txt	3	8.0	0.0	0.5	-0.157	-0.031	16	
7/14/14 13:00	M3_1.0_1000_10s_0D_test3.txt	3	8.0	0.0	0.5	0.157	0.031	16	0
7/17/14 11:09	M3_2.0_1000_10s_0D_test1_edited.txt	3	8.0	0.0	1.0	0.314	0.063	32	2

Table B.4: Summary of all tests done in the overconsolidated kaolin clay bed

Date	Filename	Diameter (in)	Embedment (D)	Moment Arm (D)	Target Tilt (deg)	Target Disp (in)	Rate of Lateral Disp (in/s)	Motor Speed (rpm)	Final Vertical Settlement (mm)
7/30/14 14:20	M2_OC_0.5_50_10s_2.5D_test1.txt	2	10.5	2.5	0.5	0.200	0.040	6	
7/31/14 12:43	M2_OC_0.5_1000_10s_2.5D_test2.txt	2	10.5	2.5	0.5	0.192	0.038	20	
7/31/14 15:41	M2_OC_monotonic_2.5D_test1.txt	2	10.5	2.5			0.002	1	
8/4/14 13:17	M2_OC_0.5_1000_10s_5D_test1.txt	2	8.0	5.0	0.5	0.192	0.038	21	
8/4/14 16:11	M2_OC_monotonic_5D_test1.txt	2	8.0	5.0			0.002	1	
8/7/14 15:36	M2_OC_monotonic_5D_test2.txt	2	8.0	5.0			0.002	1	
8/8/14 10:37	M2_OC_0.5_100_10s_5D_test1.txt	2	8.0	5.0	0.5	0.192	0.038	20	0
8/8/14 11:53	M2_OC_0.5_1000_10s_5D_test2.txt	2	8.0	5.0	0.5				25
8/11/14 12:10	M2_OC_0.5_1000_10s_5D_test3.txt	2	8.0	5.0	0.5				10
8/12/14 12:35	M2_OC_0.5_1000_10s_5D_test4.txt	2	8.0	5.0	0.5				11
12/4/14 14:48	M2_small_tank_load_controlled.txt	2	8.0	5.0			Varies	-	
12/5/15 10:47	M2_load_controlled_small_tank.txt	2	8.0	5.0			Varies	-	
8/6/14 12:04	M1_OC_0.5_1000_10s_5D_test1.txt	1	8.0	5.0	0.5	0.150	0.030	15	0
8/6/14 15:02	M1_OC_monotonic_5D_test1.txt	1	8.0	5.0			0.002	1	
8/6/14 15:24	M1_OC_monotonic_5D_test2.txt	1	8.0	5.0			0.002	1	
8/7/14 11:56	M1_OC_0.5_1000_10s_5D_test2.txt	1	8.0	5.0	0.5	0.150	0.030	15	0
8/7/14 14:52	M1_OC_monotonic_5D_test3.txt	1	8.0	5.0					
8/28/14 14:05	M1_OC_monotonic_4D_test1.txt	1	9.0	4.0					

Table B.5: Summary of tests done in normally to moderately overconsolidated kaolin clay bed with direct lateral soil pressure measurements

Date	Filename	Diameter (in)	Embedment (D)	Moment Arm (D)	Target Tilt (deg)	Target Disp (in)	Rate of Lateral Disp (in/s)	Motor Speed (rpm)	Final Vertical Settlement (mm)
10/23/14 15:16	M4_0.5_1000_10s_5D_p.txt	4	8.0	5.0					
10/28/14 15:16	M4_0.5_1000_10s_5D_p_test2.txt	4	8.0	5.0					2-3
10/28/14 14:26	M4_monotonic_5D_p_test1.txt	4	8.0	5.0					
10/30/14 10:02	M4_0.25in_20_10s_5D.txt	4	8.0	5.0	0.3				
10/30/14 10:08	M4_0.60in_20_10s_5D.txt	4	8.0	5.0	0.5				
10/30/14 10:21	M4_1.0in_20_10s_5D.txt	4	8.0	5.0	1.0				
10/30/14 10:39	M4_2.0in_20_10s_5D.txt	4	8.0	5.0	2.0				
10/30/14 14:10	M4_monotonic_5D_2014_11_18.txt	4	8.0	5.0			0.006	3	
11/20/14 15:00	M4_static_load_controlled_2014_11_20.txt	4	8.0	5.0			Varies	-	
11/25/14 13:04	M4_load_controlled_2014_11_25.txt	4	8.0	5.0			Varies	-	
12/4/14 11:39	M4_load_controlled_2014_12_04.txt	4	8.0	5.0			Varies	-	
12/5/14 11:35	M4_load_controlled_2014_12_05.txt	4	8.0	5.0			Varies	-	
12/8/14 11:01	M4_load_controlled_cleaned_up.N.txt								
12/12/14	M4_load_controlled. txt								
9/04/15 14:11	M4LoadControlledTest1	4	8.0	5.0			Varies		
9/04/15 14:29	M4LoadControlledTest2	4	8.0	5.0			Varies		

Table B.6: Summary of tests done in the overconsolidated kaolin clay bed with a stiff top crust

Date	Filename	Diameter (in)	Embedment (D)	Moment Arm (D)	Target Tilt (deg)	Target Disp (in)	Rate of Lateral Disp (in/s)	Motor Speed (rpm)	Final Vertical Settlement (mm)
12/8/14 14:00	M2_small_tank_load_controlled.txt	2	8.0	5.0			Varies	-	
12/12/14 12:37	M2_load_controlled.txt	2	8.0	5.0			Varies	-	

Table B.7: Summary of tests done in overconsolidated Gulf of Mexico clay bed

Date	Filename	Diameter (in)	Embedment (D)	Moment Arm (D)	Target Tilt (deg)	Target Disp (in)	Rate of Lateral Disp (in/s)	Motor Speed (rpm)	Final Vertical Settlement (mm)
12/16/14 14:39	M2_load_controlled_GOM_small_tank.txt	2	8.0	5.0			Varies	-	
12/18/14 11:25	M2_load_controlled_GOM_small_tank.txt	2	8.0	5.0			Varies	-	
1/12/15 12:21	M2_0.5_10s_5D_100_GOM.txt	2	8.0	5.0	0.5	0.2		45	0
1/13/15 11:04	M2_0.5_10s_200_5D_GOM.txt	2	8.0	5.0	0.5	0.2		45	1

Table B.8: Summary of tests done in normally consolidated Gulf of Mexico clay bed

Date	Filename	Diameter (in)	Embedment (D)	Moment Arm (D)	Target Tilt (deg)	Target Disp (in)	Rate of Lateral Disp (in/s)	Motor Speed (rpm)	Final Vertical Settlement (mm)
4/09/15 13:36	NC_GoM_Clay_M1_Monotonic_Load_Controlled_Test1.txt	1	8.0	5.0			Varies	-	
4/10/15 11:53	NC_GoM_Clay_M1_Monotonic_Load_Controlled_Test2.txt	1	8.0	5.0			Varies	-	
4/13/15 14:13	M2_8D_1.0deg_20s_25cyc_test1.txt	2	8.0	5.0	1.0	0.4		45	0
4/13/15 11:11	M2_NC_GoM_0.5deg_100cyc_10s_test2.txt	2	8.0	5.0	0.5	0.2		45	0
4/15/15 11:51	M2_NC_GoM_disp_controlled_monotonic_test1.txt	2	8.0	5.0					